CZECH TECHNICAL UNIVERSITY IN PRAGUE

12105 Department of Mechanics, Biomechanics and Mechatronics

MASTER'S THESIS

Fatigue Life Prediction in Welded Structures

Martin Tomek 2015/2016

Declaration

This thesis is a presentation of my original research work. Wherever contributions of others are involved, every effort is made to indicate this clearly, with due reference to the literature, and acknowledgement of collaborative research and discussions.
The work was done under the guidance of Ing. Josef Jurenka Ph.D., at the Czech Technical University, Prague.

Date:.. Signature:..

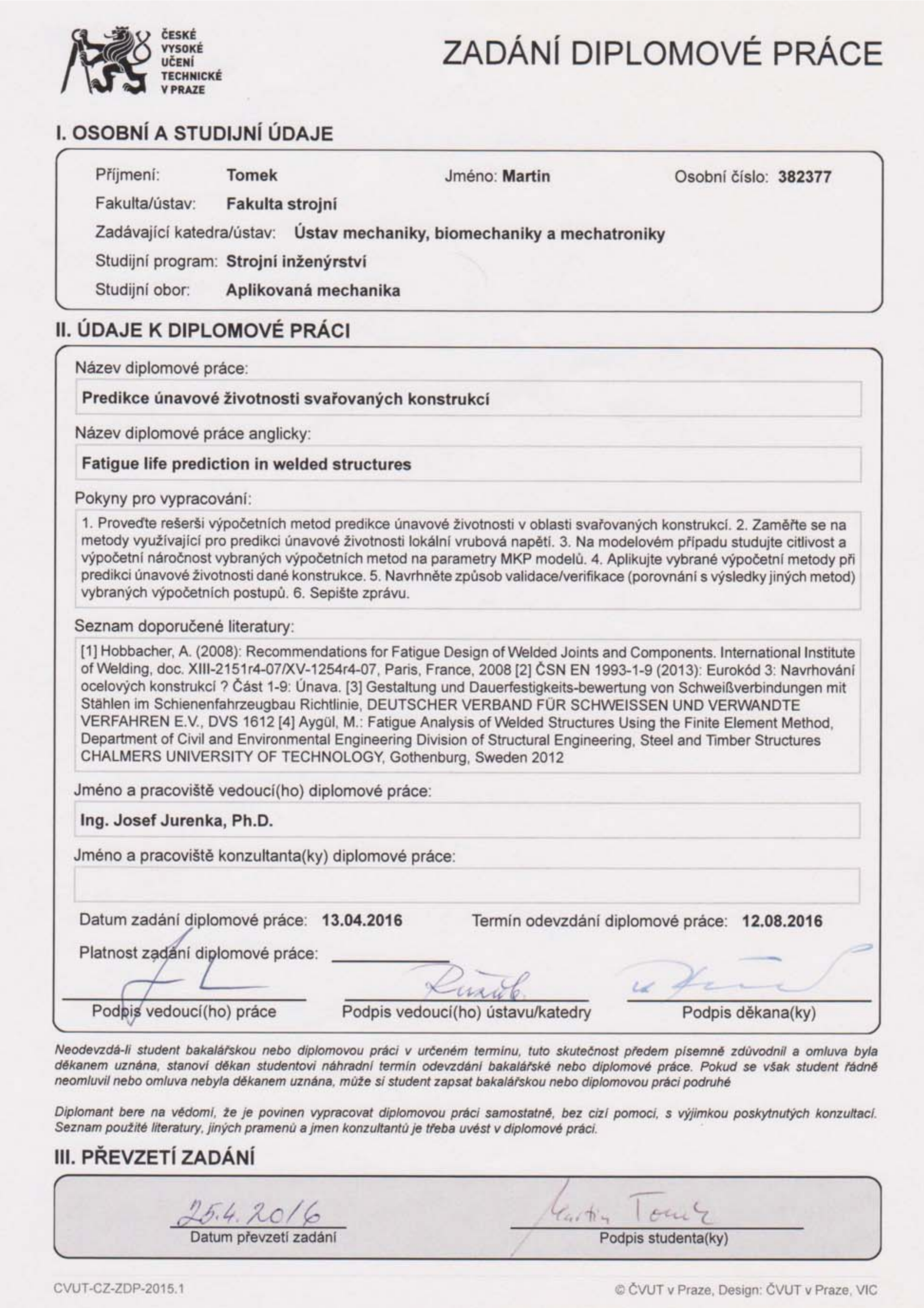

ČESKÉ VYSOKÉ UČENÍ TECHNICKÉ V PRAZE

ZADÁNÍ DIPLOMOVÉ PRÁCE

I. OSOBNÍ A STUDIJNÍ ÚDAJE

Příjmení: **Tomek** Jméno: **Martin** Osobní číslo: **382377**

Fakulta/ústav: **Fakulta strojní**

Zadávající katedra/ústav: **Ústav mechaniky, biomechaniky a mechatroniky**

Studijní program: **Strojní inženýrství**

Studijní obor: **Aplikovaná mechanika**

II. ÚDAJE K DIPLOMOVÉ PRÁCI

Název diplomové práce:

Predikce únavové životnosti svařovaných konstrukcí

Název diplomové práce anglicky:

Fatigue life prediction in welded structures

Pokyny pro vypracování:

1. Proveďte rešerši výpočetních metod predikce únavové životnosti v oblasti svařovaných konstrukcí. 2. Zaměřte se na metody využívající pro predikci únavové životnosti lokální vrubová napětí. 3. Na modelovém případu studujte citlivost a výpočetní náročnost vybraných výpočetních metod na parametry MKP modelů. 4. Aplikujte vybrané výpočetní metody při predikci únavové životnosti dané konstrukce. 5. Navrhněte způsob validace/verifikace (porovnání s výsledky jiných metod) vybraných výpočetních postupů. 6. Sepište zprávu.

Seznam doporučené literatury:

[1] Hobbacher, A. (2008): Recommendations for Fatigue Design of Welded Joints and Components. International Institute of Welding, doc. XIII-2151r4-07/XV-1254r4-07, Paris, France, 2008 [2] ČSN EN 1993-1-9 (2013): Eurokód 3: Navrhování ocelových konstrukcí ? Část 1-9: Únava. [3] Gestaltung und Dauerfestigkeits-bewertung von Schweißverbindungen mit Stählen im Schienenfahrzeugbau Richtlinie, DEUTSCHER VERBAND FÜR SCHWEISSEN UND VERWANDTE VERFAHREN E.V., DVS 1612 [4] Aygül, M.: Fatigue Analysis of Welded Structures Using the Finite Element Method, Department of Civil and Environmental Engineering Division of Structural Engineering, Steel and Timber Structures CHALMERS UNIVERSITY OF TECHNOLOGY, Gothenburg, Sweden 2012

Jméno a pracoviště vedoucí(ho) diplomové práce:

Ing. Josef Jurenka, Ph.D.

Jméno a pracoviště konzultanta(ky) diplomové práce:

Datum zadání diplomové práce: **13.04.2016** Termín odevzdání diplomové práce: **12.08.2016**

Platnost zadání diplomové práce: ____________

Podpis vedoucí(ho) práce

Podpis vedoucí(ho) ústavu/katedry

Podpis děkana(ky)

Neodevzdá-li student bakalářskou nebo diplomovou práci v určeném termínu, tuto skutečnost předem písemně zdůvodní a omluva byla děkanem uznána, stanoví děkan studentovi náhradní termín odevzdání bakalářské nebo diplomové práce. Pokud se však student řádně neomluvil nebo omluva nebyla děkanem uznána, může si student zapsat bakalářskou nebo diplomovou práci podruhé

Diplomant bere na vědomí, že je povinen vypracovat diplomovou práci samostatně, bez cizí pomoci, s výjimkou poskytnutých konzultací. Seznam použité literatury, jiných pramenů a jmen konzultantů je třeba uvést v diplomové práci.

III. PŘEVZETÍ ZADÁNÍ

25.4.2016
Datum převzetí zadání

Martin Tomek
Podpis studenta(ky)

CVUT-CZ-ZDP-2015.1

© ČVUT v Praze, Design: ČVUT v Praze, VIC

Abstract

The thesis describes fatigue assessment of welded joints by means of effective notch stress approach. Firstly, general methods for weld fatigue analysis are broadly described with focus on effective notch stress approach. Secondly, guidelines for creation and evaluation of notch stress approach models are presented. Next, notch stress approach is tested on small-scale model and compared to experimental results. Lastly, larger scale structure, boom of small sized excavator, is evaluated and comparison with other methods is discussed.

Keywords

Effective notch stress approach, fatigue of welded joints, fatigue tests, finite element method, hot-spot stress approach.

Acknowledgement

I would like to thank my supervisor Ing. Josef Jurenka Ph.D. for leadership and consultation of topics covered in the thesis. Next I would like to thank Ing. Šárka Trubelová for provision of experimental data and related consultations. I would also like to thank company Doosan Bobcat Engineering s.r.o. for provision of excavator model and loads definition and thus enabling me to perform analysis on "real life" product.

Last but not least I would like to thank my parents for their selfless and unconditional support as well as for all sacrifices they had to make in order to enable me to graduate.

Contents

Nomenclature xvi

1 Introduction 1

2 Basic concepts and nomenclature 3

2.1 Variable loading 3

2.2 S-N curves and FAT classification 4

2.2.1 S-N curves 4

2.2.2 FAT classification 6

2.3 Damage cumulation hypothesis 9

3 Overview of classical methods 11

3.1 Nominal stress approach 12

3.2 Structural (hot-spot) stress approach 14

3.2.1 Hot spot stress calculation 15

3.2.2 Reference points 17

3.3 Effective notch stress approach 19

3.3.1 Neuber's microstructural support hypothesis 19

3.3.2 Effect of multi-axiality 23

4 Guidelines for modelling of welded details by effective notch stress approach 25

4.1 Modelling of the welds 25

4.1.1 Ideal weld profile 26

4.1.2 Geometry based on the measurement 26

4.2 Mesh size and refinement 26

4.3 Utilization of sub-models 28

4.4 Link to structural stress analysis 29

4.5 2D modelling 29

4.6 Cross-section weakening 30

4.7 Misalignment and weld imperfections 30

4.8 Design S-N curves for effective notch stress approach 30

4.8.1 Correction for mild weld notches with reference radius of 1 mm . . . 31

5 Calibration of the effective notch stress approach on small scale model 33

5.1 Experiment description 34

5.2 Geometry and boundary conditions 37

5.3 Finite element model 40

5.4 Results 44

5.5 Discussion of results 50

5.5.1 Geometry type 50

5.5.2 Meshing method 51

5.5.3 Experiment difference 53

5.5.4 Comparison with other methods 53

6 Fatigue assessment of large scale model 57

6.1 Geometry and load definition 57

6.2 Finite element model 60

6.2.1 Contacts and boundary conditions 60

6.2.2 Mesh 68

6.3 Results 69

6.3.1 Stress and deformation 69

6.3.2 Endurance 74

7 Conclusion 77

Reference 79

A Analysis of geometry A 81

B Analysis of geometry B 85

C Analysis of geometry C 89

D Nomenclature used in excavator description 93

Nomenclature

$\Delta\sigma_{nom}$	Amplitude of nominal stress
$\Delta\sigma$	Stress range
$\Delta\sigma_{k,max}$	Maximum principal stress range
$max\sigma_{nom}$	Maximum value of nominal stress
ν	Poisson's ratio
$\overline{\sigma}_C$	Local fracture stress
π	Ludolph's number
ρ	Real radius of the notch
ρ^*	Substitute microstructural length
ρ_m	Material density
ρ_f	Fictitious radius
ρ_r	Reference radius
σ_Y	Yield Strength
σ_a	Stress amplitude
σ_a	Stress amplitude
σ_c	Endurance limit
σ_l	Lower stress amplitude
σ_m	Mean stress
σ_m	Mean stress
σ_u	Upper stress amplitude
$\sigma_{k,max}$	Maximum principal stress

σ_k	Effective notch stress
σ_s	Structural stress
θ	Weld flank angle
D	Fatigue damage ratio
E	Young's modulus of elasticity
i	Index for bin number in load spectrum
K_w	Weld notch factor
K_{IC}	Fracture toughness
m	S-N curve coefficient representing slope
N	Number of loading cycles, Endurance
N_i	Number of cycles to failure at design stress range $\Delta\sigma_i$
n_i	Number of cycles of design stress range $\Delta\sigma_i$ in bin i
R	Cycle asymmetry
$r_{1.0}$	Reference radius $r = 1mm$
r_{ref}	Reference radius
s	support factor
T	Period
t	plate thickness
w	Attachment width
FAT	Fatigue class specified by IIW
FEA	Finite Element Analysis
IIW	International Institute of Welding
MPC	Multi-point constraint

1 Introduction

When designing structures, loads imposed are often not constant but variable in time. Under this category one can imagine buildings loaded by snow, offshore wind turbines by waves and wind, aircraft engine rotors by accelerations, pressures, unbalances or transient temperatures and many others. When a part is loaded dynamically, a fatigue assessment needs to be done in order to come up with safe and reliable design.
When considering fatigue, all loads acting on the part need to be considered. Loads contributing to fatigue are usually called *fatigue actions*. Based on the fatigue actions the stresses and strains are calculated. It needs to be stressed out that reliable fatigue assessment can only be done when all relevant fatigue actions are considered. This puts large strain onto designers as loading is often not easily quantifiable and great deal of experience is needed to asses the loading appropriately.

This thesis is predominantly concerned with fatigue assessment of welded joints with particular interest in analysis by means of effective notch stress approach. First half of the thesis is rather theoretical and describes basic concepts of fatigue as well as existing state of the art approaches to fatigue assessment of welded joints, whereas the second half focuses on application of one of these methods - effective notch stress approach.

2 Basic concepts and nomenclature

Aim of the following section is to give an overview of the methods used in fatigue assessment of welded joints.
The existing fatigue assessment methods were developed and tested on common details and construction materials, therefore carry some limitations with them. Description of fatigue assessment methods to follow is therefore limited to welded components made of wrought or extruded products of [1]:

- ferritic/perlitic or bainitic structural steels up to $\sigma_Y = 960MPa$,
- austenitic stainless steels,
- aluminium alloys,

commonly used for welded structures. Further "the recommendations are not applicable to low cycle fatigue, where $\Delta\sigma_{nom} > 1.5\sigma_Y$, $max\sigma_{nom} > \sigma_Y$, for corrosive conditions or for elevated temperature operation in the creep range" [1].
First, several basic concepts and nomenclature related to fatigue assessment are going to be explained.

2.1 Variable loading

Variable loading that structures in operation are exposed to usually have complicated time dependence. In case of rotating machinery the loading can be periodic, but is seldom not superimposed with chaotic loads. For majority of constructions the loading has stochastic behaviour. Nevertheless, fatigue analysis is best described on case of simple periodic loading. After grasping the fundamentals, expanding the theory for complex loading is straightforward.
This type of loading can, for example, be found in rotating shafts. We can plot the stress-time dependence as a sinusoid curve and describe it by three parameters σ_l , σ_u and T that denote lower and upper stress amplitudes and period respectively. In fatigue design two parameters derived from these are usually used. Mean stress σ_m and stress amplitude σ_a. Both appear in the two most important diagrams in fatigue design: S-N and

Haigh diagrams. Last important parameter is called cycle asymmetry R and is computed as:

$$R = \frac{\sigma_l}{\sigma_u} \tag{1}$$

This parameter's importance lies in different fatigue resistance behaviour of materials with respect to symmetry of loading. Different types of constant amplitude loading are displayed in Figure 1.

As was mentioned before, loading is seldom so simple. In case of complex time dependence, loading is decomposed into a histogram and the impact of each loading range on structure is superimposed in fatigue analysis in order to get combined fatigue resistance.

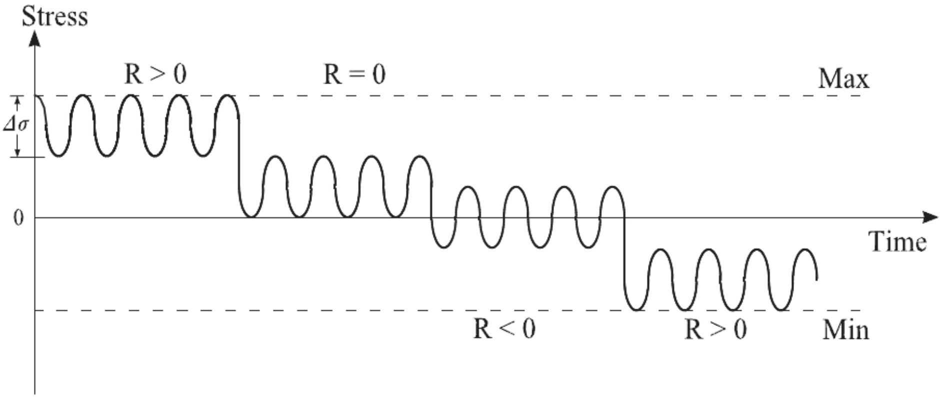

Figure 1: Types of constant amplitude loading [7].

2.2 S-N curves and FAT classification

2.2.1 S-N curves

One of the main postulates of fatigue analysis is that for the occurrence of the fatigue fracture, not total operating time, but number of loading cycles is critical. Based on the experimental testing of the specimens we can determine a relationship between number of cycles leading to failure N, stress amplitude σ_a and mean stress σ_m for a given material (see Figure 2a). Because this relationship is based on experimental measurement and the number of cycles leading to failure can be enormous, it is not practical to define this relationship as a function of all three parameters. Therefore the worst case scenario:

symmetric tension-compression loading ($R = 0$) with $\sigma_m = 0$ is usually considered and for this stress amplitude σ_a or stress range $\Delta\sigma$ as a function of number of cycles leading to failure is plotted. This plot is called S-N (Stress-number of cycles) or Wöhler curve (see Figure 2b).

The S-N curve is usually plotted in semi-logarithmic scale and based on the stress amplitude can be divided into two major zones: finite and infinite strength. The infinite strength zone goes from 0 to σ_c and corresponds to the amplitude stress levels that do not cause fatigue failure. σ_c is called Fatigue limit or Endurance limit. Above σ_c loading causes part to fail within finite amount of cycles. In engineering, the amount of cycles connected to endurance limit is usually taken as $N = 10^7$ or $N = 10^8$. In recent decades it has been found that fatigue failure can occur in the infinite life region as well, however slope of the S-N curve is much lower than in the finite region and is considered in special cases only.

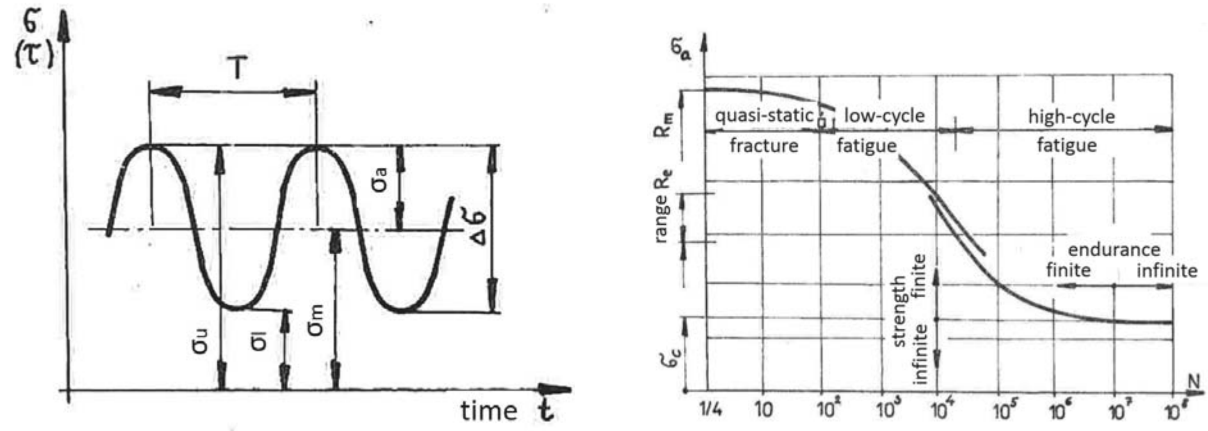
σ
(τ)
T
σa
Δσ
σu
σl
σm
time t
σa
Rm
range Re
σc
quasi-static
fracture
low-cycle
fatigue
high-cycle
fatigue
endurance
finite
infinite
strength
finite
infinite
N
1/4
10
10²
10³
10⁴
10⁵
10⁶
10⁷
10⁸

Figure 2: **a**) Constant amplitude stress cycle. **b**) S-N curve [8].

Based on the number of cycles to failure the S-N curve can be also divided into three ranges [8]

a) **Range of quasi static fracture**, where the failure occurs after first or several decades of cycles. This is not essentially classified as fatigue driven failure because the fracture surface grows very fast and the surface exhibits marks of ductile fracture similar to static failure.

b) **Range of low-cycle fatigue**, where the fracture appears after 10^2 to 10^5 cycles. The stress levels in material are high resulting in cyclic plastic deformation. The fracture surface exhibits coarse structure with intercrystallic fracture progression and distinctive marks of plastic deformation.

c) **Range of high-cycle fatigue**, where the amount of cycles leading to failure is larger than $5 \cdot 10^4$. The fracture surface is smooth with transcrystallic structure without marks of plastic deformation.

The S-N curve in its low-cycle to high-cycle range can be mathematically described as:

$$N = \frac{C}{\Delta\sigma^m} \tag{2}$$

It needs to be said, that reliability level of low-cycle fatigue range of S-N curve is generally small. The coefficients are obtained from the experimental measurements and scaled with respect to the required reliability and confidence level. In analysis of particular details the curve is also scaled with respect to stress concentrators typical to the detail itself. These stress concentrators can be divided into three categories: first the non-linear stress concentration in the inspected area due to local geometry, second due to the quality of the surface and last due to the quality of the material itself.

As was described earlier, the fatigue resistance is dependent not only on the stress amplitude but also on the mean stress value. To respect that, Haigh diagram (also called Goodman diagram) is used. This diagram scales the endurance limit of material based on the mean stress value. Example of such diagram can be seen in Figure 3. In the diagram, various lines correspond to different theories of taking mean stress influence into account.

2.2.2 FAT classification

The above mentioned procedure is typical to most structural details, however welded joints bring several difficulties to fatigue assessment and endurance evaluation. As was mentioned in the previous paragraph, the S-N curves are specific to material and are scaled for various details based on the potential stress concentrations. This can be easily done for common details, however welded joints present several major complications. To name a few:

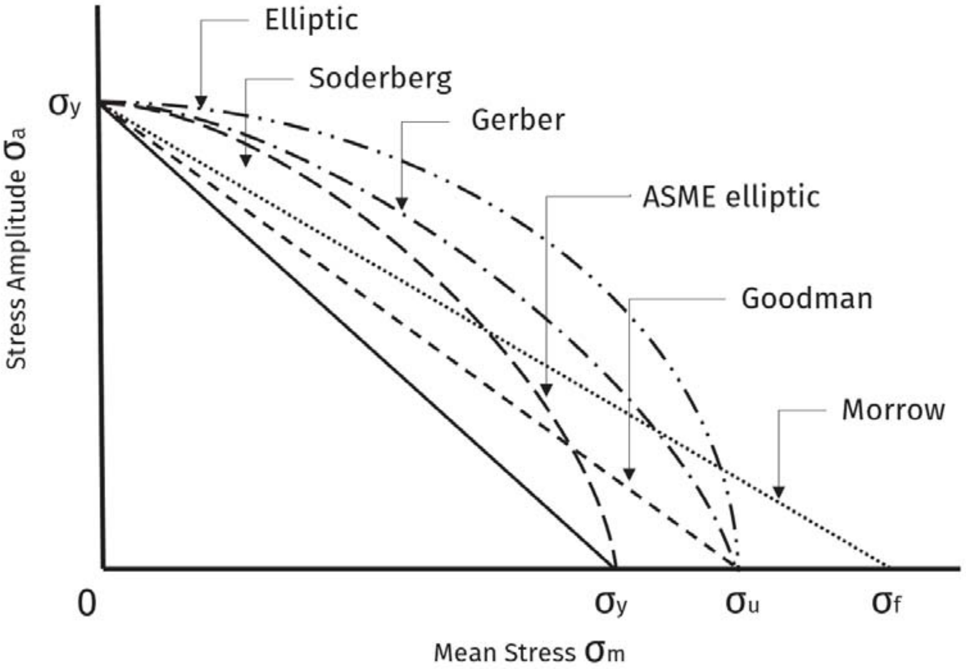

Figure 3: Example of Haigh diagram. Different curves correspond to safe zones per different theories [9].

- material inhomogeneities such as micro-cracks, voids and lack of fusion,
- large residual stresses and unknown stress gradients,
- unknown geometry of the weld,
- electrode additives resulting in base material properties alteration.

This results in low reliability and sometime even inability of classical fatigue assessment approach as described above. Because of the wide usage of welded joints there has been a considerable effort to come up with reliable method for its fatigue assessment. In general the current methods can be divided into three categories:

1) Design per standards and design codes. Country or region specific codes that specify reliable methods for fatigue assessment, that are generally applicable.
2) Design per special methodology. Company specific methods for assessment with special prerequisites (for example consideration of company material and welding quality).
3) Design per detail fatigue testing.

One of the industry acclaimed codes that is widely used and that specifies several fatigue assessment methodologies is *Recommendations for Fatigue Design of Welded Joints and Components* published by International Institute of Welding (further referred to as IIW). The IIW has tackled the problem by measurement, collection and evaluation of substantial number of fatigue tests for different details and creation of database of S-N curves with survival probability of at least 95%, calculated from the mean value on the basis of two-sided 75% tolerance limits of the mean. Each of the structural details defined in IIW recommendations is classified based on the nominal stress range. In most cases this means assessment on the basis of maximum principal stress range in the section where the failure is to occur. If the detail is not listed in IIW recommendations additional methodologies are presented with specific S-N curves. Because the details tested were manufactured using convectional welding procedures, the IIW S-N curves already incorporate the above mentioned peculiarities such as:

- stress concentration due to weld geometry,
- weld imperfections consistent with normal fabrication standards,
- high residual stresses,
- metallurgical conditions, or
- welding process.

The respective details are classified and assigned to so called fatigue classes (denoted FAT). The FAT class numerical value represents fatigue resistance of the detail in MPa at 2 million cycles (see Figure 4). The slope of the S-N curves for steel and normal stress is $m = 3$ with the amplitude knee point assumed to correspond to $N = 10^7$ cycles. In case of low to medium cycle applications the S-N curve is considered to assume constant level after $N = 10^7$ cycles. In case of very high cycle applications the S-N curve is assumed to decline further after $N = 10^7$ cycles, where the slope of $m = 22$ is recommended. This is for example typical for rotating machinery, where large amounts of cycles are accumulated quickly.

For the endurance of details assessed on the basis of shear stress the slope of S-N curve is given as $m = 5$ with the amplitude knee point assumed to correspond to $N = 10^8$ cycles. IIW also provides S-N curves for details from aluminium.

The IIW further gives a set of recommendations for S-N curves modification in case of details alteration from normal parameters such as large wall thickness, welds improvements, temperature effects and corrosion.

In case of welded joints the Haigh diagram is typically not used due to the presence of high residual stresses of unknown magnitude. It can nevertheless be used in special cases, mostly when stress state is known reasonably well (for example when the parts are heat treated for residual stress relieving) [1].

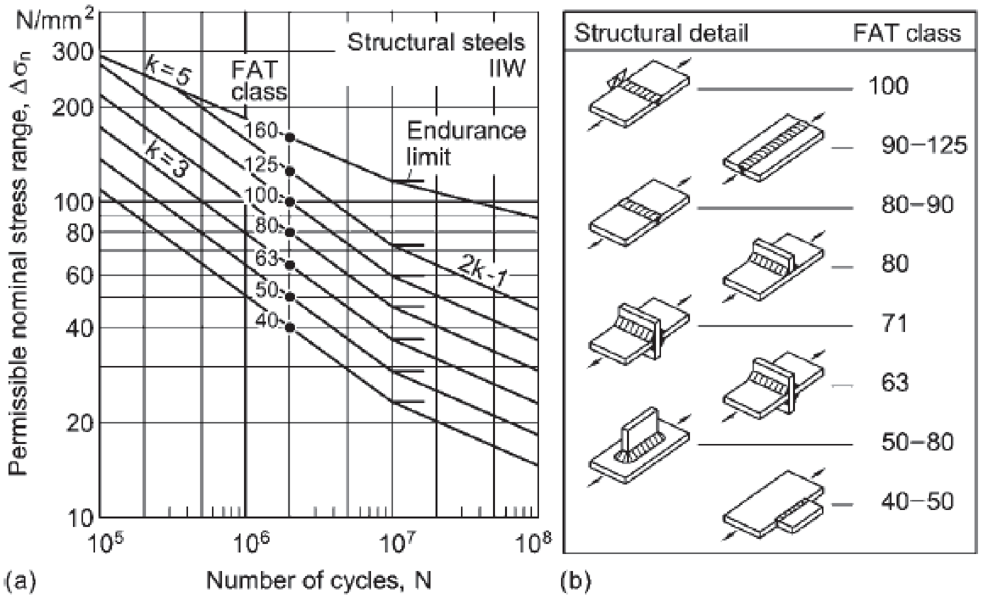

Figure 4: S-N curves by IIW and example of details and their FAT clases [4].

2.3 Damage cumulation hypothesis

In case of variable amplitude loading cumulative damage calculation should be applied. So called modified Palmgren-Miner rule is appropriate in case of welded joints. First the S-N curve is selected and the required number of cycles is determined. The endurance limit σ_C is then compared with the maximum design stress range $max\Delta\sigma$ from the load spectrum. If it is lower than the endurance limit the life of the welded detail can be assumed infinite. This is only applicable when considering the S-N curve to be constant after 10^7 cycles. Therefore this is not recommended for the details required to withstand vast amounts of cycles.

In that case the S-N curve is extrapolated beyond the 10^7 cycles as $m_2 = 2m_1 - 1$, [1]. The slope is different than the above specified for the constant amplitude loading. The load spectrum is decomposed into bins and the partial fatigue damage is computed for each load spectrum block. The hypothesis states that each block of the spectrum depletes part of the details endurance capability and its cumulative sum shall be limited. This can be written as, [1]:

$$D = \sum_{i=1}^{i} \frac{n_i}{N_i} \leq 0.5...1.0 \tag{3}$$

Where D is called fatigue damage ratio, the i is index for bin number in load spectrum, the n_i is the number of cycles of design stress range $\Delta\sigma_i$ in bin i and N_i the number of cycles to failure at design stress range $\Delta\sigma_i$. Hobbacher [1] implies that recent research has indicated $D = 1$ being too non-conservative and therefore recommends $D = 0.5$. In case of spectra with high mean stress fluctuation even lower fatigue damage ratio is recommended.

In case the actual sequence of loads becomes significant non-linear fracture mechanics damage calculation is recommended.

3 Overview of classical methods

The methods utilized in the fatigue assessment of welded joints can be divided into two categories denoted as 'global' and 'local' approaches.

The first category, global approach, is based either directly on external forces and moments or nominal stresses in the specifiedcross-sections. The stress distribution in cross-sections is considered to be constant or linear.

The second category, local approach, is based on the local strains and stresses. Knowledge of continuum mechanics is used to describe the process of cyclic crack initiation, propagation and final fatigue. The crack initiation is based on the notch stress approach, where typically the stress in the weld root is calculated. The propagation of the crack and the final fracture are based on the crack propagation approach.

The intermediate approach between global and local method is structural stress approach, that involves stress concentration due to macrogeometry and the notch effect is considered by adjustment of S-N curve.

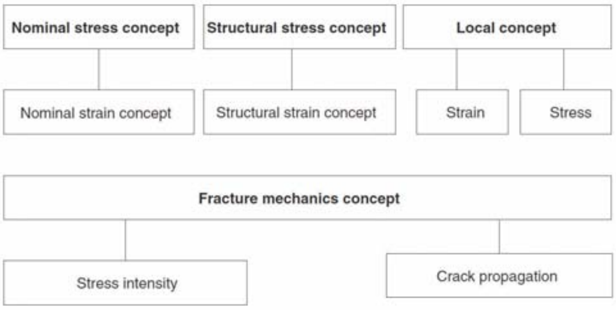
Nominal stress concept
Structural stress concept
Local concept
Nominal strain concept
Structural strain concept
Strain
Stress
Fracture mechanics concept
Stress intensity
Crack propagation

Figure 5: Fatigue assessment methods. [Sonsino, Radaj, 2008].

The definition of different types of stresses upon which the fatigue assessment is built are displayed in Figure 6. The main approaches applied in the fatigue assessment of the welded joints therefore are:

1. Nominal stress approach,
2. Structural (hot-spot) stress approach,
3. Effective notch stress approach,
4. Fracture mechanics,

5. Component testing.

More elaborated subdivision is illustrated in Figure 5. In the following sections approaches 1-3 are going to be described briefly.

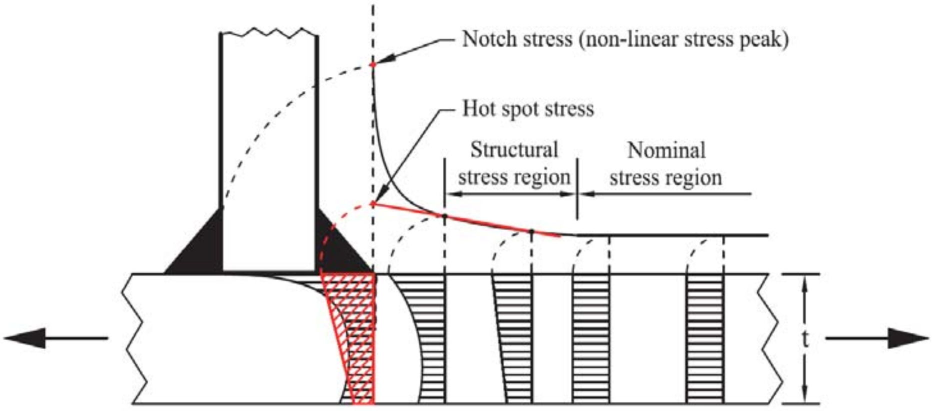

Figure 6: Stress distributions across the plate thickness and along the surface in the vicinity of a weld toe [2].

3.1 Nominal stress approach

Nominal stress approach was the most widely used method for assessment of endurance of welded details. This approach uses nominal stress amplitudes calculated in the cross sections of the base plate and compares them to the S-N curve to determine number of cycles the detail will last till failure. The stress is calculated disregarding the local stress raising effects of the welded joint, nevertheless macrogeometric shape of the component and load concentrations in the close vicinity of the weld need to be considered (see Figure 7). Both of those can influence redistribution of membrane stresses and generate severe bending stresses. Misalignment of the welded components also needs to be considered as long as it is larger that tolerance already included in the S-N curves.

Nominal stress for simple joints can be calculated using the beam theory. For complex geometry FEA (Finite Element Analysis) can be used. Mesh can be coarse, however large attention needs to be paid to exclude any stress concentrations arising from structural details of the weld.

The S-N curve is depended on material (steel or aluminium), detail class and weld quality class. Notch/detail classes are assigned to sets of uniform S-N curves which are gener-

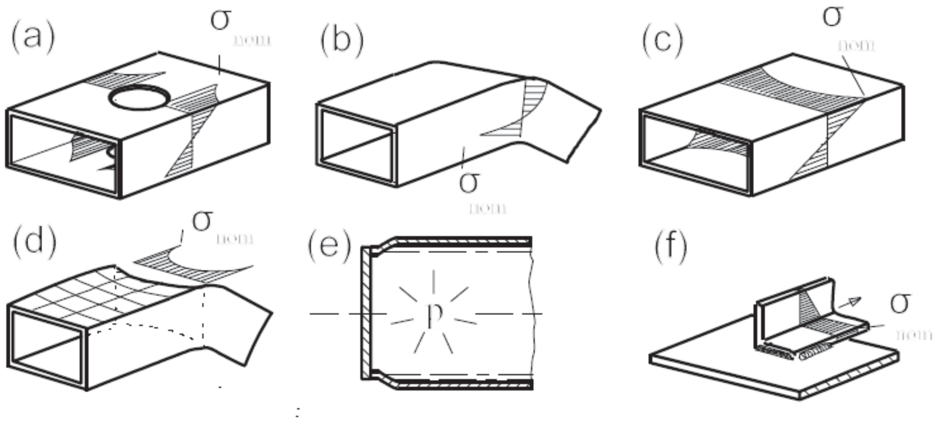

Figure 7: Examples of macrogeometric effects [1].

ally "linearised, parallelised and equidistantly positioned in logarithmic scales of the parameters S and N" [4].

Design codes grade typical weld details and assign them to different detail classes (FAT) representing S-N curves based on the results of the fatigue tests (see Figure 4). To see other example of these tabulated details see recommendations by IIW [1].

Nominal stress S-N curves are substantially lowered due to the presence of high tensile residual stresses that are typically introduced by welding [4]. The S-N curves are independent of mean stress because presence of high tensile residual stresses is expected, that keeps the initiated cracks open permanently. In case where compressive residual stresses were artificially introduced, IIW recommends to use fatigue enhancement factors for certain details.

Nominal stress approach is widely used in construction of bridges, cranes, ships, pipes and many others. Typically where lightweight design and damage tolerance are not necessary.

Nominal stress approach is typical to design per design codes. Examples of such codes are: IIW recommendations, European design codes (EUROCODE 3), ASME boiler and pressure vessels, British codes, German standards, Japanese standard.

If detail is loaded by a spectrum of stress amplitudes, Miner damage accumulation rule is recommended for fatigue assessment.

3.2 Structural (hot-spot) stress approach

In the hot-spot stress approach, stress at so the called hot-spot is used as reference value for fatigue evaluation. Stress at hot-spot includes all stress-raising effects of evaluated detail apart from stress contribution due to the presence of the weld profile itself. In other words the non-linear peak of the stress caused by the notch in weld toe is excluded from hot-spot stress. Figure 8 gives examples of hot-spot stress distributions in various details that include stress variation due to effects of macro-geometric features.

Structural stress approach is used when nominal stress is difficult or impossible to determine due to geometric complexity or where the detail is not classified in the design codes.

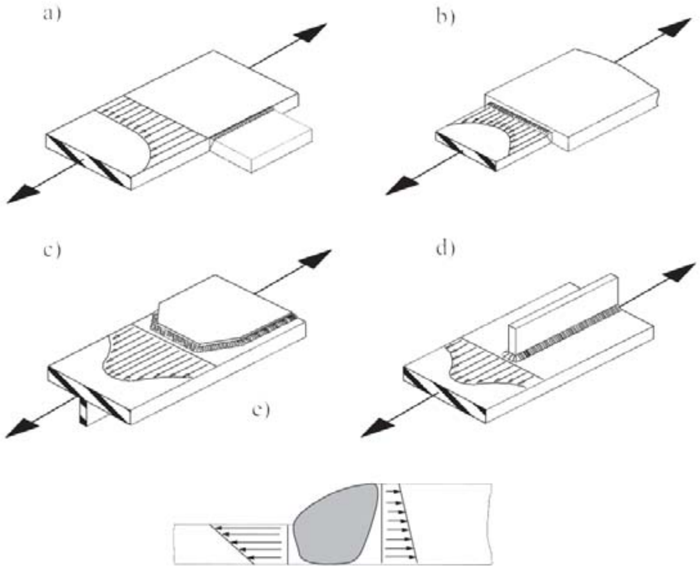

Figure 8: Examples of hot-spot stress distributions including the effect of macro-geometric features [1].

Hot-spot stress is stress extrapolated from reference points in vicinity of the weld as indicated in Figure 6.

When the stress is biaxial across at the plate surface, IIW recommends to use principal stress which acts perpendicular to the weld toe within $\pm 60^\circ$.

IIW classifies two types of hot-spots according to their location on the plate and their orientation with respect to the weld toe (see Figure 9). *Type a* where weld toe is located on the plate surface whereas *type b* where weld toe is located at the edge of the plate. The hot-spot stress at the location is determined from the FEA and by extrapolation of nodal values or by strain measurement and subsequent extrapolation.

Due to non-linearity of actual stress distribution a special procedure needs to be adopted. First reference points are established at the surface of the plate, second the hot-spot stress is calculated by extrapolating the stress from the reference points to the weld toe. Due consideration needs to be given to the choice of reference point closest to the weld toe in order to avoid any influence of the notch originating from the weld. IIW recommends to use distance $0.4t$, where t is the plate thickness.

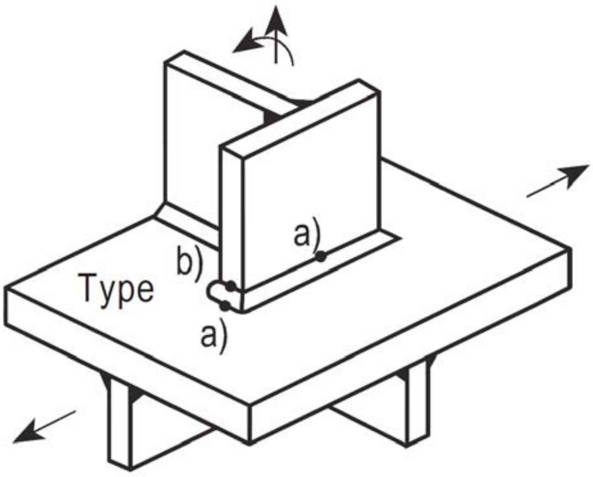

Figure 9: Types of hot-spot stress [1].

It is of utmost importance to correctly identify fatigue critical locations and corresponding reference points. This is done either by measurements at several locations, analysis of the FEA results or experience with existing components.

3.2.1 Hot spot stress calculation

Determination of the structural hot-spot stress is almost exclusively done by application of FEA. This is because parametric solutions of the analysed details do not exist due to structural discontinuities and model complexities.

Hot spot stress is calculated assuming idealized perfectly aligned welded joint. It is however also possible to take misalignment into account by its explicit modelling in the FEA model or by applying an appropriate magnification factor.

Generally plate, shell or solid elements are used in the model. "The elements must allow

for steep stress gradients and formation of plate bending" [1].
In model with shell elements, elements are placed in the mid-plane of the welded plates. The 8-noded elements are recommended to capture steep stress gradients. The geometry of the welds is not modelled in simplified models, however when the results would be affected by local bending in the area of the weld, the welds need to be included. The welds can be modelled either by inclined shell elements with appropriate stiffness or by rigid links between the relevant nodes.
For more complex models solid elements are preferred. The displacement function of the solid elements must allow for steep stress gradients and plate bending with line stress distribution in the plate thickness direction. An example of such element is 20-node isoparametric prismatic element with mid-side nodes at the edges. Model constructed of those elements can have one layer of elements across the plate thickness only due to the quadratic displacement function and linear stress distribution. "By reduced integration the linear part of the stresses can be directly evaluated at the shell surface and extrapolated to the weld toe" [1]. When multiple layers of elements are used, the stress can be linearised over the plate thickness directly at the weld toe. Figure 10 shows typical meshes used for hot-spot stress approach evaluation.
As was described earlier, hot spot stresses are extrapolated from nodes adjacent to the weld toe. The length of the elements is therefore influenced by the choice of reference points selected for stress evaluation. To avoid the influence of the stress singularity at the weld toe, the stress closest to the hot spot is evaluated at the first nodal point. The length of the element closest to the weld is therefore driven by the distance from the first reference point. Width of solid elements or two shell elements should not be larger that attachment width (see "w" in Figure 10). If fine mesh is used, refinement in direction

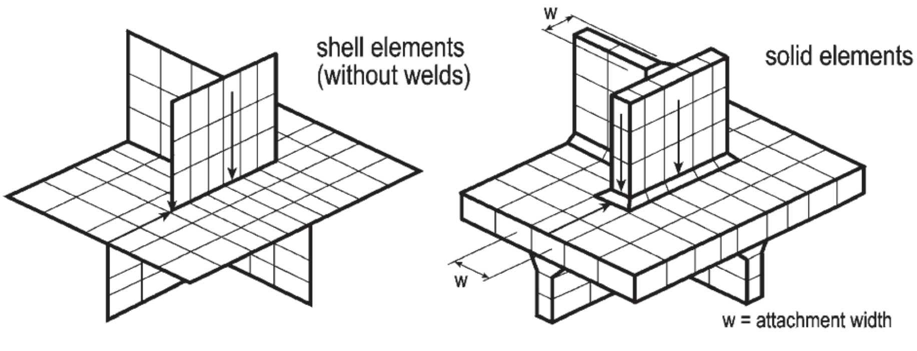

Figure 10: Typical models from shell and solid elements [1].

of thickness shall be introduced.

3.2.2 Reference points

Hot spot stress is determined by extrapolation from two or more reference points. Typical paths for extrapolation are marked in Figure 10. The extrapolation method varies based on the type of hot-spot (see Figure 9), number of reference points, refinement of the mesh and loading. Generally the most important division is based on the type of hot spot stress as defined above. For type "a" of hot spots the stress is dependent on the plate thickness. All the extrapolation equations are therefore function of plate thickness and the reference points are spaced in its fractions. Type "b" is independent on the plate thickness and the reference points are spaced in predefined lengths from the weld toe. Recommended extrapolation techniques are apparent from Table 1.

As discussed, the stress values in reference points can be taken either from FEA or measured by strain gauges.

Hot-spot	Mesh	Extrapolation	Description
A	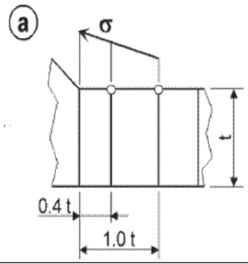	$\sigma_S = 1.67\sigma_{0.4t} - 0.67\sigma_{1.0t}$	-Fine mesh -Element length no longer than $0.4t$ at hot spot -Linear extrapolation
A	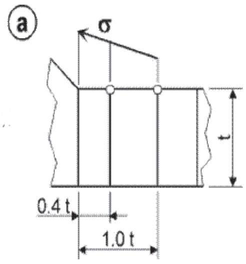	$\sigma_S = 2.52\sigma_{0.4t} - 2.24\sigma_{0.9t} + 0.72\sigma_{1.4t}$	-Fine mesh -Element length no longer than $0.4t$ at hot spot -For pronounced non-linear peaks and sharp changes of applied force -Quadratic extrapolation
A	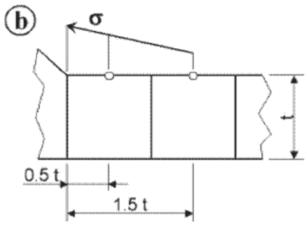	$\sigma_S = 1.50\sigma_{0.5t} - 0.50\sigma_{1.5t}$	-Coarse mesh with higher order elements -Element length equal to plate thickness -Evaluation at mid side points -Linear extrapolation
B	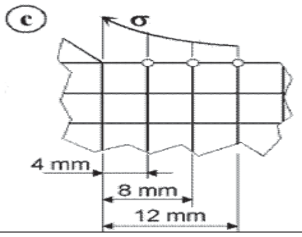	$\sigma_S = 3\sigma_{4_{mm}} - 3\sigma_{8_{mm}} + \sigma_{12_{mm}}$	-Fine mesh -Element length no longer than $4mm$ at hot spot
B	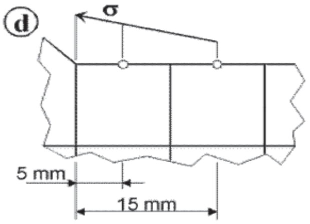	$\sigma_S = 1.5\sigma_{5_{mm}} - 0.5\sigma_{15_{mm}}$	-Coarse mesh -Element length 10 mm at hot spot -Evaluation at mid side nodes

Table 1: Extrapolation techniques based on mesh size and hot-spot type [1].

3.3 Effective notch stress approach

Goal of the effective notch stress approach is to find stress directly at the location from where fatigue crack initiates. Conceptually, the paramount step of effective notch stress approach is the substitution of the actual geometry with an effective one. There are several reasons behind this. The most important reason comes from what is called '*microstructural notch support hypothesis*'. Under the term microstructural support we can imagine fatigue behaviour of an inhomogeneous material structure under stress gradient. This hypothesis says that maximum notch stress according to the theory of elasticity is not decisive for crack initiation and propagation but instead some lower local stress gained by averaging of the notch stresses over a material-characteristic small length, area or volume at the notch root. It further implies that final stress therefore also depends on the microstructural length of material (material property) and radius of the notch in addition to other usual parameters.

There are different microstructural hypotheses used for the stress assessment with '*stress averaging concept*' proposed by Neuber being the most common in the fatigue assessment of welded joints. This concept is used mainly in the form of fictitious notch rounding and is also known under the name *effective notch stress approach*. Other main microstructural hypotheses are: stress gradient approach (Siebel and Stieler 1955), critical distance approach (Peterson 1959) and highly stressed volume approach (Kuguel 1961, Sonsino 1993 and 1995).

3.3.1 Neuber's microstructural support hypothesis

Fatigue crack initiation and propagation at the root of sharp notches presents highly localized process of material damage. The initiation and accumulation of this damage takes place on microstructural and submicrostructural level by means of dislocation movements, microcracks inititation and propagation [5]. This complex phenomena has been described by microstructural cracking theories, which enabled deeper understanding of the complicated processes involved and thus identification of critical microstructural parameters that can be used in structural materials processing optimization.

Although more detailed, the microstructural theories are not optimal as engineering methods for fatigue life or strength assessment, where the classical continuum theories are usually used. One of such continuum theories is *microstructural support hypothesis* proposed by Neuber in 1937 and is going to be described in this section. This hypothesis is of particular interest to us due to the popularity it has adopted in the fatigue assessment of welded joints.

It is well known that strength of sharply notched specimens is not reduced as severely as elastic stress concentration suggests. The microstructural support hypothesis assumes that the macrocracks initiation at the notch occurs not when the notch root stress exceeds the endurance limit, but when the limit is exceeded by a stress averaged across a small material volume characterized by the *substitute microstructural length* ρ^*. This is consistent with the observation mentioned above. Furthermore Neuber combined the microstructural support hypothesis with the *fictitious notch rounding concept* "in order to avoid the (at the time) labourious stress averaging procedure at the notch root" [5]. The concept of fictitious notch rounding lies in artificial enlargement of the notch size in such a way that the root stress in the enlarged notch is equal to the stress averaged across the substitute microstructural length ρ^* of actual notch. The fictitious enlargment size is equal to the microstructural length multiplied by the *support factor* s. The microstructural length is a material property whereas support factor depends on the stress multiaxiallity at the root of the notch and considered failure criterion.

Based on the micrustructural length determined by Neuber on the basis of reversed tensile and bending loaded notched specimens, the radius for sharply notched weld toes was approximated as $\rho_r = 1$ mm. It needs to be said that Neuber's tests did not take crack closure effects into consideration, therefore the support effect of the material was overrated [5].

Neuber gave the fictitious notch rounding in the following form:

$$\rho_f = \rho + s\rho^*, \tag{4}$$

where ρ_f represents the fictitious notch radius and ρ the real notch radius. As was already mentioned, the microstructural support length ρ^* depends solely on the material and its microstructural condition. This can be expressed by means of yield limit in fatigue loading σ_Y proposed by Neuber or by the fracture toughness K_{IC} and the averaged local fracture stress $\overline{\sigma}_C$ in static loading as described by Weiss (1971) as [5]:

$$\rho^* = \frac{2}{\pi}\left(\frac{K_{IC}}{\overline{\sigma}_C}\right)^2 \tag{5}$$

Up to this point, all types of sharp notches were discussed. It was Radaj who in 1969 proposed to predict high-cycle fatigue strength of welded joints (in root and toe regions) based on the fictitious rounding. The conservative approach for the mild steel assumes the actual notch radius as singularity $\rho = 0$ mm. Root and toe locations of welds can be viewed as a cast steel for which the substitute microstructural length is equal to $\rho^* = 0.4$ mm. The substitute microstructural length for other materials is depicted in Figure 11. For the plane strain conditions at the roots of sharp notches combined with von Mises multiaxial strength criterion for ductile materials Radaj in 1990 proposed the value of support factor $s = 2.5$. By substitution of these values to Equation 4 the fictitious radius is assumed as $\rho_f = 1$ mm. To respect the fact that this rounding radius corresponds to the conservative case, and not the actual geometry, where the actual notch size is not equal to zero, we call it *reference radius* and mark it as r_{ref} or $r_{1.0}$.

It is worth noting, that the same reference radius can be applied for aluminium details, even though the microstructural support length for aluminium is smaller. This is consistent with the results of experiments performed by Morgenstern [5].

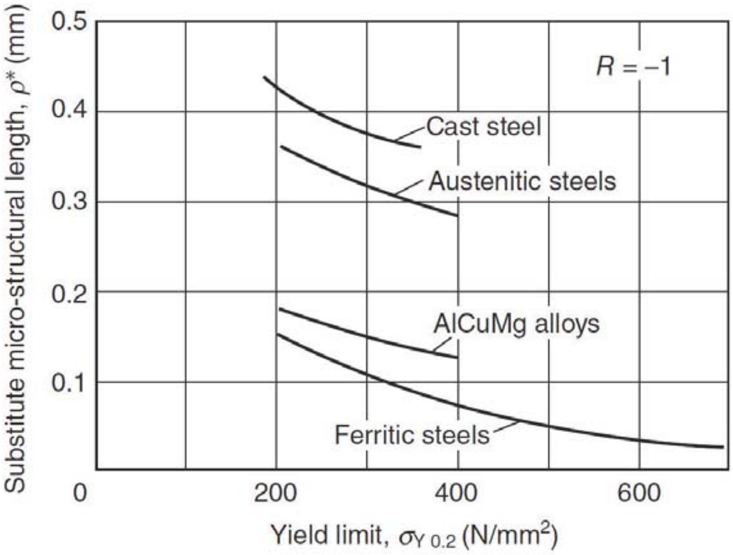

Figure 11: Substitute microstructural length dependent on yield limit for various materials (Neuber, 1968) [3].

For infinite life the effective stress from the effective model is then compared with the endurance limit of the parent material. In case of finite life it is recommended to correct the final stress values with respect to residual stresses by using the normalized S-N curve. IIW recommendation in this regard is to use FAT225 curve. Non-zero static mean stress can be incorporated into the analysis in terms of Haigh diagram, however care needs to be taken as Neuber microstructural hypothesis has not yet been verified for non-zero static mean stress [4].

The fictitious rounding needs to be carried out with care as in case of some details the modification of geometry can cause undercuts and therefore result in larger stress concentration. The rounding is also debatable in case of purely tensile or compressive loading in direction of crack, where in the ideal case no stress rise occurs, but in case of rounded geometry a substantial stress concentration is created [4].

The attractiveness of the effective notch stress approach for designer is that for any type of detail the principal stresses are found in critical weld locations and compared with endurance limit of the material. The method therefore neutralizes influence of various geometries and loading modes on the fatigue strength of the detail as opposed to nominal stress approach that relies on a list of tabulated details. Additionally it allows for comparison of different geometrical configurations and further optimization.

This approach has nevertheless several limitations, which need to be mentioned:

- As with other local methods, an experience of the designer is required to apply effective notch stress approach correctly. User needs to be aware of both strengths and shortcomings of this method. It is advised to always approach the results critically and compare/validate with other methods.

- There is a limitation with respect to thickness of welded plates that this reference radius can be applied to. This comes from the effect of comparatively large cross section reduction and hence stress modification caused by the fictitious notch rounding. Therefore for the thin walled welded joints ($t < 5$ mm) reference radius $r_{ref} = 0.05$ mm is commonly being adopted. This value was derived on completely different hypothesis than the above discussed . "*The background of the smaller reference radius $r_{ref} = 0.05$ mm is the relationship between the stress-intensity factor and the notch stress (...) as well as the crack tip blunting*" [6]. The value is also a compromise between the ability of modelling by FEA and calculation of reasonable

stress components.
According to Sonsino [6] the reference radii size of $r_{ref} = 1$ mm and $= 0.05$ mm are also based on empirical observations and assumptions. The radius of 1 mm is often observed in untreated as-welded thick walled joints. As for the thin walled joints, the smaller radius corresponds to the approximate size of low to medium strength feritic steel grains and in many cases to the radius of the notch root of spot-welds or laser welded joints.

- Impact of multiaxiallity and boundary conditions. This is discussed in the next section.

3.3.2 Effect of multi-axiality

Only a small percentage of details can be considered to be subjected to one stress component only. In case of real constructions the welded joint is often subjected to multiaxial state of stress and its evaluation can have direct impact on the fatigue assessment. When the weld is subjected to more than one stress component, we can generally distinguish two cases [3]:

1. the principal stress directions are constant which is usually associated with proportional stress components, or
2. the principal stress change direction, which is associated with non-proportional stress components and which is produced by out of phase loading components.

If the loading falls under the first category, the largest principal stress range that acts within a sector of $\pm 45°$ perpendicular to the weld line should be considered as a fatigue resistance main determining parameter [3]. The equivalent stress range is in this case usually smaller and fatigue prediction can be non-conservative. This assessment is similar to case with uni-axial loading.
In the second case, the welded detail is subjected to predominantly in-plane shear load. Hence the equivalent stress range can be larger than the maximum principal stress range. If the second principal stress has different sign than the other two, fatigue assessment

using equivalent stress is appropriate. Additional option is to use one of the stress components interaction formula[1] [2] to get the fatigue relevant parameter. In case that stress in the notch is based on the stress concentration factors applied to the different stress components, "account should be taken of the fact that the locations of the corresponding peak stresses might differ" [3].

---

[1] Sonsino C M and Wiebesiek J (2007): Assessment of Multiaxial Spectrum Loading of Welded Steel and Aluminium Joints by Modified Equivalent Stress. IIW-Doc. XIII-2158r1-07/XV-1250r1-07, International Institute of Welding.

[2] Hobbacher A (2009): Recommendations for Fatigue Design of Welded Joints and Components. IIW Doc.1823-07, Welding Research Council Bulletin 520, New York.

4 Guidelines for modelling of welded details by effective notch stress approach

Although the theory of fictitious notch rounding may seem rather straightforward, its application by means of finite element method is generally not. The results can largely vary based on several aspects intrinsic to modelling itself such as notch placement, element size, element type or displacement function of the elements. Generally speaking a sufficient discretization is needed so the task is to find balance between the precision and numerical difficulty. In order to come up with reliable results consistent with reality a set of recommendations should therefore be followed. In the proceeding section core recommendations are summarized, based mostly on the *Recommendation for fatigue design of welded joints and components* [1] and *Guideline for the fatigue assessment by notch stress analysis for welded structures* [3]. If further informations are needed, please consult these publications.

In the effective notch stress analysis a linear elastic material behaviour is usually assumed and deemed sufficient. A great care nevertheless needs to be taken if large displacements are present. This can be the case for thin-walled structures where non-linear analysis may be required. This is also applicable if contacts are assumed. "However, contact between non-welded root faces is not usually assumed, leading mostly to conservative results" [3]. The welded details can be modelled as 2D or 3D depending on the exact geometry of the detail. If the variation of the loading and geometry can be neglected in the third direction, 2D analysis is usually sufficient and plane strain conditions are assumed as the stresses in the notch are biaxial due to the restraint in the third direction.

4.1 Modelling of the welds

Generally two cases can be considered:

- Modelling of the idealized weld profile where the weld has constant flank angle and toe or root radius is equal to reference radius.

- Modelling of the weld based on the measurement of the actual geometry that is approximated by simple geometrical entities such as circular or straight lines.

4.1.1 Ideal weld profile

The weld geometry can be characterized by flank angle θ and radius r. Figure 12 shows typical idealized weld profiles of butt and fillet welds. It is evident, that in case of non-penetrating fillet welds, two shapes can be used. Either keyhole or U-shaped notch can be inserted. In case of U-shaped notch the high stress concentration for loading parallel to the non-welded face is reduced, but can also lead to an underestimation of the notch stress in the weld throat. The vertex point of the circle needs to be located at the weld root in order to retain the length of non-welded root faces. Note that by placement of the notch, thickness of the base plate can be reduced. This is referred to as *cross-section weakening*. In case of thin-walled profiles this cross-section weakening can lead to higher stresses and overconservative results and needs to be accounted for.

4.1.2 Geometry based on the measurement

If direct weld profile measurement is utilized, the point-wise measurement is first smoothened and approximated by straight and circular lines with tangential transitions. The weld profile modelled directly from the measurement points may result in unrealistic stress concentrations in the concave corners of the profile and therefore overconservative results. Depending on the approach the root and the toe radius can be either modelled as measured or enlarged to be consistent with the micro-structural support effect of the material.

4.2 Mesh size and refinement

Welded parts or details are usually meshed relatively coarsely with gradual refinement toward the notched area. Proper mesh should take force flow and deformation behaviour of the whole structure into account to simulate loading of the notched area correctly. Of particular interest is the "bending behaviour of structures (that) has to be considered by

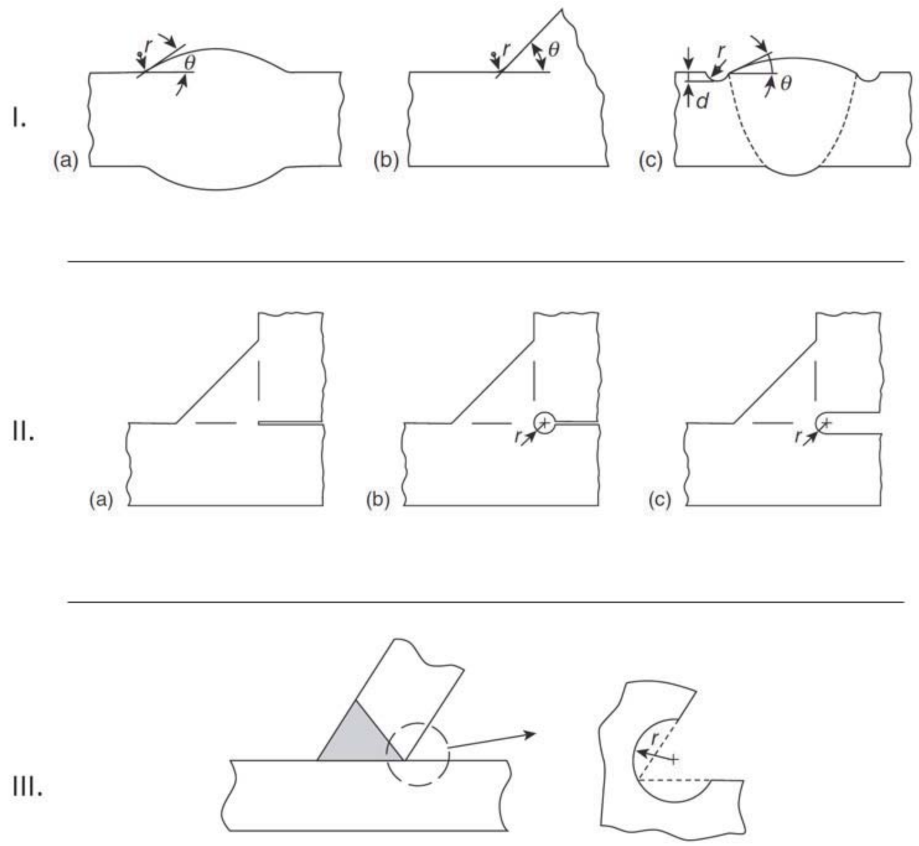

Figure 12: Modelling of the idealized weld profile. **I.** Rounding of weld toes of (a) a butt-weld, (b) a fillet weld and (c) a butt weld with undercuts. **II.** Rounding of the weld root of a non-penetrating fillet weld (a) by a keyhole (b) and U-shaped notch(c). **III.** Notch rounding of the weld root of a Y-joint [3].

appropriate elements and subdivision" [3]. The refinement must be such as to describe steep stress gradients that appear in vicinity of the notch. Both tangentially and normally to the notched surface the elements size and shape must be fine enough to yield accurate results.

In case of weld toes with flank angle $\theta = 45°$ this level of accuracy is achieved by placement of at least three elements with quadratic displacement function along the curve of the radius. Considering reference radius $r_{ref} = 1mm$ this corresponds to the maximum element size of $0.25mm$. Elements with linear displacement function can also be used, however their number has to be substantially increased (at least 5 elements per $\theta = 45°$ radius). It is also advised to use same size of elements at faces directly adjacent to the root and the toe radii before gradually increasing them in order to capture stress peaks close to this transition. The accurate depth-wise stress gradients can be achieved by using inflation of elements, in other words to have several layers of gradually increasing elements normal to the notch surface. When 3D analysis is performed, the lengthwise dimension of the elements needs to correspond to the stress gradients expected, if low then relatively long elements are suitable. The size recommendations are summarized in Table 2.

Notch stresses are evaluated on the circular surface where the stress state corresponds to the plane stress condition. Usually the stress is evaluated in the nodes of the elements. It should be always checked that the stress changes smoothly when approaching the notch surface. If not, the mesh may be too coarse. This is mostly applicable if linear elements with constant stress distribution are used. For this type of elements it is also necessary to ensure that the stress has been extrapolated well to the free notch surface.

Element type (displacement function)	Relative size	Size for $r = 1mm$	Size for $r = 0.05mm$	No. of elem. over $45°$arc	No. of elem. over $360°$arc	Estimated error
Quadratic	$\leq r/4$	$\leq 0.25mm$	$\leq 0.012mm$	≥ 3	≥ 24	$\approx 2\%$
Linear	$\leq r/6$	$\leq 0.15mm$	$\leq 0.008mm$	≥ 5	≥ 40	$\approx 10\%$

Table 2: Recommendation for element sizes (length-wise and depth-wise with respect to notch surface) [3].

4.3 Utilization of sub-models

Due to the requirement for mesh refinement in the area of the notch, sub-modelling is extremely useful technique used in the effective notch stress analysis. The sub-modelling can be described by two steps:

1. Computation of stresses and displacements in the relatively coarse global model suitable for structural stress evaluation.
2. Computation of the notch stresses in a local fine-meshed sub-model that is loaded by prescribed displacements or stresses taken from the global model.

The sub-model must be extracted from the global model in such a way that "the boundary effects on the notch stresses are negligible" [3]. Usually the nodal displacements at the boundary are extracted form the global model and extrapolated suitably to boundary nodes of the sub-model. Due care needs to be taken to incorporate all local acting loads to the sub-model, such as pressure. Another possibility is to extract and apply sectional forces and moment, or stresses acting at the boundaries.

The most important condition for appropriate sub-modelling is that the section of global model and corresponding local model to have the same stiffness. If this condition is not met, notch stresses will not be evaluated correctly. In case the global model stiffness is larger than that of sub-model, the notch stresses in the sub-model will be too small because the displacements applied at the boundary were underestimated. If forces and moments are prescribed at the boundary, the stresses will be evidently overestimated. "The relevant part of the overall model should be created in such a way that local deformations can fully develop; in particular, local bending, which might be partly prevented by the element behaviour. In the case of non-penetrating welds, the non-fused region should be included in the overall model and the weld should be able to deform in the same way that it does in the sub-model" [3]. To check if the analysis of the sub-model is done correctly is advised to compare stress distribution at the boundaries of the sub-model where the displacements are applied and stress distribution on the corresponding cross-section of the global model. No need to say they should be the same. If forces and moments were applied at the boundaries, it is displacements that need to be the same.

4.4 Link to structural stress analysis

The notch stress concentration is limited to the close vicinity of the notch. It is therefore possible to consider the undisturbed stresses in the hot spot superimposed by a weld notch factor K_w as a first approximation. The detailed effective notch stress analysis can be then performed on the sub-model only, with the boundary conditions (stresses or displacement field) taken from the structural stress model.

4.5 2D modelling

As was mentioned before, sometimes 2D model is sufficient. If one wants to use 2D model, the following two conditions need to be met. First, the loading of the weld needs to act predominantly in the plane perpendicular to the weld. Only in that case normal and shear stresses acting lengthwise, with respect to the weld profile, can be neglected. Second, the weld geometry must not change in the area where the 2D model should be valid. Only in that case the 2D model is truly representative.

4.6 Cross-section weakening

Due to the substitution of the real notch in the weld by a fictitiously enlarged notch a so-called cross-section weakening phenomenon can be met. By introduction of this larger notch a stress concentration can occur. Ideally the stress raising effect due to the cross-section weakening should be subtracted from the notch stress to "separate the support effect represented by fictitious notch rounding" [5]. Radaj proposes [5] to take this into account by reducing the fatigue effective notch stress on the basis of tensile and bending stress increase in the equally weakened unnotched plate.

4.7 Misalignment and weld imperfections

The misalignment of the base plates can have large impact on the notch stresses and therefore needs to be considered. There are two possible ways of approaching this phenomena:

- Inclusion of the misalignment of the welded detail into the model based on the measurement of particular detail, manufacturing tolerances or worst case assumptions.
- Modelling of the welded detail perfectly aligned and magnification of the notch stresses by magnification factors (for example given in [1]).

4.8 Design S-N curves for effective notch stress approach

The concept of FAT curves was described in the beginning of this thesis and is going to be broadened further in this section. The FAT classes for effective notch stress approach are based on the maximum principal stress in the notch. Although not advisable, it is possible to use equivalent Von Mises stress for evaluation, however smaller FAT class needs to be applied. This is because equivalent Von Mises stress is usually smaller in the sharp notches than maximum principal stress. When Von Mises stress is used, reduction by at least one FAT class is recommended. Table 3 gives the recommended FAT classes for various materials when carrying out effective notch stress analysis.

Material	Characteristic fatigue strength $(P_s = 97.7\%, N = 2x10^6)$ $r_{ref} = 1mm$	Characteristic fatigue strength $(P_s = 97.7\%, N = 2x10^6)$ $r_{ref} = 0.05mm$
Steel	FAT225	FAT630
Aluminium alloys	FAT 71	FAT 180
Magnesium	FAT 28	FAT 71

Table 3: Characteristic fatigue strength of welds for different materials based on effective notch stress with $r_{ref} = 1mm$ and $r_{ref} = 0.05mm$, assuming assessment by maximum principal stress) [3].

4.8.1 Correction for mild weld notches with reference radius of 1 mm

If the notch is relatively mild, despite the added fictitious radius, FAT curve needs to be modified. This, for example, applies to the transverse butt welds with almost no overfill, welds with very small flank angle, welds that have been grounded or welds on thin plates. In these cases, the stress concentration factor in the notch is close to one. This means, that the life assessed on the basis of FAT225 curve is overestimated and the FAT class should be reduced.

To deal with this phenomena a special variable called *notch factor* K_w is introduced and defined as effective notch stress σ_k divided by structural stress σ_s:

$$K_w = \frac{\sigma_k}{\sigma_s} \tag{6}$$

The structural stress can be either determined by the hot-spot stress approach, or stress at the distance of 2 mm from the transition between straight and curved part can be taken [3]. The resulting SN curve for mild notches is then a combination of the FAT225 curve and FAT 160 curve multiplied by the notch factor and is displayed in Figure 13.

Class FAT 160 corresponds to the endurance of the parent material and by inspection of the afore mentioned figure it is evident that the parent material governs design in the low to medium cycle fatigue, especially for small K_w. The notch factor $K_w = 1.6$ is recommended as lowest bound, even though in some cases the K_w calculated strictly following the formula may be smaller.

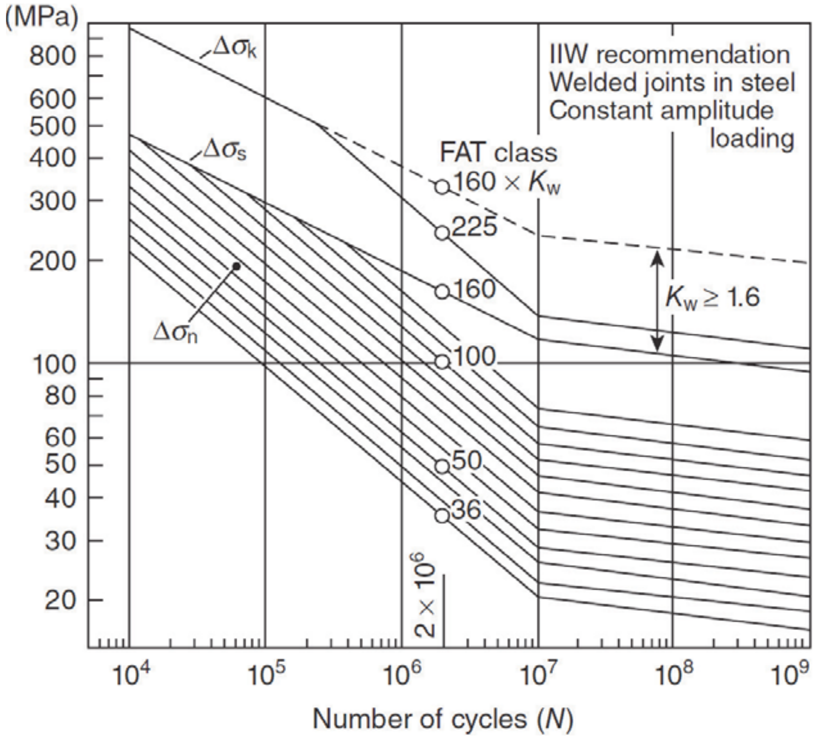

Figure 13: S-N curve for mild notches for endurance determined on the basis of effective stress approach with $r_{ref} = 1mm$ [3].

5 Calibration of the effective notch stress approach on small scale model

In order to test sensitivity of the effective notch stress approach on meshing and modelling methods a small scale model was prepared, analysed and evaluated. The backbone of the analysis was a fatigue test of simple welded specimen that was performed by Doosan Bobcat Engineering s.r.o. A simplified specimen geometry is depicted in Figure 14. The exact dimensions of the specimen are not disclosed as they present potentially sensitive data. The specimen can be classified as longitudinal fillet welded gusset with smooth transition and fillet weld around end. The thickness of the plate and the size of the non-penetrating fillet weld is equal to 6 mm. Material of the parts is structural steel S235 J2C. Similar type of detail can be found on booms of excavators and heavy duty machinery, where the actuators are attached by pins through the holes in the vertical plates.

In the experiment 10 specimens were divided into three sets that were then loaded on varying levels in order to achieve parameters necessary for construction of S-N curve and determination of FAT class corresponding to this specific detail. Further, the specimens were strain-gauged in order to evaluate hot spot stress in the weld notch directly. The results of the experiment are extremely useful for calibration and evaluation of the effective notch stress analysis.

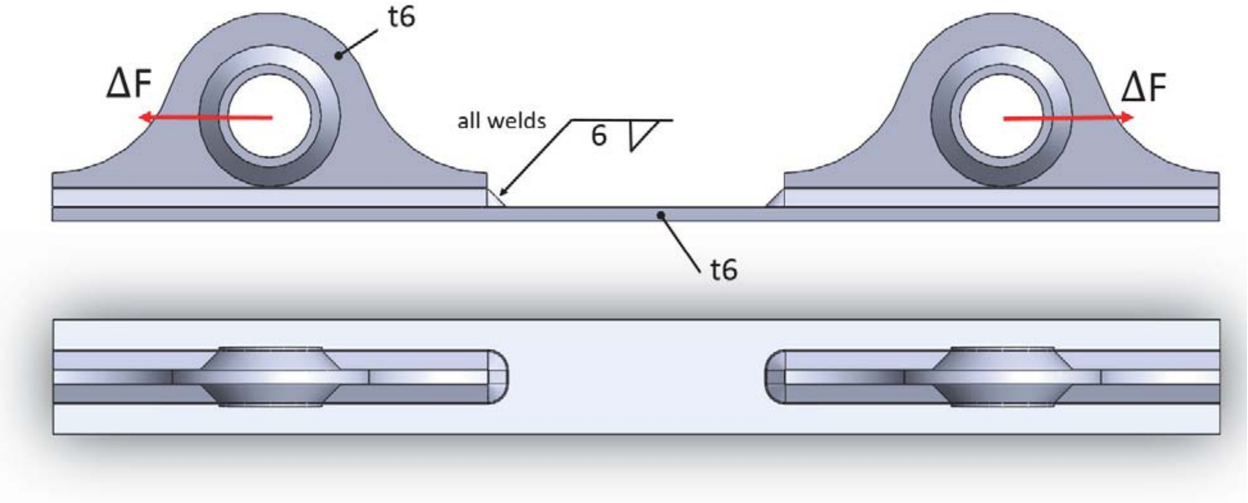

Figure 14: Simplified geometry of the test specimen.

5.1 Experiment description

Specimens were loaded axially as indicated in Figure 14. Figure 15 shows five of the specimens in as-tested condition. Table 4 gives details of loading and number of specimens in each set. The specimens were loaded on three different load levels. Endurance of respective specimens is recorded in Table 5. Test was interrupted when visible crack appeared on the surface (see Figure 17).

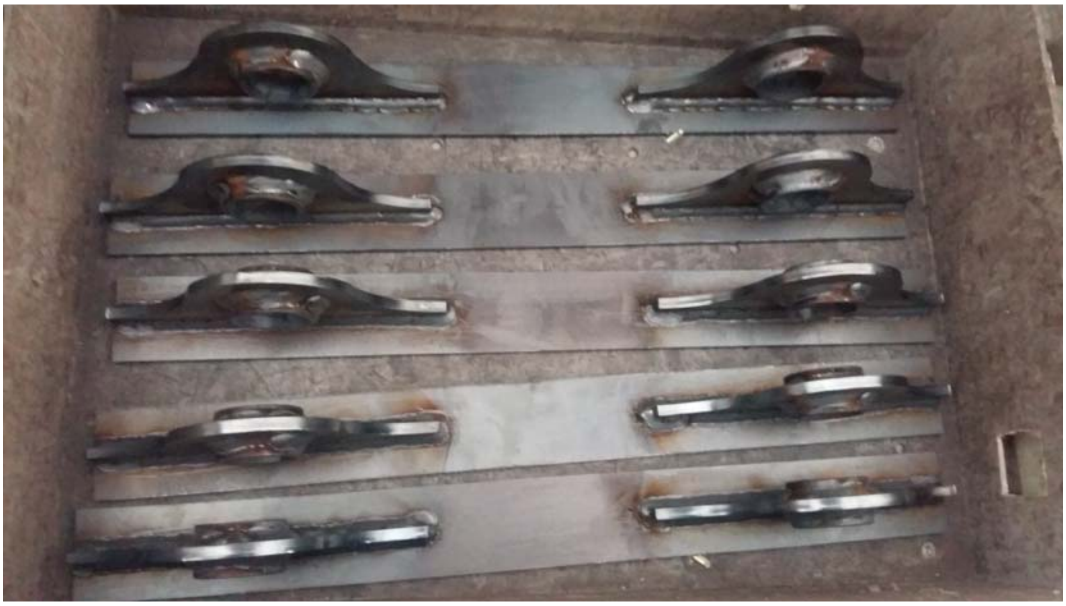

Figure 15: Photograph of five specimens in as-tested condition.

Amplitude $F_A[N]$	Mean load $F_M[N]$	Cycle asym. R	Minimum load $F_{min}[N]$	Maximum load $F_{max}[N]$	No. of spec. $n[-]$
1 200	1 300	0.040	100	2 500	4
1 050	1 150	0.045	100	2 200	5
850	950	0.056	100	1 800	1

Table 4: Loading of specimens in the experiment.

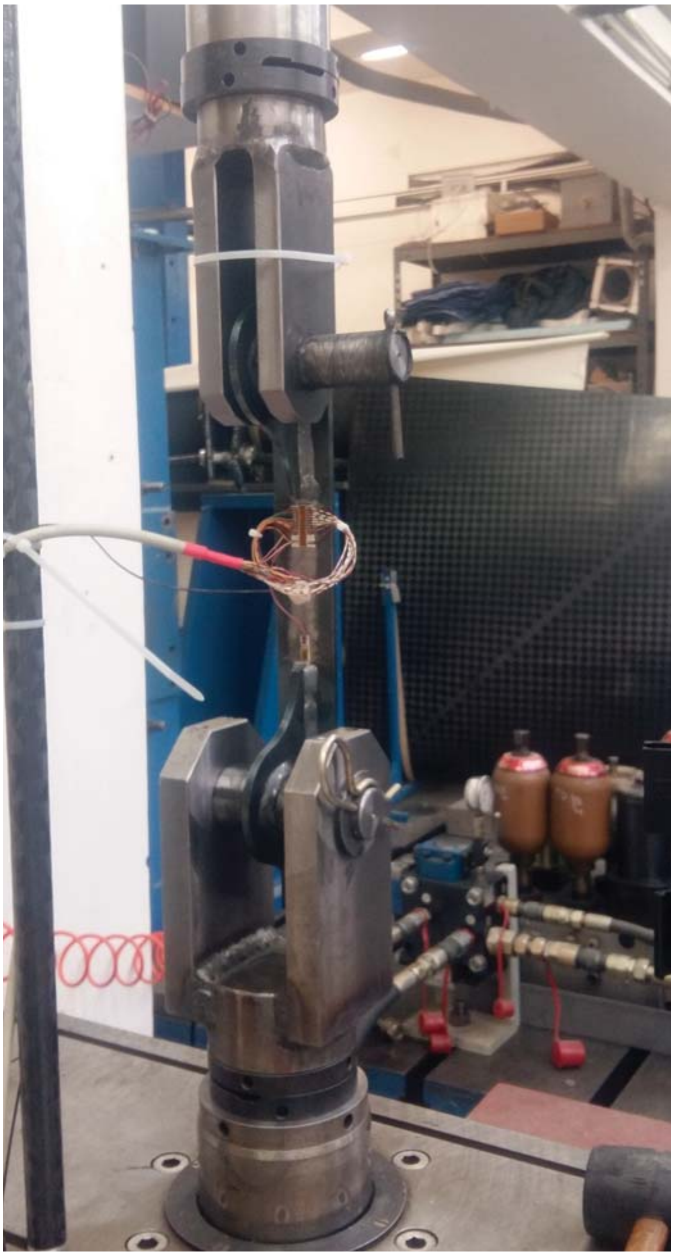

Figure 16: Photograph of specimen during testing.

Specimen no. $n[-]$	Maximum Load $F_{max}[N]$	Endurnace $N[-]$
1	1 800	no crack
2	2 200	300 000
3	2 200	150 000
4	2 200	130 000
5	2 200	163 000
6	2 200	105 000
7	2 500	77 000
8	2 500	75 000
9	2 500	42 000
10	2 500	62 000

Table 5: Endurance of test specimens.

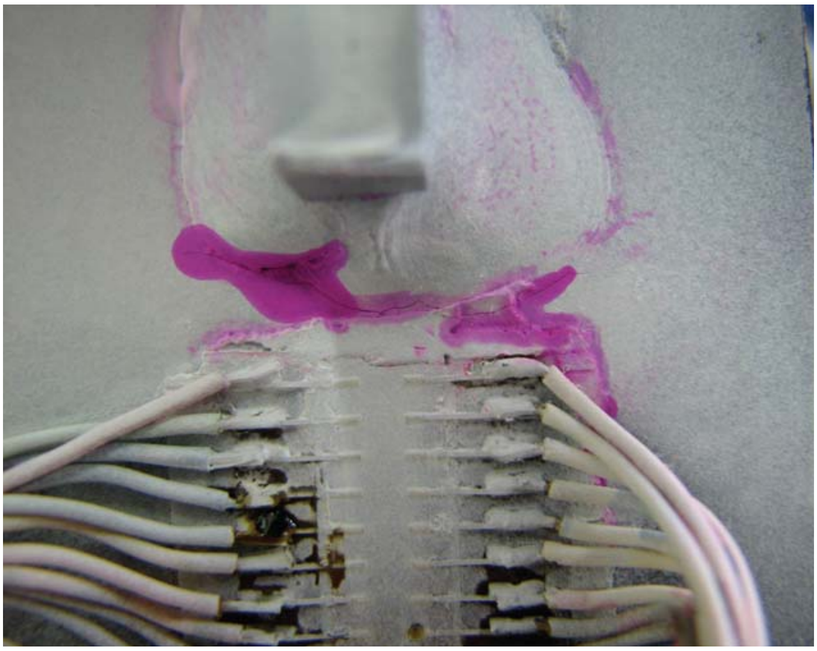

Figure 17: Specimen no.2 after the test with visible crack, $N = 300000$.

5.2 Geometry and boundary conditions

Due to overall symmetry of the model as well as the loading, only one-quarter of the model was necessary to be evaluated with loads adjusted appropriately.

As was described in the section about modelling, according to effective notch stress approach, weld profile geometry needs to be incorporated into the model. It is obvious from the nature of the specimen loading that the largest stress can be expected in the weld toe region at the edge of the vertical plate. It is therefore of the utmost importance to model this section correctly.

It comes as no surprise that this section is hardest to model appropriately because the longitudinal direction of the weld changes into the transverse at the edge forming a sharp turn of 90°. Three possible ways to model this transition were investigated in the analysis for the sake of understanding their impact on the results. The respective variants are displayed in Figure 18. Variant A shows straight transverse weld bead with radius transition. Variant B also incorporates straight transverse section, but with straight transition from longitudinal direction. Variant C represents more complex geometry as the weld toe is modelled as 180° arc. This nevertheless produces weld profile that does not have same size lengthwise. The indicated naming convention (A, B, C) is going to be followed further down in the text.

It needs to be stressed out that the geometry of the weld bead in the model can differ from the actual parts (see Figure 19). This is the impact of the welding process itself, where variety of parameters can influence the outcome. This uncertainty is nevertheless already included in the FAT class of the welded details as it is based on a large number of statistically evaluated tests.

The weld root and toe radii were modelled in accordance with Section 4. Figure 20 shows placement of the reference radii $r_{ref} = 1mm$. Placement of the reference radii in the transverse section of the welds is apparent from Figures 18 and 21.

As for the weld joining circular tube with the gusset (see Figure 22), no reference radii were placed, because this area is not life limiting and the notches, if placed, would not have impact on the stresses in the actual life limiting location (edge of the plate).

In all other aspects the model respects geometry of the test specimens.

Figure 23 displays model reduced to one quarter. On faces painted in yellow, the symmetry boundary conditions were applied. Load in the longitudinal direction was

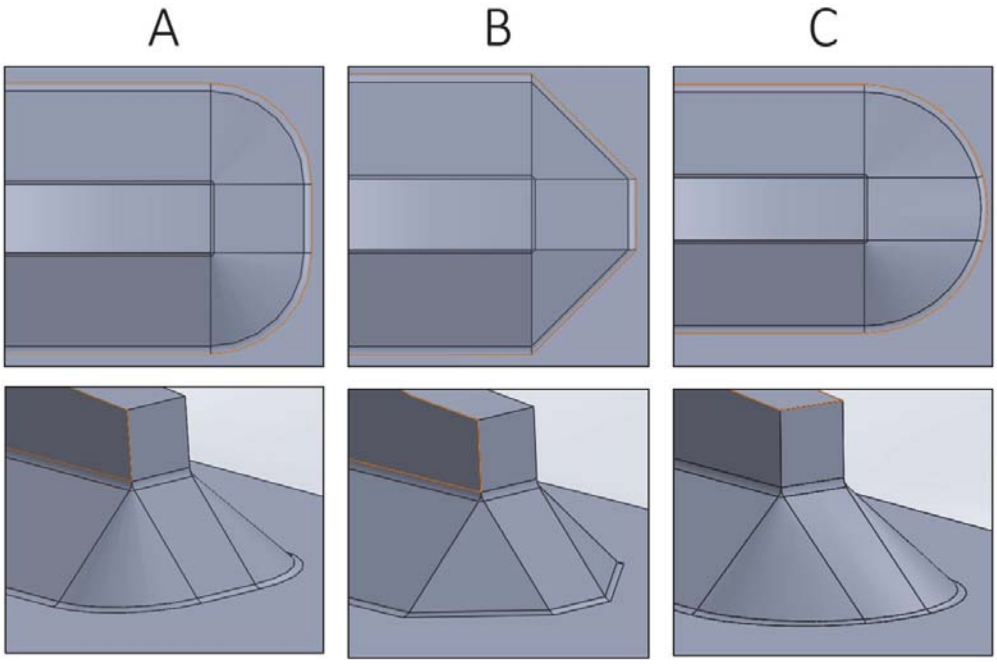

Figure 18: Three possible variants of the weld bead transition.

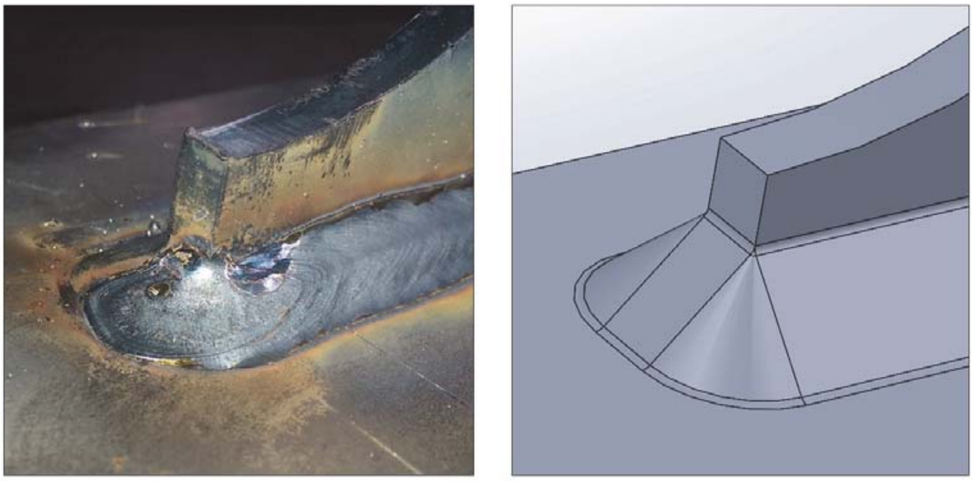

Figure 19: Weld edge on one of the specimens as compared to the model (geometry A).

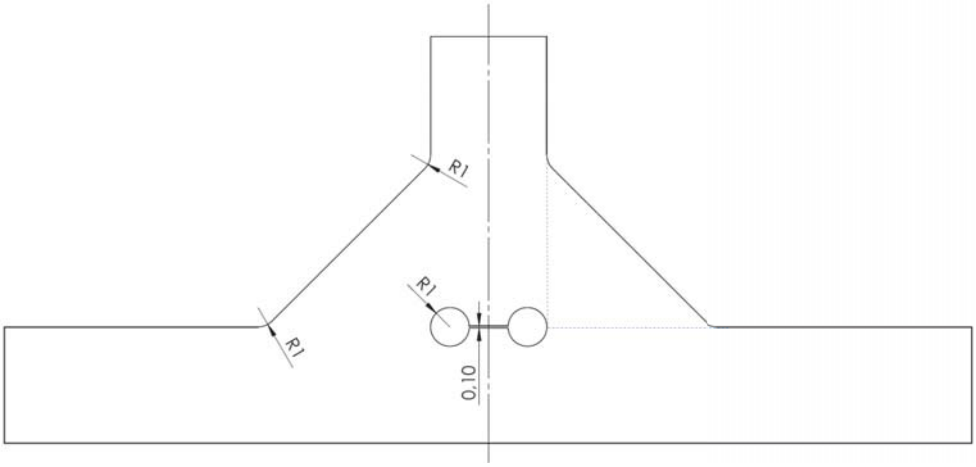

Figure 20: Reference radii in the weld toe and root of the longitudinal section of the weld.

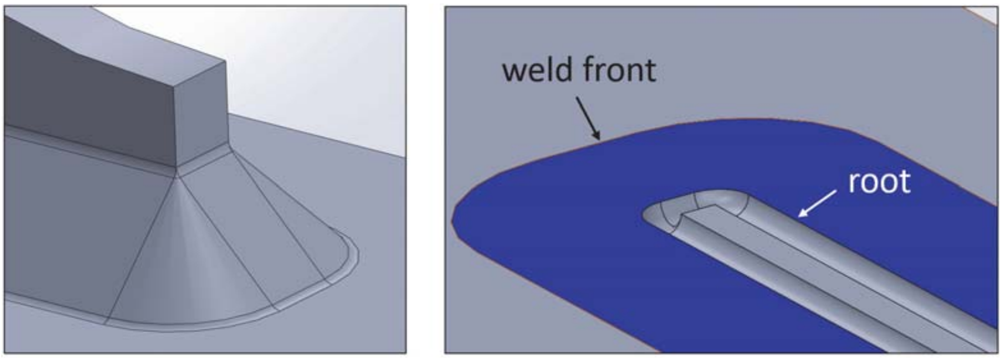

Figure 21: Reference radii in the weld toe and root of the transverse section of the weld.

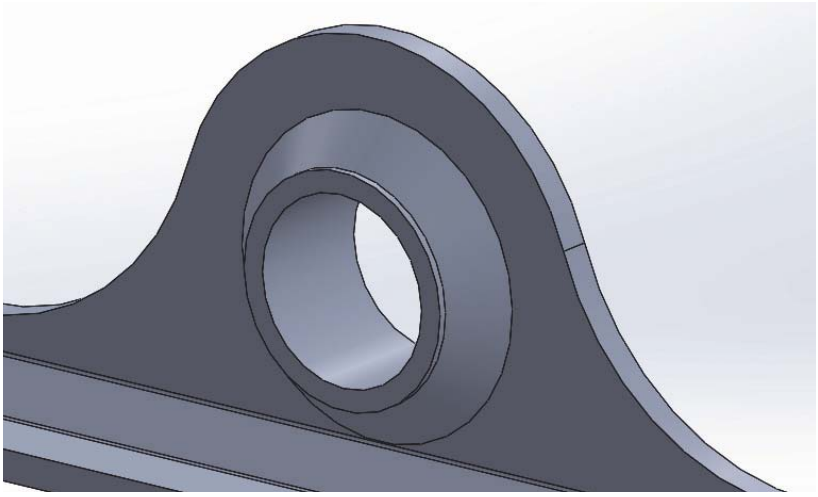

Figure 22: No reference radii were placed in the weld around circular tube.

applied in the center of the pivot as a remote force. Two load levels of $F = 2500N$ and $F = 2200N$ were investigated based on the experiment (see Table 5). The load applied to the model was decreased by half in order to respect the symmetry boundary conditions.

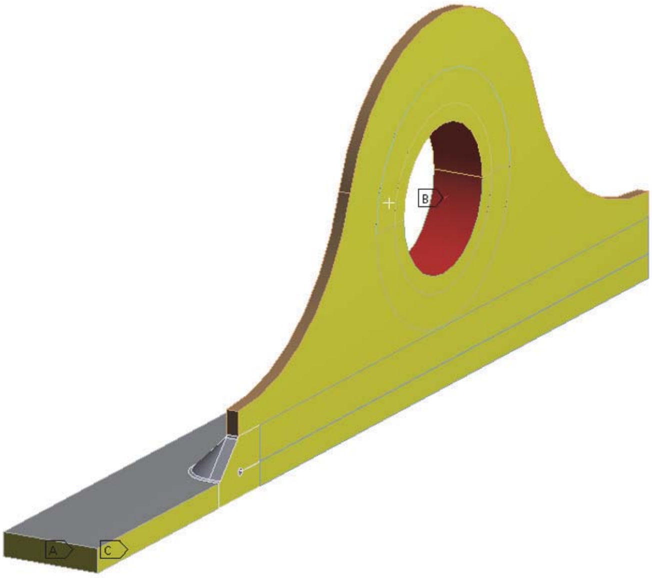

Figure 23: Boundary conditions of the quarter-model.

5.3 Finite element model

Linear elastic finite element models were prepared up in $ANSYS$ 16.0 for all three varints of weld edge geometry. Sub-modelling method was used to get the most precise stress results in the weld toe region. Figure 24 shows partitioning of the model into a global model discussed in the previous section as well as sub-model. Mesh of global model representing weld edge geometry A can be seen in Figure 25. The model was predominantly meshed by sweeping quadratic brick elements. In the section of the transverse part of the weld, where solely brick meshing was impossible, hex-dominant quadratic mesh was used. Element size was set as $1mm$ for the whole model except for the weld root and toe radii where the size was set to $0.5mm$. Global models for other geometries can be found in Appendices B and C.

From these global models, sub-models were created (Figure 26). Meshing of the regions in vicinity of the weld toe with brick elements comprises considerable effort. In order to see the sensitivity of endurance on type of elements (meshing method) used, three

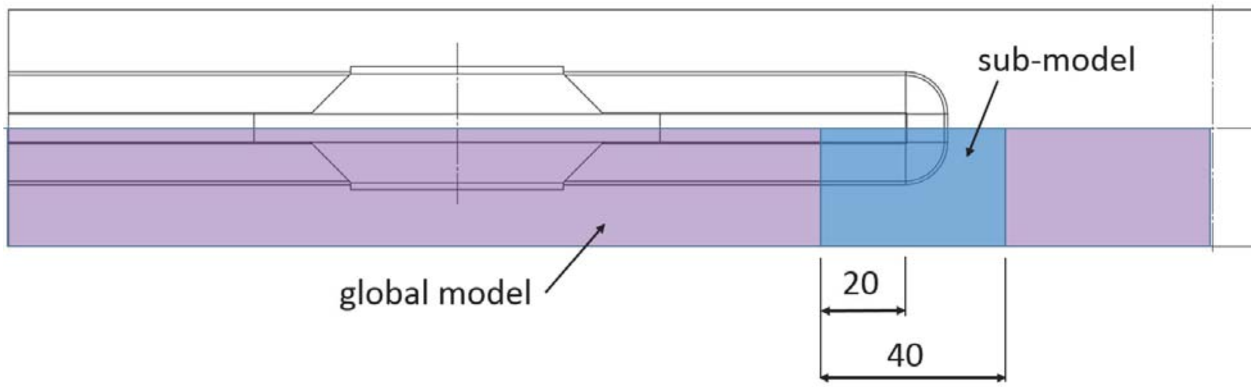
sub-model
global model
20
40

Figure 24: Global and sub section of the model used in analysis.

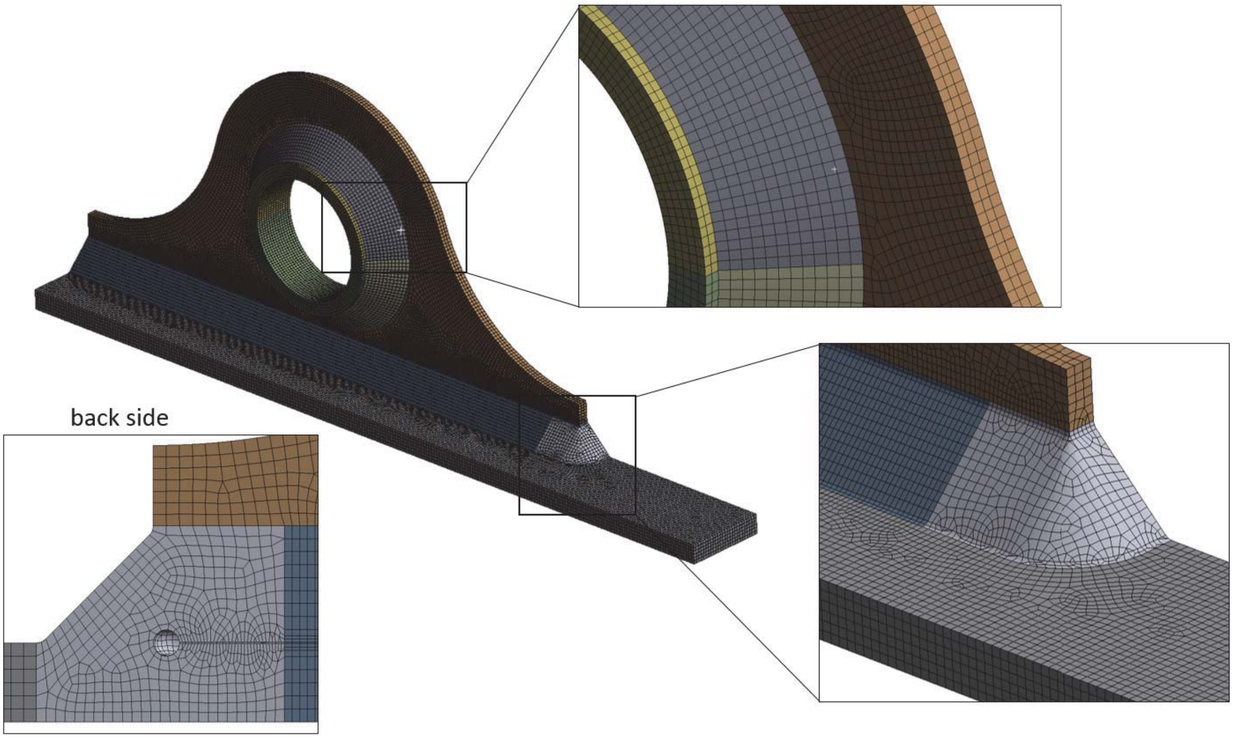

Figure 25: Global mesh for the weld edge geometry A.

different methods readily available in Ansys were employed. These three methods of meshing are further in the text referred to as:

tetra Tetrahedral patch conforming mesh. Inflation is used in weld notch areas in order to increase depth-wise precision.

hex dominant Free hex dominant mesh where majority of the elements is converted to hex elements with the rest being tetra and pyramid. This method is recommended by Ansys for bodies that cannot be swept.

hexa Manual partitioning of the model to sweepable zones that are meshed with hex (brick) elements only. Unsweepeble zones of the model are meshed with hex dominant mesh.

An example of the three meshing methods in weld toe of geometry A are displayed in Figures 27 and 28. Mesh differences for geometries B and C can be observed in Figures 69, 70, 71, 75, 76 and 77 included in Appendix.

The overall element minimum size for all sub-models is $0.5mm$ whereas in the weld toe region the size is set to $0.15mm$. This is in compliance with the recommendation ($\leq 0.25mm$). The displacement field from the global model was applied at the boundaries

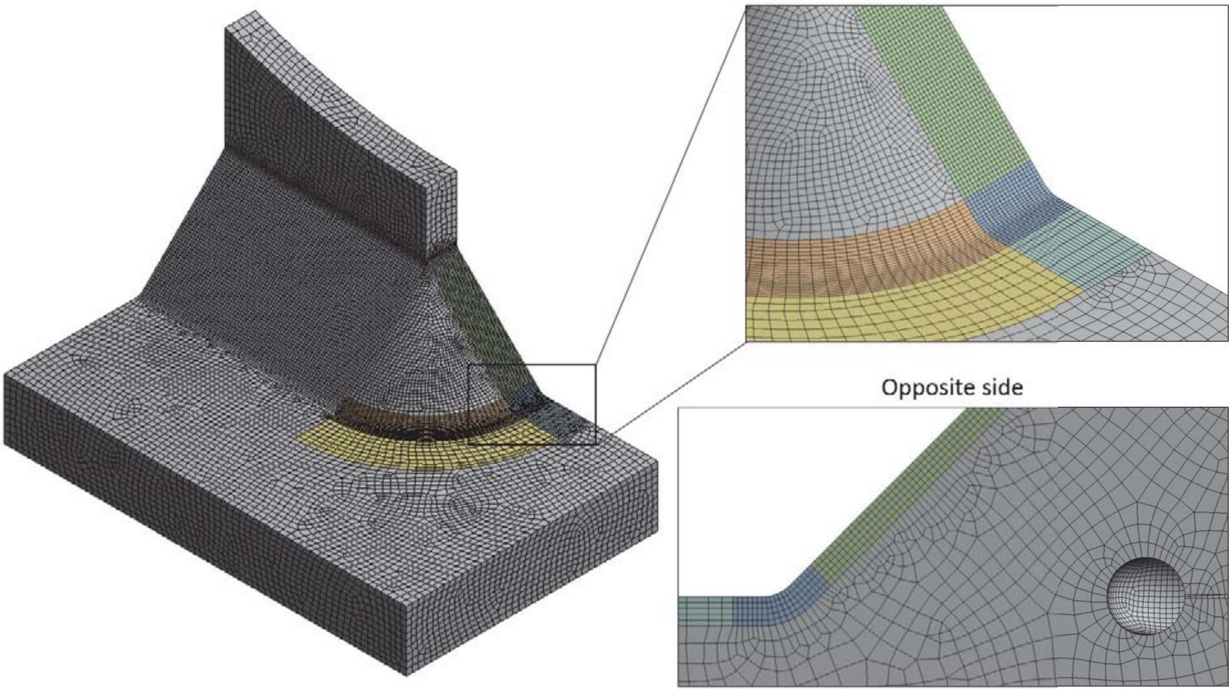

Figure 26: sub-model mesh for the weld edge geometry A.

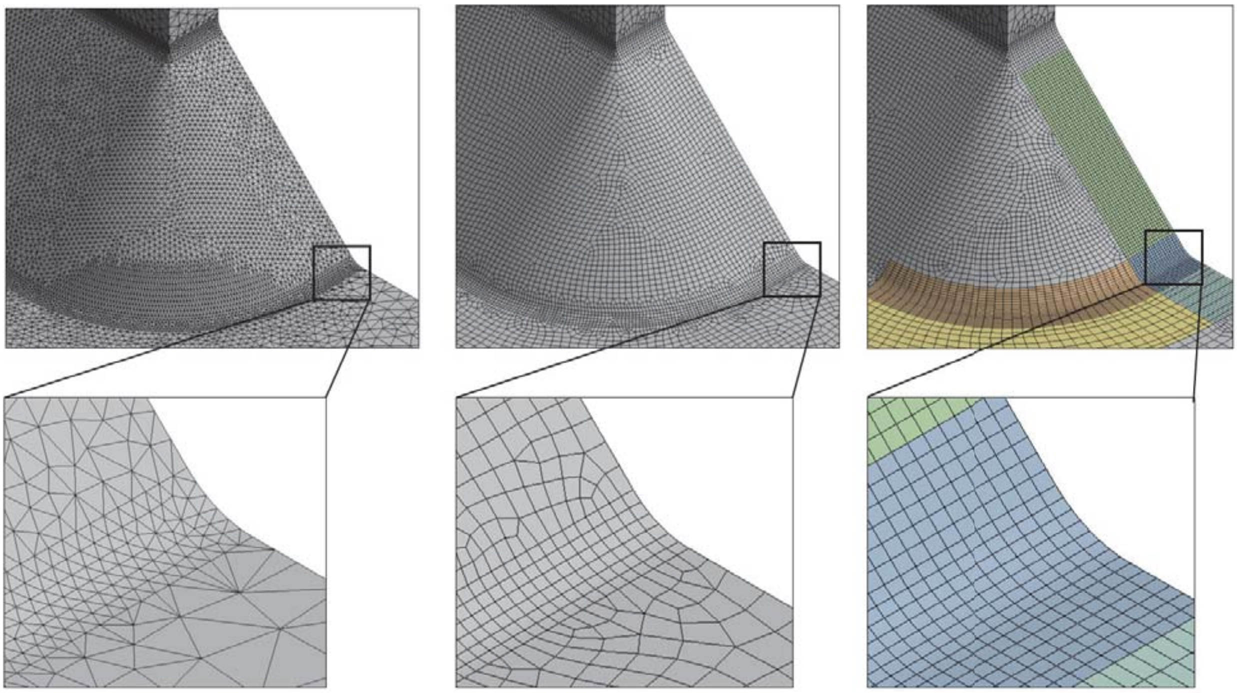

Figure 27: Comparison of mesh for geometry A. Transverse part of the weld. Meshing method from the left: tetra, hex dominant, hexa.

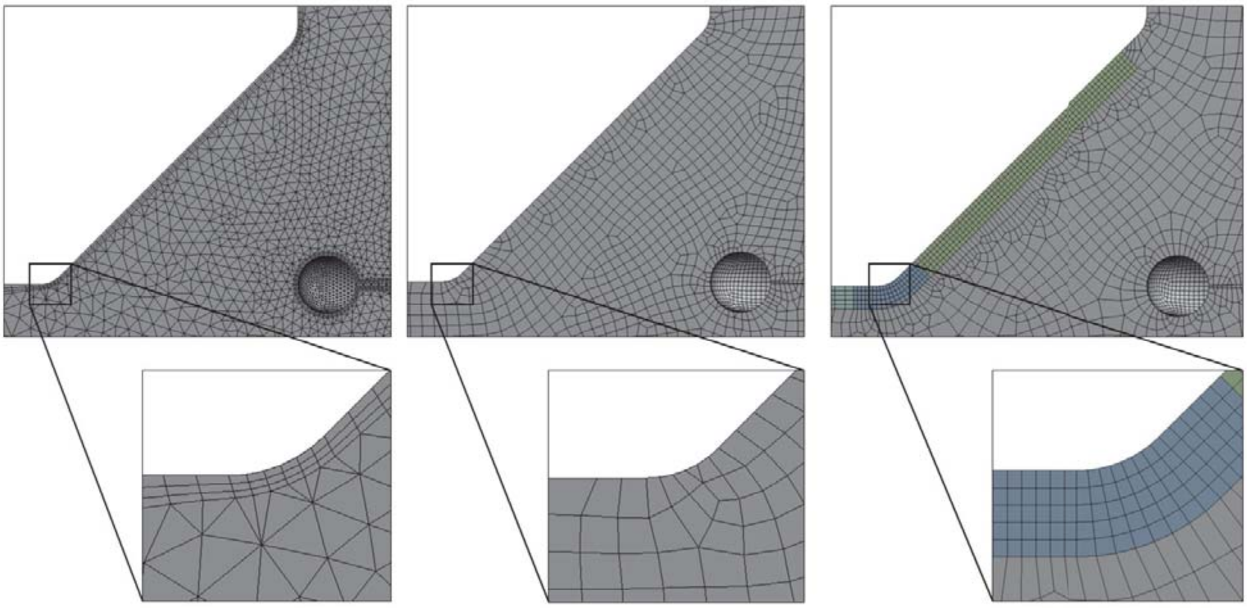

Figure 28: Comparison of mesh for geometry A. Backside of detail. Meshing method from the left: tetra, hex dominant, hexa.

of the sub-model. Sufficient number of high quality elements (good size and aspect ratio) is used both length wise an depth wise with respect to the weld toe radius in order to describe the stress gradient in the critical location well enough.
Table 6 lists the number of elements and nodes of the respective models. This can serve as an indication of computational cost and size of the models. In general hex dominant meshing method produced largest models with same conditions imposed on element size.

Geometry	Global model		Sub-model		
	nodes	elements	mesh	nodes	elements
A	636 758	144 513	tetra	537 424	259 929
			hex. dom.	1 139 889	317 245
			hexa	877 210	247 355
B	809 943	185 321	tetra	519 339	251 144
			hex. dom.	1 108 029	305 906
			hexa	1 145 388	317 341
C	583 904	132 864	tetra	539 963	261 379
			hex. dom.	1 060 813	316 090
			hexa	1 137 550	296 967

Table 6: Number of elements and nodes for corresponding models.

5.4 Results

Figure 29 shows lateral view of the deformed global model for geometry A (2.9 deformation scale) with maximum principal stress map. It can be seen that the baseplate is predominantly loaded in bending with the most loaded spot being the weld toe at the vertical plate edge. The mesh (see Figures 25, 68 and 74) is too coarse to give representative effective notch stress, therefore sub-model results are needed.
Results from the sub-model of geometry A meshed by hexahedral elements can be seen in Figure 30, 31 and 32. From the principal stresses vector plot it is apparent, that the stress state on the notch surface is bi-axial, as we would expect, and therefore in fatigue assessment maximum principal stress value shall be used (in accordance with section 3.3.2). The maximum principal stress is equal to $\sigma_{k,max} = 1140.3MPa$. Figure 32 displays

principal stress as a function of a a lengthwise coordinate (x-axis) from the stress peak. It is evident that in the critical location the sign of all principal stresses is positive. This further confirms the maximum principal stress being the best candidate for fatigue resistance evaluation. It is also evident that the stresses are largely non linear.

Table 8 gives condensed results for stresses and endurance of respective models as well as comparison with the experimental values (averaged). For geometry B duplicitous values are present. This stems from the fact that due to modelling of the weld profile itself a new stress concentration was created, where the stress reaches its global peak. This is not coincident with the stress peaks in the other models (see Figure 34). Therefore a second value placed in parentheses is included that can be easier compared to the rest of the geometries and corresponds to the maximum at the plane of symmetry. Endurance was determined based on the fatigue curve corresponding to FAT class 225. Official recommendation is to use the default curve that represents survival probability of 97.7%. To compare the results with the experiment, where only a statistically insufficient number of specimens was tested for each of the two load levels (see Table 7), the curve was offset to represent survival probability of 50.0%. The offset of the SN curve was based on standard deviation of $logN = 0.250$ and is in compliance with recommendation proposed by IIW [1]. The representation of both curves can be seen in Figure 33, where results from analysis of geometry A with hexa mesh are displayed for both load levels.

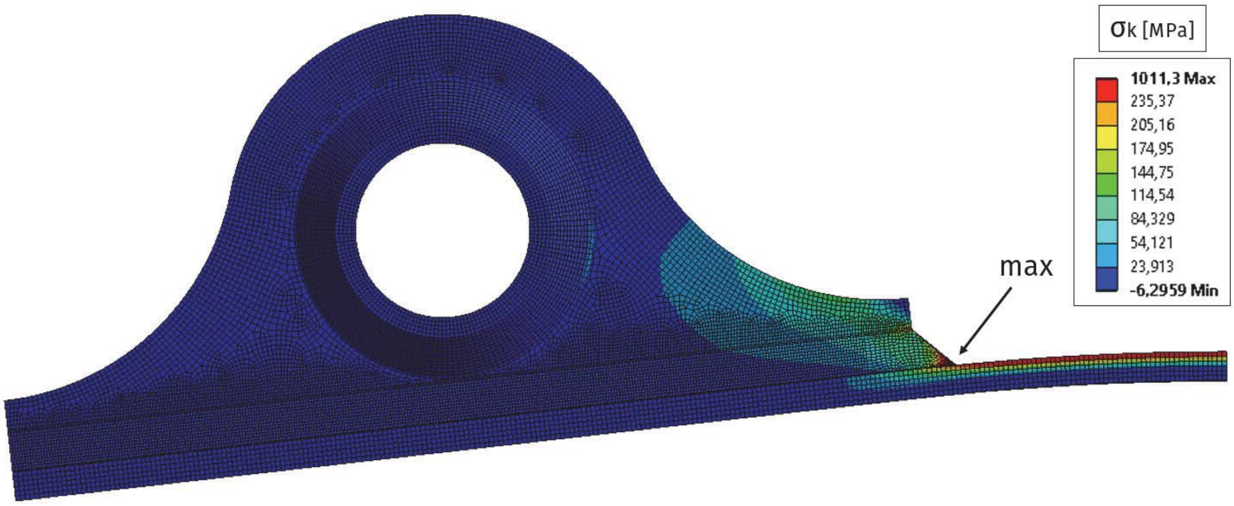

Figure 29: Maximum principal stress in the global model for weld edge geometry A. Load $F = 2\,500N$.

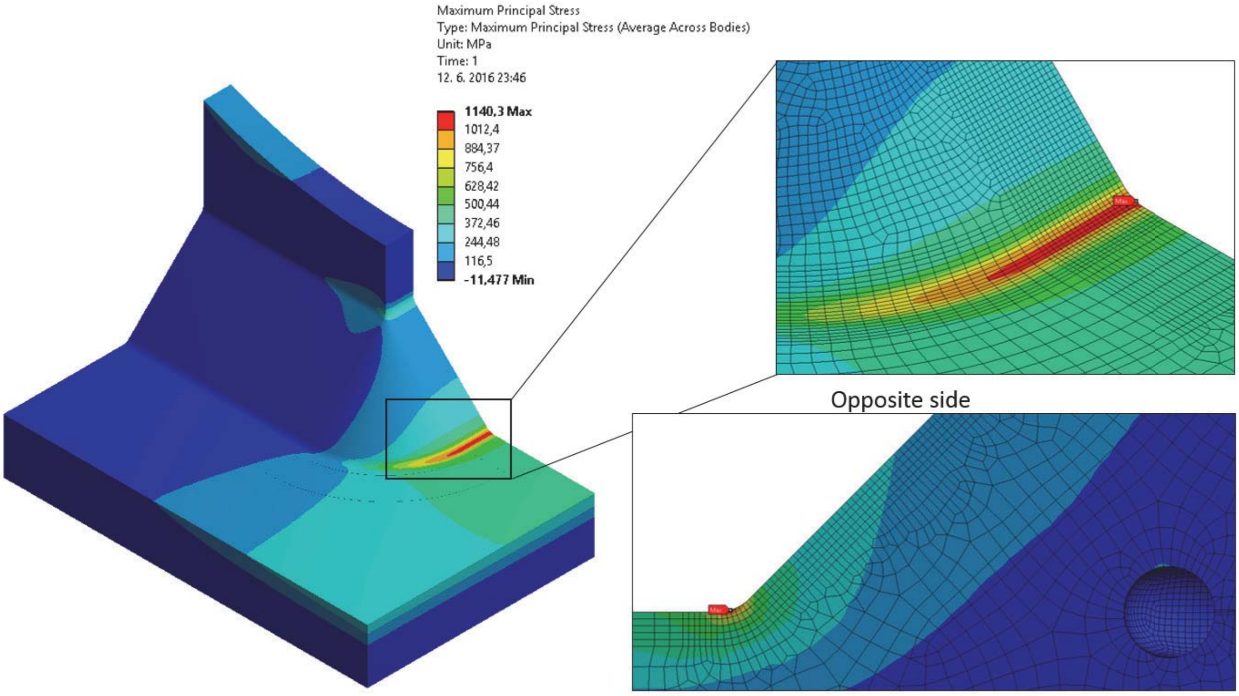
Maximum Principal Stress
Type: Maximum Principal Stress (Average Across Bodies)
Unit: MPa
Time: 1
12. 6. 2016 23:46
1140,3 Max
1012,4
884,37
756,4
628,42
500,44
372,46
244,48
116,5
-11,477 Min
Opposite side
Max
Max

Figure 30: Maximum principal stress in the sub-model for weld edge geometry A; meshing method - hexa. Load $F = 2\,500 N$.

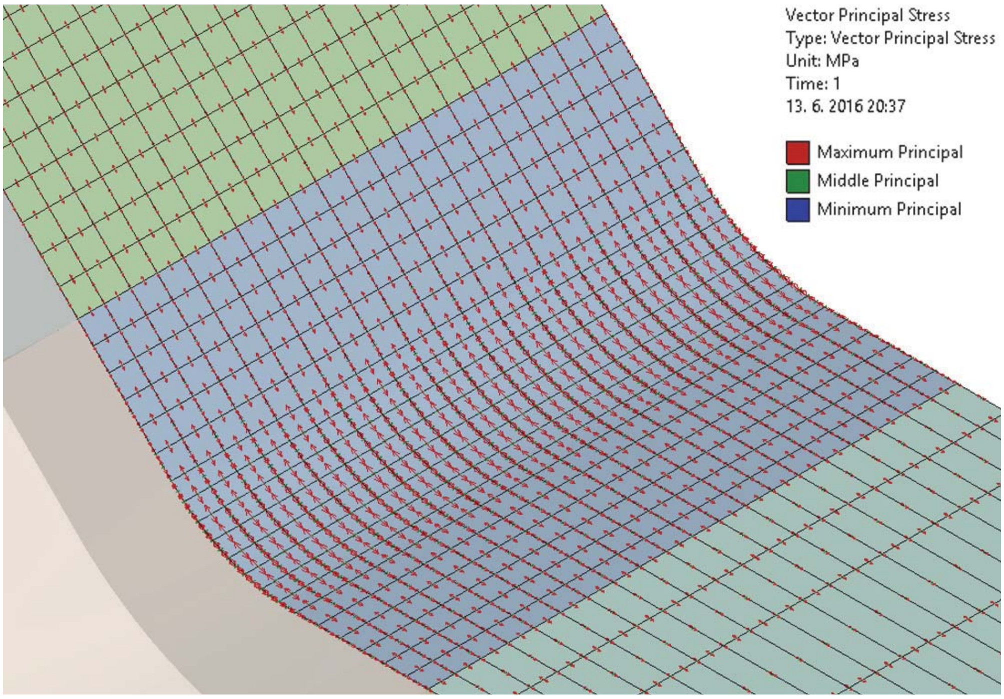
Vector Principal Stress
Type: Vector Principal Stress
Unit: MPa
Time: 1
13. 6. 2016 20:37
Maximum Principal
Middle Principal
Minimum Principal

Figure 31: Vector plot of the principal stresses in the weld toe region for the sub-model for weld edge geometry A; meshing method - hexa. Load $F = 2\,500 N$.

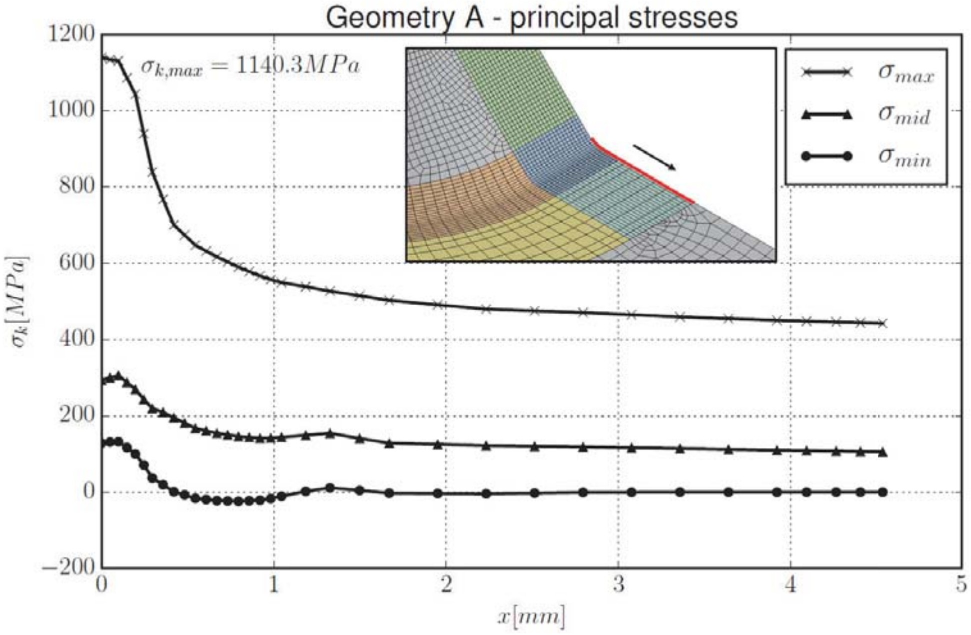

Figure 32: Maximum principal stress along path from the stress peak forward for the weld edge geometry A; meshing method - hexa. Load $F = 2\,500N$.

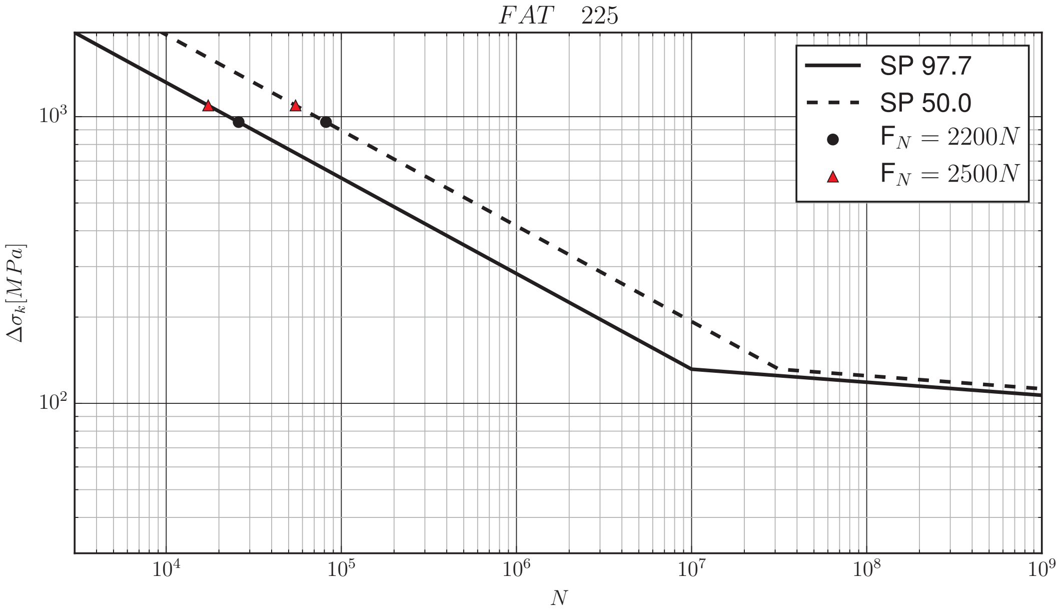

Figure 33: S-N curve FAT 225 for survival probabilities of 97.7% and 50.0% for geometry A with hex meshing. Points correspond to endurance at the two analysed load levels ($F = 2200N$ and $F = 2500N$).

Specimen no. $n[-]$	Maximum Load $F_{max}[N]$	Endurance $N[-]$	Average $N[-]$
1	1 800	no crack	not evaluated
2	2 200	300 000*	137 000
3	2 200	150 000	
4	2 200	130 000	
5	2 200	163 000	
6	2 200	105 000	
7	2 500	77 000	64 000
8	2 500	75 000	
9	2 500	42 000	
10	2 500	62 000	

Table 7: Average endurance of test specimens. **This specimen was disregarded in the average value calculation because the loading plot from the test showed fluctuations and inconsistencies.*

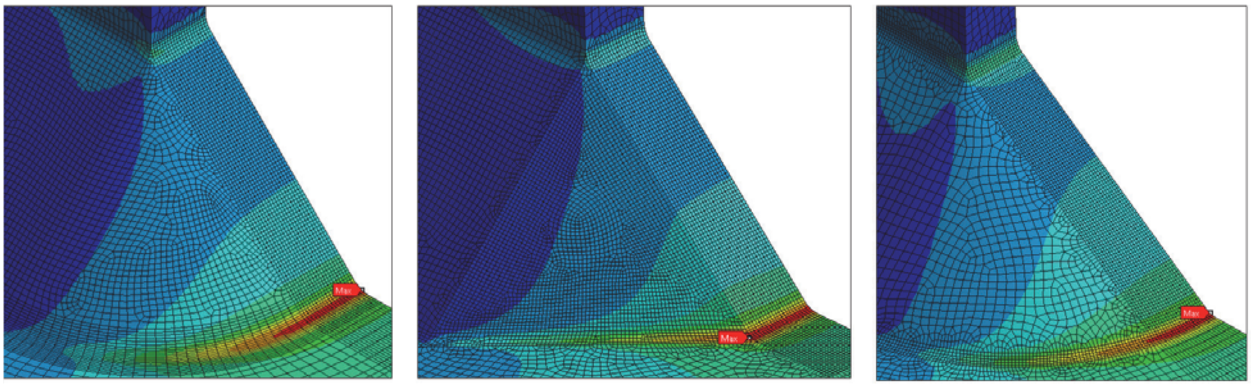

Figure 34: Difference in stress peak location for the three investigated geometries. Load $F = 2\,500N$, meshing method-hexa. From left: Geometry A, B, C.

Load	Experiment	Geometry	Global model	Sub-model					
$F[N]$	avg. endurance $N_{exp,a}[-]$	$[-]$	max.principal $\sigma_{Gk,max}[MPa]$	mesh $[-]$	max.principal $\sigma_{Sk,max}[MPa]$	max.p. range $\Delta\sigma_{Sk,max}[MPa]$	end. SP 97.7 $N_{97.7}[-]$	end. SP 50.0 $N_{50.0}[-]$	experiment dif. $\Delta_{50.0}[\%]$
2 200	137 000	*A*	889.9	tetra	1 025.1	978.5	24 316	76 690	−44.0
				hex. dom.	1 007.8	962.0	25 590	80 707	−41.1
				hexa	1 003.5	957.9	25 920	81 749	−40.3
		B	1 009.6 (954.9)	tetra	1 123.9	1 072.8	18 450	58 191	−57.5
					(1 066.9)	(1 018.4)	(21 568)	(68 024)	(−50.3)
				hex.dom.	1 104.3	1 054.1	19 450	61 344	−55.2
					(1 026.1)	(979.5)	(24 245)	(76 466)	(−44.2)
				hexa	1 003.5	1 063.5	18 942	59 740	−56.4
					(1 057.1)	(1 009.1)	(22 174)	(69 934)	(−49.0)
		C	933.2	tetra	981.9	937.2	27 672	87 274	−36.36
				hex. dom.	1 003.8	958.2	25 897	81 676	−40.4
				hexa	984.25	939.5	27 471	86 640	−36.8
2 500	64 000	*A*	1 011.3	tetra	1 164.9	1 118.3	16 289	51 374	−19.7
				hex. dom.	1 145.3	1 099.5	17 140	54 057	−15.5
				hexa	1 140.3	1 094.7	17 366	54 772	−14.4
		B	1 147.2 (1 085.2)	tetra	1 277.2	1 226.1	12 359	38 979	−39.1
					(1 212.2)	(1 163.7)	(14 456)	(45, 592)	(−28.8)
				hex.dom	1 254.9	1 204.7	13 030	41 095	−35.8
					(1 166.0)	(1 119.4)	(16 243)	(51 229)	(−20.0)
				hexa	1 266.1	1 215.5	12 687	40 014	−37.5
					(1 202.5)	(1 154.4)	(14 808)	(46 704)	(−27.0)
		C	1 060.5	tetra	1 115.6	1 071.0	18 545	58 491	−8.6
				hex. dom.	1 140.4	1 094.8	17 362	54 757	−14.4
				hexa	1 114.3	1 069.7	18, 610	58 696	−8.3

Table 8: Summary of results of the analysis. (For geometry B, the maximum stress was found on the sharp weld corner, values in brackets correspond to location comparable with other geometries)

5.5 Discussion of results

Following discussion stands mostly on the results presented in Table 8.

5.5.1 Geometry type

It was already stated in the section about modelling of the weld geometry that ideal design-intended profile of the weld is hardly achieved in reality (recall Figure 19). Nevertheless the actual geometry of the weld bead can have detrimental effect on the results. Three various geometries were investigated with difference only in modelling of transition between the longitudinal and transverse part of the weld. Figure 35 gives the results in terms of maximum principal stresses $\sigma_{K,max}$ in a more illustrative fashion. Results for geometry B were taken from the location where the stress peaks in other two geometries are present (not from the artificial stress peak at the weld's sharp edge, see Figure 34). The stress is directly connected to endurance, therefore the impact of geometry on life can be observed as well.

First of all it is apparent that modelling of the transition as linear, as in geometry B, is not optimal approach. The stress peak occurs at a location that was artificially created and is in fact a singularity. Perhaps if additional rounding of sharp edges was incorporated (based on microstructural support hypothesis) stresses would be lowered to more meaningful levels. Nevertheless by using sharp liner transition between the longitudinal and transverse weld sections the amount of material is reduced compared to the other two geometries and hence the stress at the middle of transverse section is generally increased. This is clearly visible in Figure 35. Geometry A produces more conservative stresses than geometry C. This could be also connected with the amount of material of the transverse weld bead section. Due to the fully circular transition the weld angle is milder than that of geometry A and the amount of material is slightly higher. Moreover as the notch is milder, stress concentration is smaller as well. Based on those results, geometry A seems preferable as it gives consistent not-overly conservative results and the geometry conforms with the design intent the most of the three.

Last result that is going to be presented in this section is comparison of maximum principal stress distribution perpendicular to the weld toe critical location in the x-axis direction that can be seen in Figure 36. Maximum principal stress is essential y the same

for the three geometries 5 mm from the critical location. This further proves that the zone of various weld geometry influence on stress is relatively small.
It needs to be stressed out again that none of these geometries are however met in the real specimens that were tested. This is inherent to analysis by effective notch stress approach. One may then wonder, why bother with such modelling, when the reality and model can differ so much. The answer lies in the processing of the results, where flaws and imperfections are not included in the model itself, but rather in the fatigue curve (or FAT class) and the process of how it was derived (large number of all different detail tests). This means that results based on those curves have tendency to be conservative, but its a price that needs to be paid due to all uncertainties that are associated with welding process itself. This further implies that if one follows welding quality processes strictly, thoroughly a above most consistently, he or she should be able to safely alter the SN curves to less conservative areas. This would allow for production of more lightweight design, but can be only achieved after confirmation by means of testing and analyses validation.

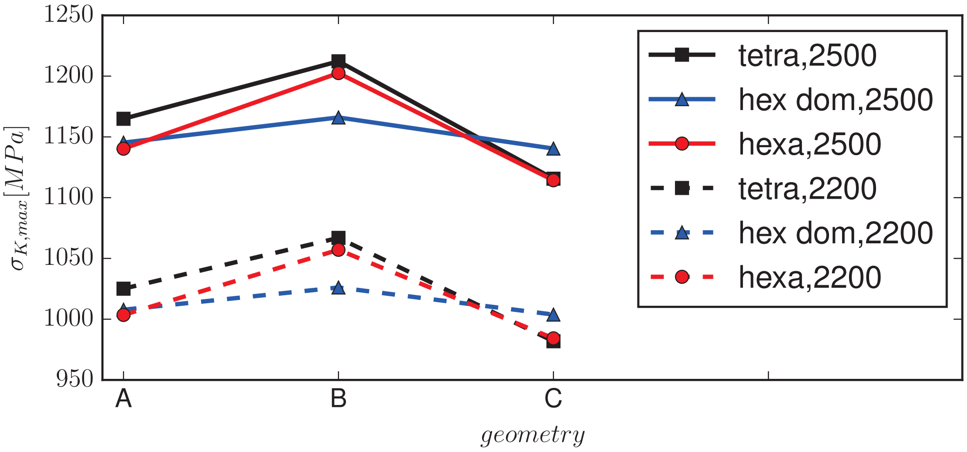

Figure 35: Fluctuation of maximum principal stress as a function of geometry and meshing method used.(For geometry B, values in parentheses from Table 8 were used.)

5.5.2 Meshing method

Figure 35 also provides an insight into the influence of three different meshing methods on the results. In two of the three geometries the tetrahedral mesh produces most con-

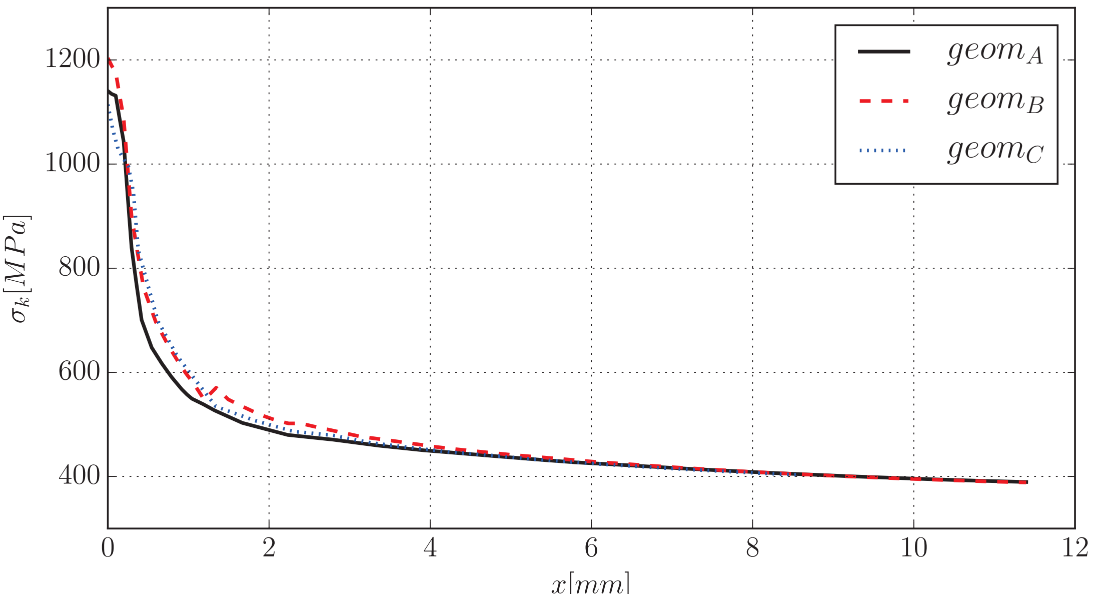

Figure 36: Length-wise maximum principal stress distribution for various geometries. Hexa mesh.

servative results. The hex dominant mesh produces results somewhere in the middle of the rest. Also looking at Figure 28 one can see that the element size for hex dominant mesh in depthwise direction was coarser than in other meshing methods. This may have caused larger local stiffness and consequently less precise calculation of steep stress gradient.

As to the actual differences, all methods, except for geometry B, produce results that are within three percent to each other and therefore do not have significant impact on the fatigue resistance. Based on these result, the tetrahedral mesh is comparable with strictly hexagonal mesh and therefore recommended as the model preparation is easier and least time consuming. Before it was mentioned that tetrahedral meshing method produces larger models in terms of number of elements. If the investigated model had more elements, the greater necessary computational effort would eventually out-weight the gains coming from easier modelling and strictly hexagonal mesh would be advantageous. Strictly hexagonal mesh also brings pros in terms of greater discretization consistency and better control over mesh quality.

To close this topic, the relatively low sensitivity of the element type on the results indicates, that once the element size becomes fine enough, element type is of low significance in terms of results quality. At that moment, one needs to decide if the effort is spent on longer time of computation or lengthier mesh preparation.

5.5.3 Experiment difference

Looking on Tables 5 and 8 it is apparent, that endurance based on the analysis is in general much more conservative than based on the results of experiment. It can be said, that even 50% survival probability FAT 225 S-N curve produces conservative results in this particular case. One however needs to bear relatively statistically insignificant number of test samples in mind. Based on the preceding discussions regarding geometry and mesh influence the geometry A with hexagonal mesh could be taken as the most representative candidate without the knowledge of the actual weld geometry. The accuracy is -40.3% and -14.4% for load levels $2\,200N$ and $2\,500N$ respectively.

Nevertheless results of geometry C provide even better match. This indicates, that the real weld geometry may have been closer to this particular geometry. Indeed, looking at Figure 19 one can notice that weld flank angle is actually smaller than $45°$ and therefore somewhat closer to the weld geometry C. It needs to be said that the aim of the analysis was not to model the actual geometry but to see the sensitivity of different geometry modelling on the results. The aim of these fatigue assessment methods is to reliably predict life of details when only design intended geometry is known. Therefore it cannot be bluntly said that geometry C is a better modelling approach in general. If one wanted to get the best match with the experiment, direct measurement and modelling of actual weld bead geometry is advised.

5.5.4 Comparison with other methods

In order to validate the results from effective notch stress calculation, structural stress was calculated from the existing model and endurance in critical location was compared between the two methods. Hot-spot stresses from analysis results were extrapolated in accordance with IIW recommendations. Example of such analysis hot-spot stress linear extrapolation is illustrated in Figure 38. Based on the IIW tabulated details, sample was assigned with FAT 90 S-N curve for hot-spot stress based endurance calculation (see Figure 37). Aligned with the preceding methodology, FAT 90 was offset to 50% survival probability rate. The selected detail no. 552 do not correspond exactly to the tested

specimen geometry, nevertheless no better match in terms of geometry was listed.
The results are given in Table 9. Strictly hex elements meshing was considered as the most representative therefore no other meshing methods are taken into account in the table. The table also gives endurance of the specimens and the comparison with effective notch stress approach as well as with experimental data (averaged endurance).

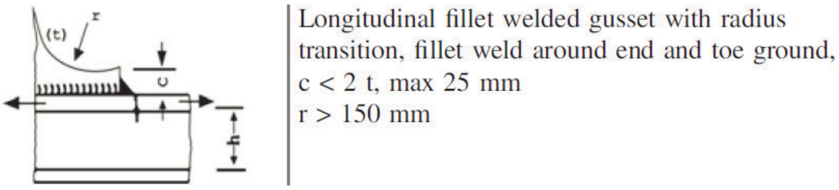

Longitudinal fillet welded gusset with radius transition, fillet weld around end and toe ground,
c < 2 t, max 25 mm
r > 150 mm

Figure 37: FAT class assigned to investigated detail. Per IIW [1] detail no. 522, FAT 90.

Load $F[N]$	Geometry $[-]$	Hot-spot stress $\sigma_S[MPa]$	End. FAT 90 SP 50.0 $N[-]$	Diff. FAT 225 $\Delta_{225}[\%]$	Diff. exp. $\Delta_{exp}[\%]$
$2\,200$	A	429.1	$58\,214$	$-28,8$	$-57,5$
	B	462.7	$46\,430$	$-33,6$	$-66,1$
	C	440.1	$53\,930$	$-37,8$	$-60,6$
$2\,500$	A	490.4	$38\,998$	$-28,8$	$-71,5$
	B	528.8	$31\,104$	$-33,4$	$-77,3$
	C	503.0	$36\,124$	$-38,5$	$-73,6$

Table 9: Linearly extrapolated hot-spot stress for respective geometries and difference with respect to experiment (averaged values, see Table **??**). Meshing method: hexa.

Looking at the results we can see that endurance based on the FAT 90 is even more conservative than ones produced by effective notch stress approach. This may be accredited to inappropriate FAT class selection (differences in actual detail's geometry and loading might be too different from the IIW selected detail) or better manufacturing quality of the detail. The author believes it is in fact combination of both. If one would like to match the effective notch stress approach with hot-spot stress based approach FAT100 produces results that are essential similar. Due to large disparity in the average endurance for the two load levels based on experiment it is not possible to select FAT class that would produce good match at both load levels. For lower load level $F = 2\,200$ N fairly

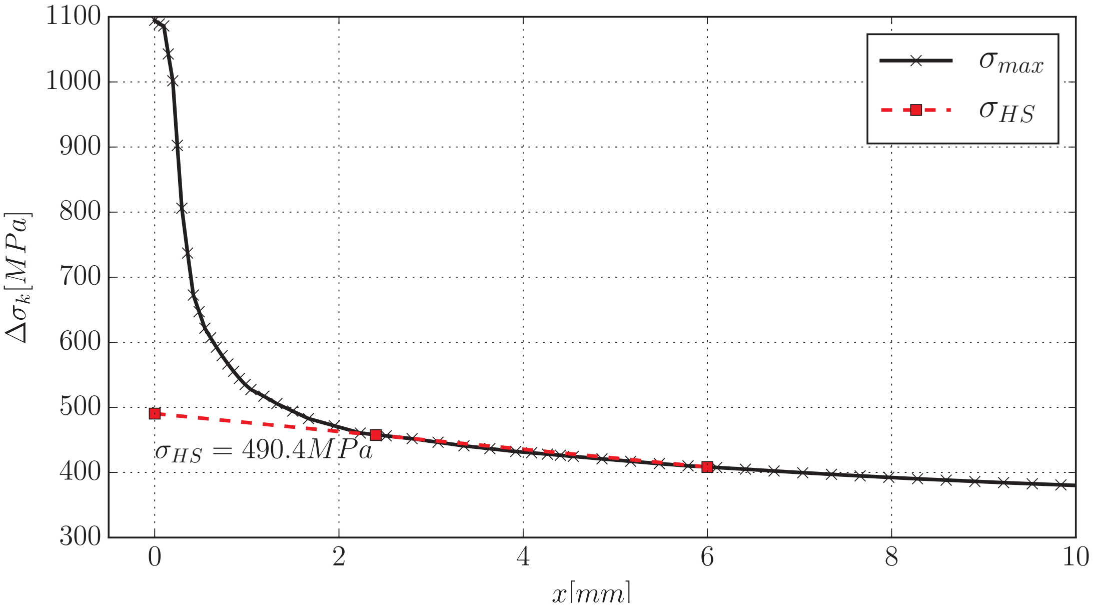

Figure 38: Hot spot stress for geometry A, meshing method hexa, load level $F = 2\,500N$.

good match with experiment is produced with FAT 125. For higher load level $F = 2\,500$ N FAT105 is deemed acceptable. Respective endurance results for these FAT classes are listed in table 10.

Load $F[N]$	**Geometry** $[-]$	**FAT 90** $N_{90}[-]$	**FAT 100** $N_{100}[-]$	**FAT 105** $N_{125}[-]$	**FAT 125** $N_{140}[-]$
2 200	A	58 214	79 854	92 442	155 966
	B	46 430	63 690	73 729	124 394
	C	53 930	73 978	85 639	144 488
2 500	A	38 998	53 495	61 927	104 482
	B	31 104	42 666	49 391	83 332
	C	36 124	49 553	57 364	96 783

Table 10: Endurance based on hot-spot stress for different FAT class SN curves.

6 Fatigue assessment of large scale model

Final part of this thesis consists of fatigue assessment of a large scale model - welded boom of an excavator E26 that can be seen in Figure 39. The model has been provided by Doosan Bobcat Engineering s.r.o. and was selected due to endurance test that was performed in the past. Only part of the model was provided, nevertheless sufficient to analyse endurance of critical location, from which the cracks initiated during the endurance test. The aim of this fatigue assessment was mostly to utilize effective notch stress approach analysis, that was described in earlier sections, on "real world" engineering example.

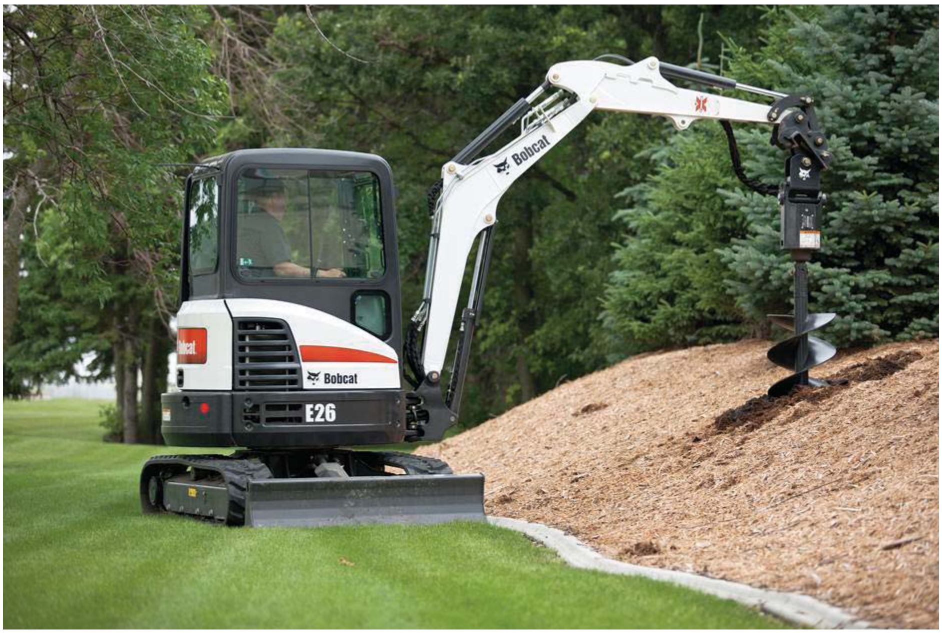

Figure 39: Lateral view of excavator with the boom that was modelled [11].

6.1 Geometry and load definition

Geometry as well as loading sequence was obtained from Doosan Bobcat. Only part of the actual geometry was provided, missing both castings of boom as well as dipper and bucket (see Figure 40). Location of important mechanism points, pins in locations A and B and points of action loads, were nevertheless obtained. Model respects the as tested configuration. For the purpose of the endurance test the boom was mounted onto stationary platform (see Figure 40) and actuators were replaced by welded rigid links made from sheet metal. This enabled to lock boom mechanism configuration for the purpose of the testing. The standard bucket, as seen in Figure 40, was replaced by non standard part, which accommodated installation of actuators for loads excitation. Model with loads nomenclature as well as established loads coordinates is depicted in Figure 41. The image serves for illustrative purposes only, as the tested bucket was not included in boom model that was provided, only location and coordinate system of the loads. Nomenclature used for description of excavator geometry and model is displayed in Appendix D.

Load sequence definition is listed in Table 11 as well as depicted in Figure 42. Loads in pairs ($[F_1 + F_2]$ and $[F_3 + F_4]$) were spatially symmetric and identical in each step of the loading sequence. Loading is assumed to be combined of repeating sequence 01 and 02 in this order, after sequence count of each sequence was reached (9 times sequence 01, 11 times sequence 02, 9 times sequence 01 and so on). Each sequence consist of 6 cycles. Complete repetition of both sequences therefore consists of 120 cycles ($6 \cdot 9 + 6 \cdot 11$).

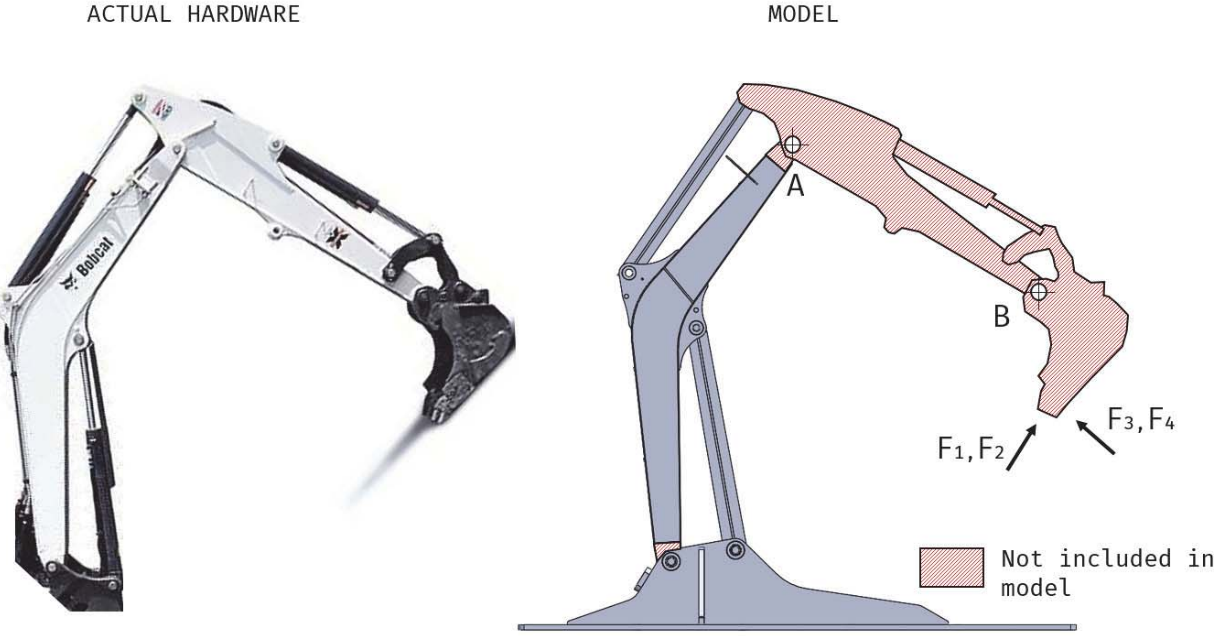

Figure 40: Comparison of actual hardware and model that was obtained for fatigue assessment (left image courtesy of [10]).

Model was first prepared for numerical model creation. This was achieved by removal of structurally insignificant elements such as plates chamfers, small holes or boom attachments. The base of the model was considered stiff enough to be removed and replaced in the pins region by a set of fixed points. Afterwards the model was partitioned and

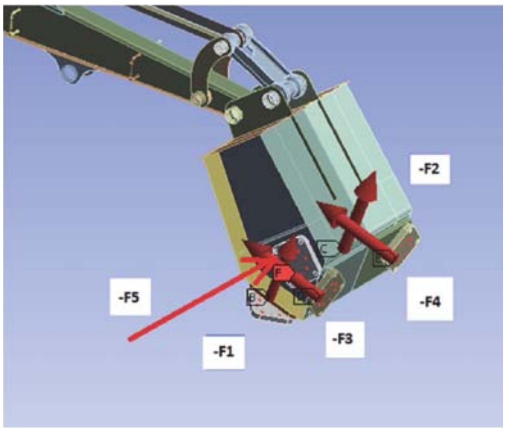

Figure 41: Loads nomenclature and coordinate system definition. Loads in picture are shown in negative direction.

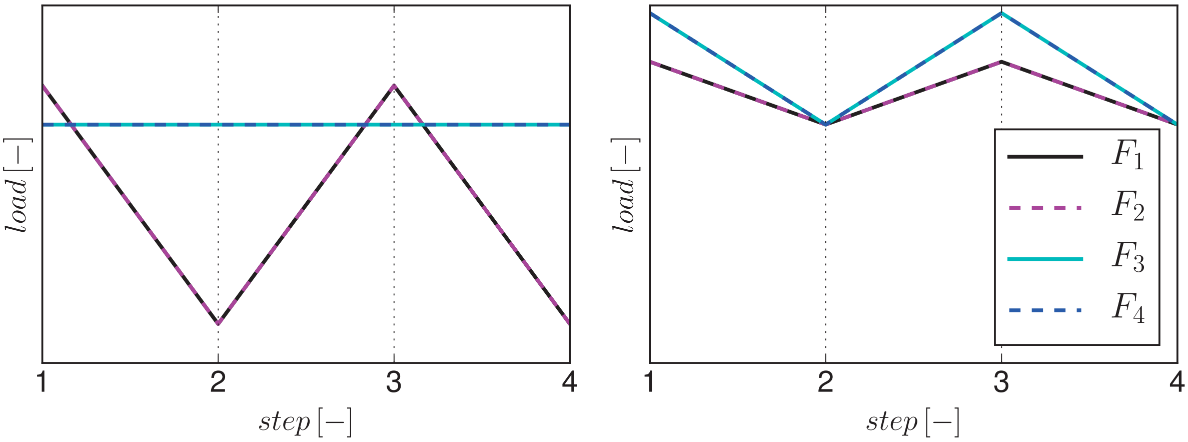

Figure 42: Excavator loads definition for two simulated sequences. **Left**: sequence 01; **Right**: sequence 02. In each sequence step $1-2-3$ is repeated 6 times. (To protect potentially sensitive data, the exact loads values are not displayed)

Sequence n.	Step	Loads				cycles in seq.	Seq. count
$[-]$	$[-]$	$F_1[N]$	$F_2[N]$	$F_3[N]$	$F_4[N]$	$[-]$	$[-]$
01	1	F	F	0	0	6	9
	2	$-5.11F$	$-5.11F$	0	0		
02	1	$1.61F$	$1.61F$	$2.86F$	$2.86F$	6	11
	2	0	0	0	0		

Table 11: Load sequence definition. One sequence consists of 6 cycles. During loading each sequence is repeated given amount of times before next sequence is initiated. (To protect potentially sensitive data, the exact loads values are not displayed)

simplified for easier meshing. This consisted of replacement of solid plates and actuator replacements by mid-plane shells. The bushings as well as location close to fatigue critical location was kept as solid bodies. Finally, the dipper was replaced by sufficiently stiff beam. Geometry of the model on which basis numerical model was constructed is depicted in Figures 43 and 44. All of the above mentioned adjustments were done following philosophy, that the model needs to retain stiffness essentially similar to the real boom, but doesn't need to be very precise in the areas far from the critical location.
In the critical location (see Figure 44) weld profile of size $a5$ was model with reference radius $r_{ref} = 1$ mm in the weld toe. Notch rounding in the root was not performed.
All members of the model were considered to be made of structural steel with following mechanical properties: $\rho_m = 7850\,kg/m^3$,$E = 2.0e5\,MPa$ and $\nu = 0.3$. In the loading of the beam, load from gravitational acceleration was not considered as precise weight distribution was unknown for the dipper and bucket. The assumption was made, that loading from gravitational acceleration on whole structure is of small significance when compared to the external loads imposed on the bucket.

6.2 Finite element model

6.2.1 Contacts and boundary conditions

Based on the model geometry described in the previous section numerical model was created. First pined joints were modelled.

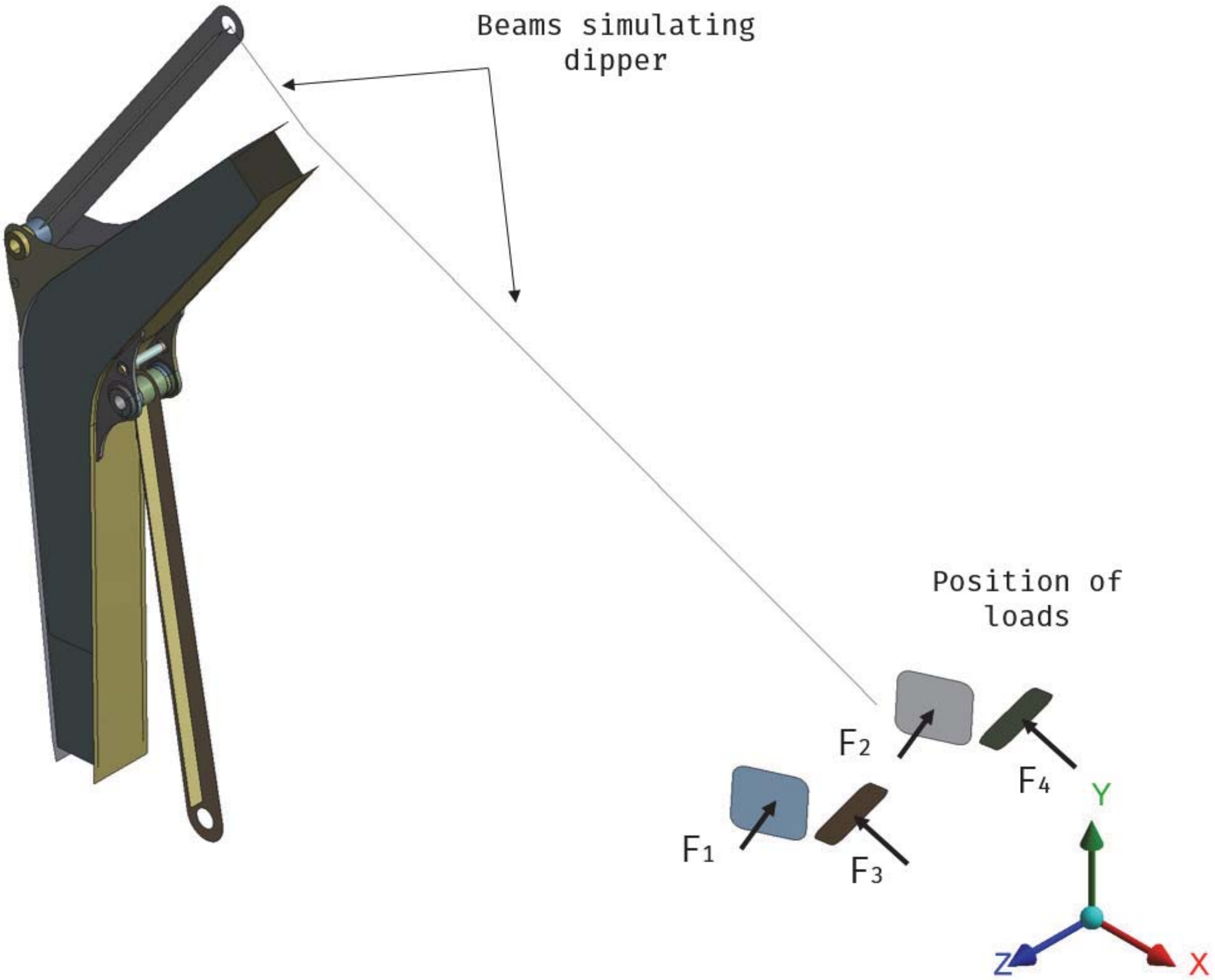
Beams simulating dipper
Position of loads
F1
F2
F3
F4
Y
Z
X

Figure 43: Overall view of simplified geometry of the boom.

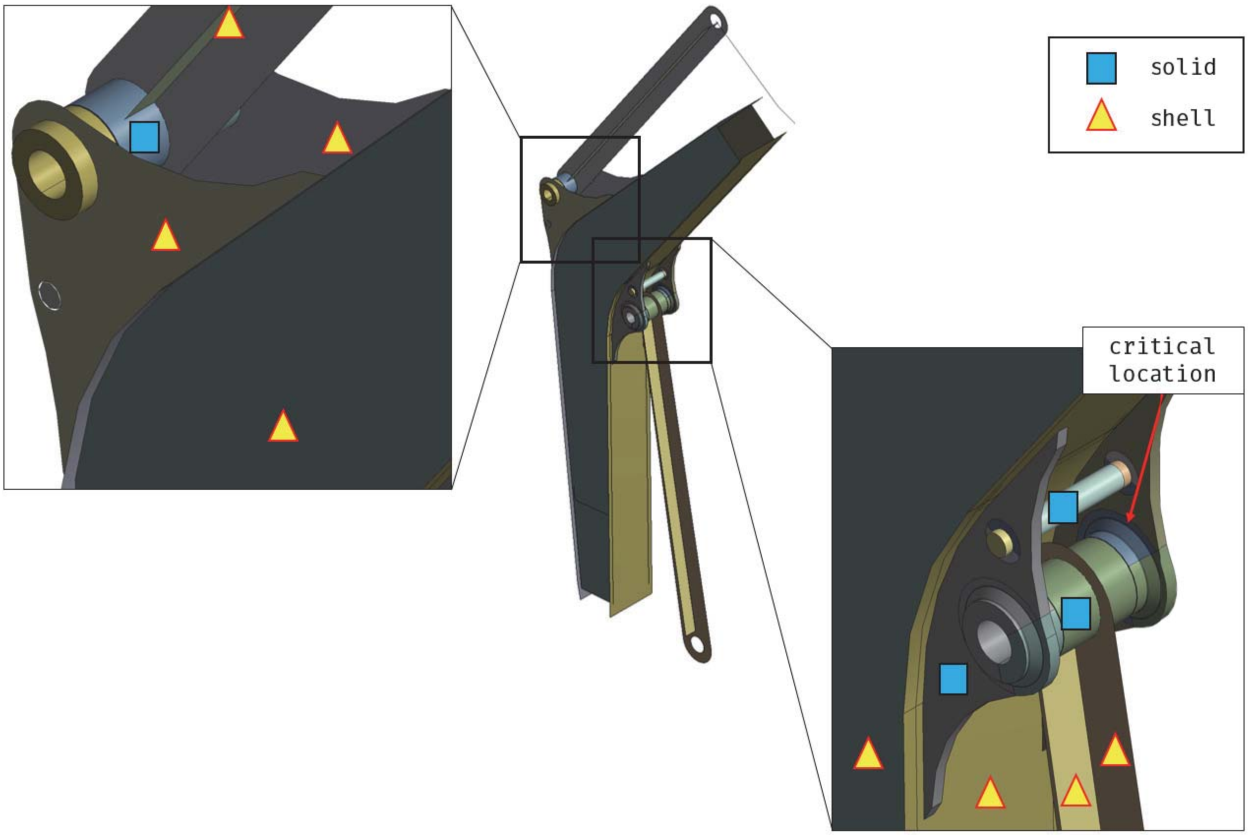

Figure 44: Detail view of simplified geometry of the boom.

Location of discussed pined joints is indicated in Figure 45. Pined joints in the figure can be divided into two categories: pins that can rotate and represent one of the rotational joints of the boom (1 and 3) and pins, that are welded between the plates and serves as stiffening members (2 and 4). The pin in the critical location (1) was modelled as a beam divided into two halves. Each outermost end vertex of the beam was connected to the two respective outer bushings with revolute condition, while the center vortices were connected together and then coupled with the center bushing. Closest stiffening pin (2) was modelled as solid body connected with both sides of the solid plates by means of MPC bonded connection. This configuration was chosen on the basis of pins proximity and their influence to the critical location where weld simulated by MPC connection introduces additional stiffness. Upper rotational joint pin (3) was modelled by imposing revolute condition between bushings only. Last stiffening pin (4) was modelled as a beam connecting circular edges of both outer plates.

Upper joints (3 and 4) were modelled much simpler than the lower ones (1,2). This is because the exact stress distribution is not needed in the upper part as it is located relatively far away from the fatigue critical location. Based on the later results this approach was deemed as sufficient.

Next contacts and other joints were established in the model.

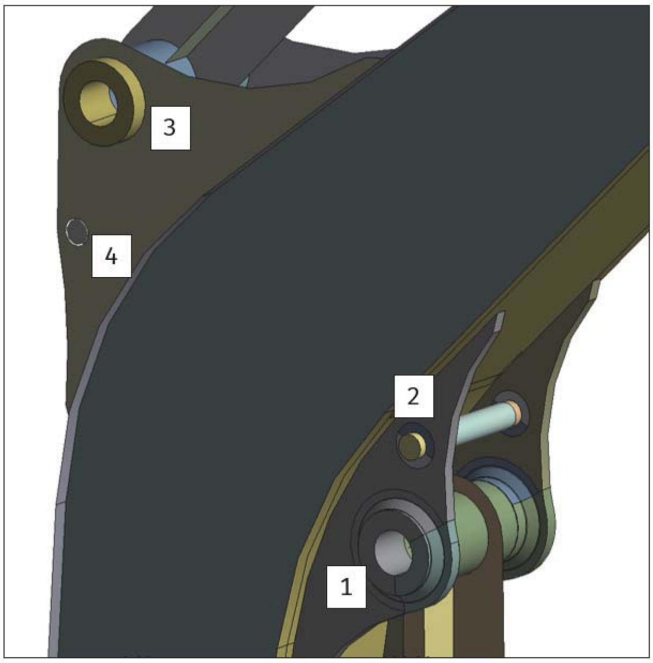

1 Divided beam coupled with middle bushing + revolute at sides

2 Solid pin coupled by MPC with plate sides

3 Bushings coupled with revolute joint

4 One beam connecting two oposite edges

Figure 45: Simulation of pinned joints.

1) Bonded MPC contact

This contact represents inseparable linear contact between entities for small deformations that adds constraint equations to tie the displacement of respective surfaces together. MPC stands for *multi-point constraint* and in this particular model simulate stiff welded joint between parts. Respective contacts can be seen in Figure 46.

2) Revolute joint

This type of joint was already mentioned above, when discussing pinned joints. This contact constricts all degrees of freedom between the contact surfaces apart from mutual rotation about coincident centerline. This type of contact can simulate non-deformable pinned joints. All revolute joints utilized in the model can be seen in Figure 47 together with their description.

3) Fixed joint

This type of connection directly constraints all degrees of freedom between connected entities and is used to lock position of respective entities. All fixed joints utilized in the model can be seen in Figure 48 together with their description.

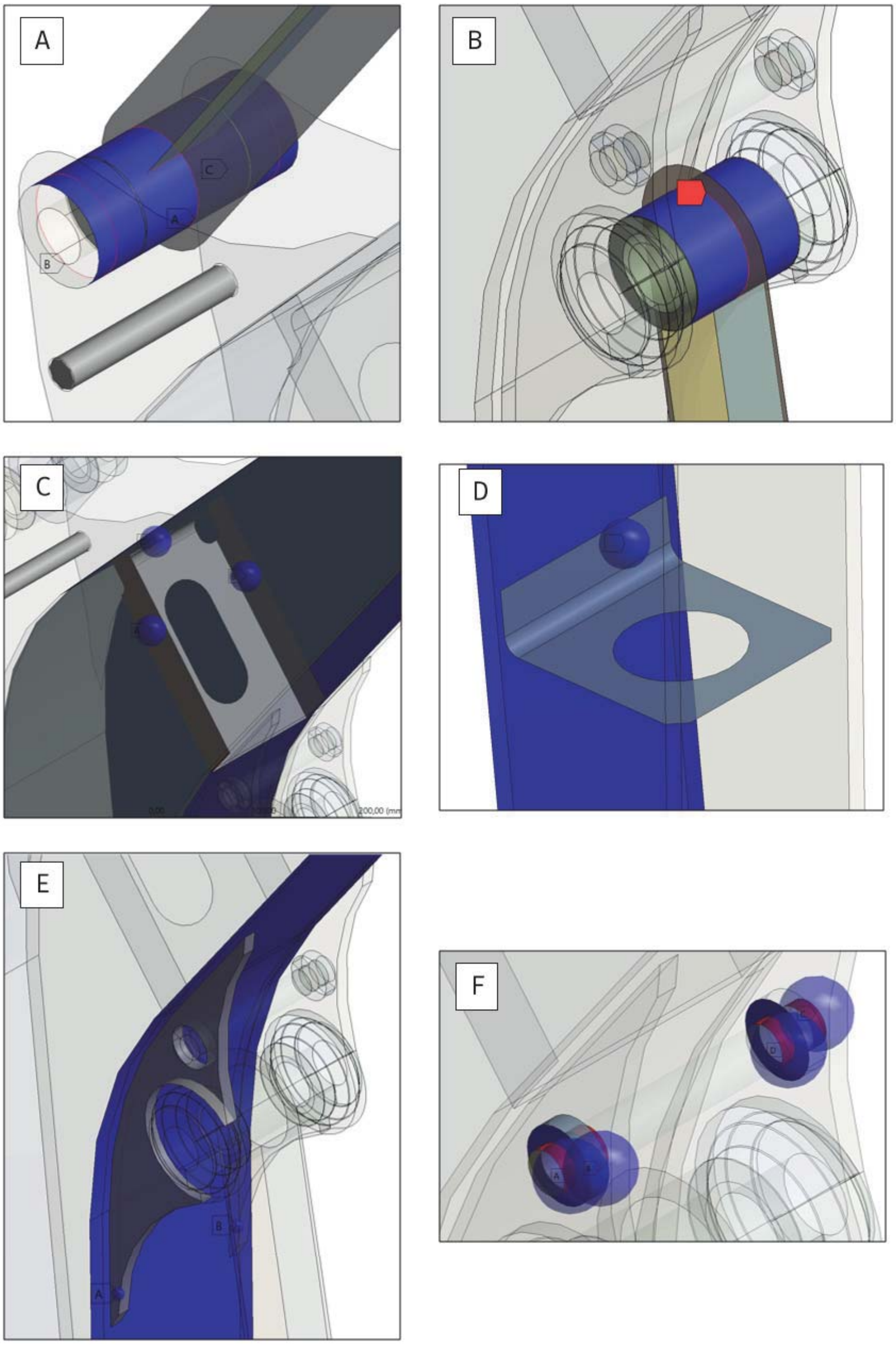

Figure 46: Bonded MPC contacts in the model. All contacts simulate welded connection. Contact between: **A)** Top solid bushing and actuator replacing link shells/top side plates shells, **B)** bottom solid bushing and actuator replacing link shells, **C)** upper internal stiffening plate shell and side plate shells, **D)** lower internal stiffening plate shell and side plate shells, **E)** bottom side solid plates and bottom side plate shells, **F)** solid pin and solid side plates.

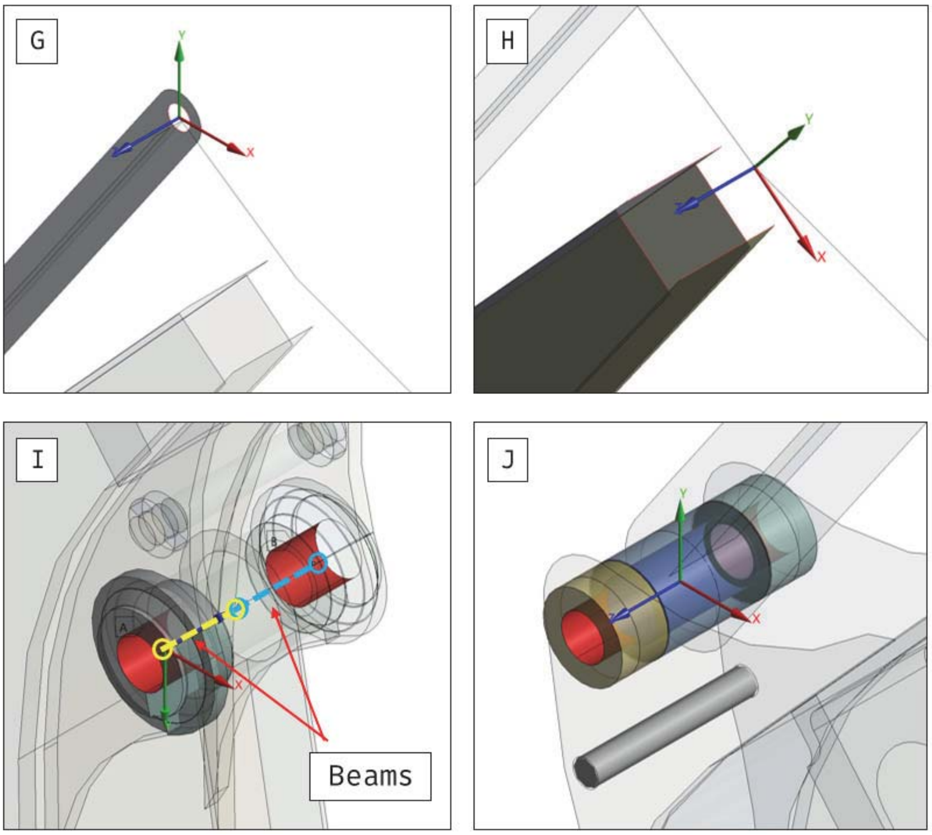

Figure 47: Revolute joints in the model. Revolution is established between: G) dipper short beam section end vertex and circular hole in upper actuator replacing link shell, H) end of the boom plate shells and vertex connecting two dipper beam sections (this enables rotation of the boom end with respect to dipper), I) end vertices of beams representing pinned joint and inner faces of outer bushings, J) inner faces of upper pinned joint outer bushings and inner face of the center bushing.

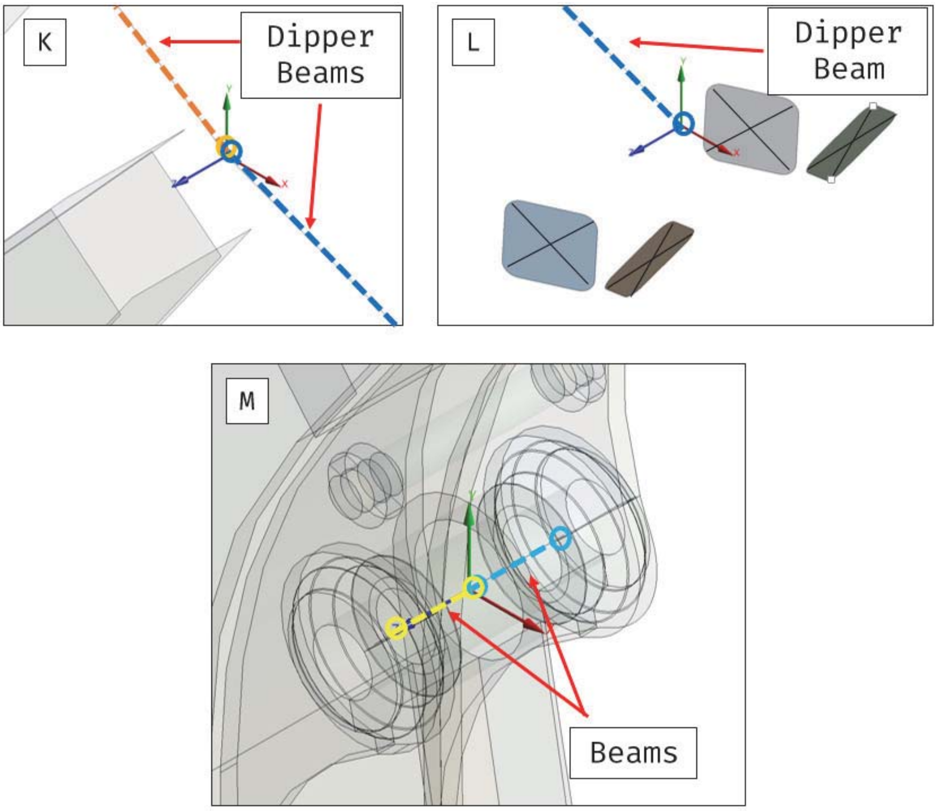

Figure 48: Fixed joints in the model. Fixed connection is established between: **K)** short an long part of the beam replacing dipper (this connection locks angle at which those two beams intersect), **L)** end vertex of the long dipper beam section and four shells the loads are imposed to, **M)** two beams end vertices representing lower pinned joint.

To finalize the model constriction, two boundary conditions are implemented representing connection of the boom with the platform. Both connections are modelled as remote displacement where all coordinates are set to location of the actual connection except for rotation about z axis which is left unconstrained. Both remote displacements are displayed in Figure 50.

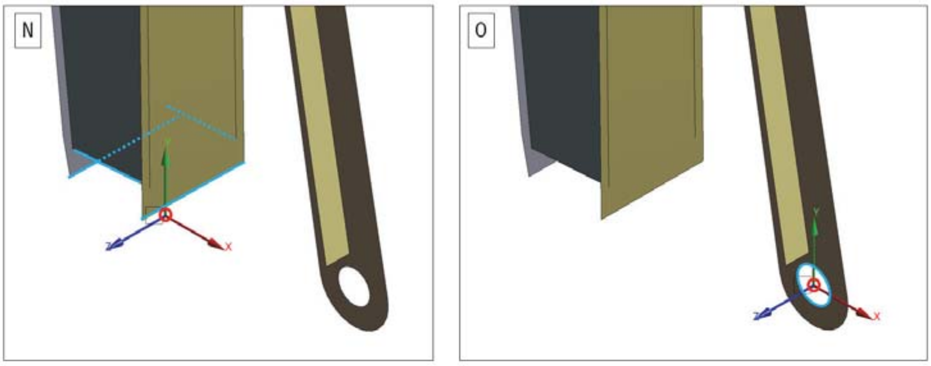

Figure 49: Remote displacement boundary conditions. Remote displacement is applied to: **N)** edges of the plate shells at the bottom of the boom, **O)** edge of the hole in lower link replacing actuator. Both parts can rotate freely about z axis.

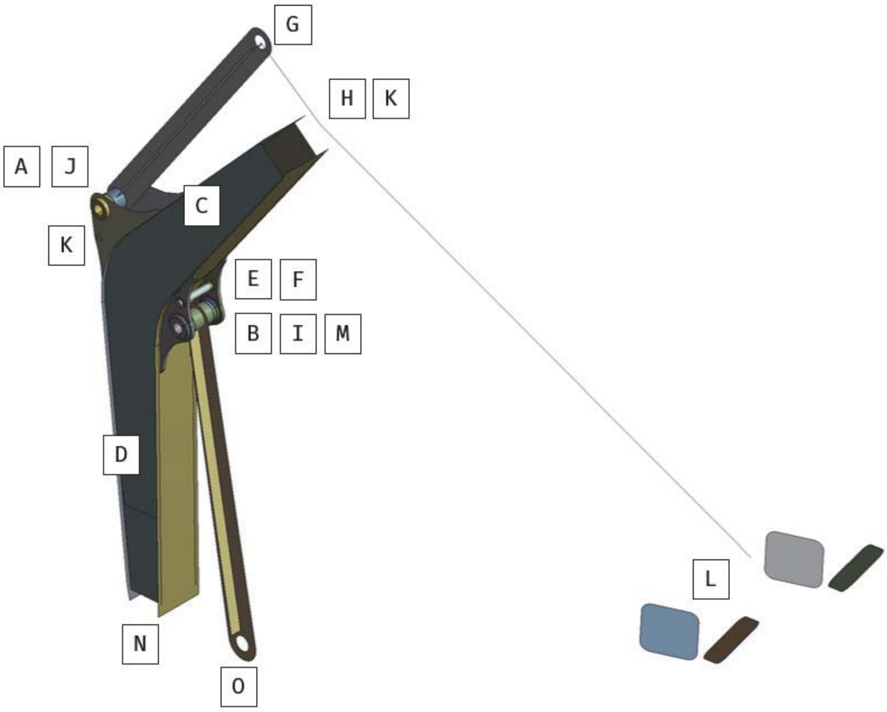

Figure 50: Location of all contacts and boundary conditions utilized in the model. For respective contacts see Figures 46,47,48 and 50.

6.2.2 Mesh

As in case of small scale model in the previous section two models were constructed. Global model included all structural elements discussed in the previous section. Figure 51 shows mesh for the global model. The shell sections were meshed by SHELL181 4 noded elements. The solid sections were meshed by both hexahedral 20-node SOLID186 and tetrahedral 10-node SOLID187 elements (see left most detail in Figure 51). Mesh also contained substantial number or contact elements due to large amount of specified contacts. For the plates around the lower pin where fatigue critical place was expected, the size of elements approximately corresponded to 3 mm. The overall size of elements was however decided by global setting of *curve and proximity* size function and *aggressive mechanical* shape checking which satisfies refinement of the mesh in the area of contacts. Number of elements and nodes is listed in Table 12.

Sub-model geometry can be seen in Figure 52. Similar to global model, the geometry was decomposed into a set of zones enabling better mesh quality in critical areas. Displacement from global model was imposed on the boundaries of the sub-model. Mesh of sub-model is displayed in Figure 53. Fatigue critical area of weld toe and vicinity of upper pin was meshed by 20-node hexahedral SOLDID186 elements. Rest of the model was meshed by 10-node tetrahedral SOLID187 elements. Size of the elements in the toe

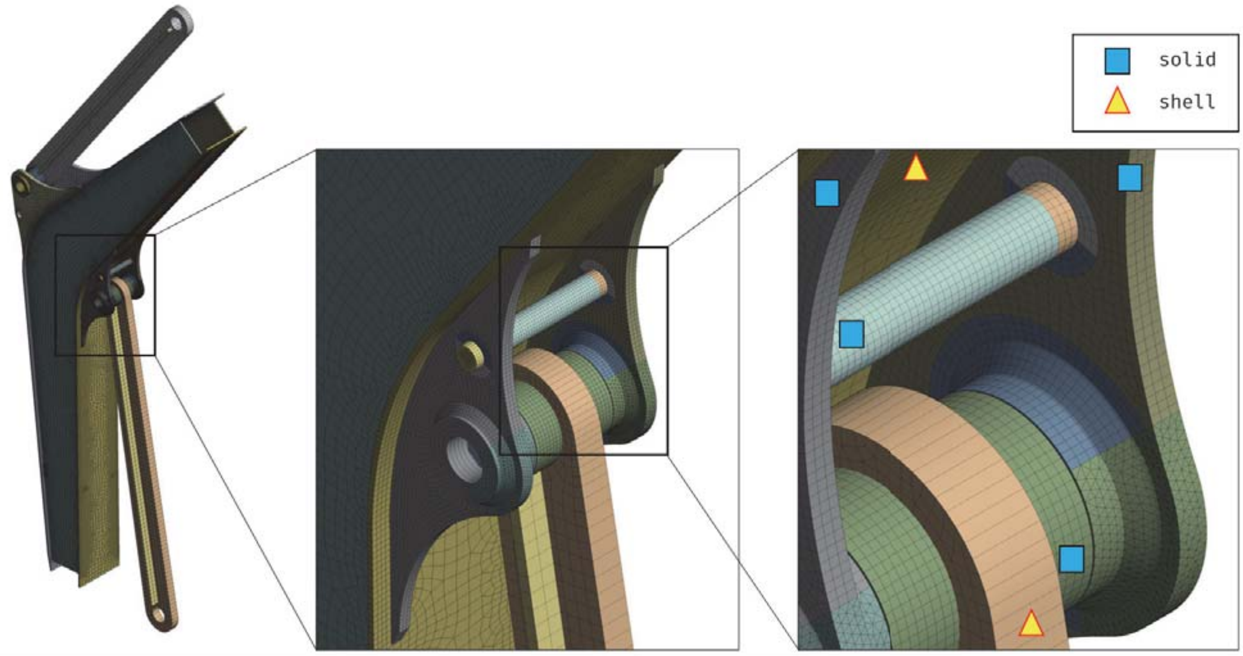

Figure 51: Global mesh of excavator boom.

of the weld was set to 0.15 mm. Size of tetrahedral elements was based on *curve and proximity* size function. Number of nodes and elements is listed in Table 12.

Model $[-]$	Number of elements $[-]$	Number of nodes $[-]$	CPU time $t_{CPU}[s]$
global	$100\,328$	$250\,081$	367.2
sub	$736\,657$	$1\,166\,210$	970.6

Table 12: Number of elements and nodes of global and sub model.

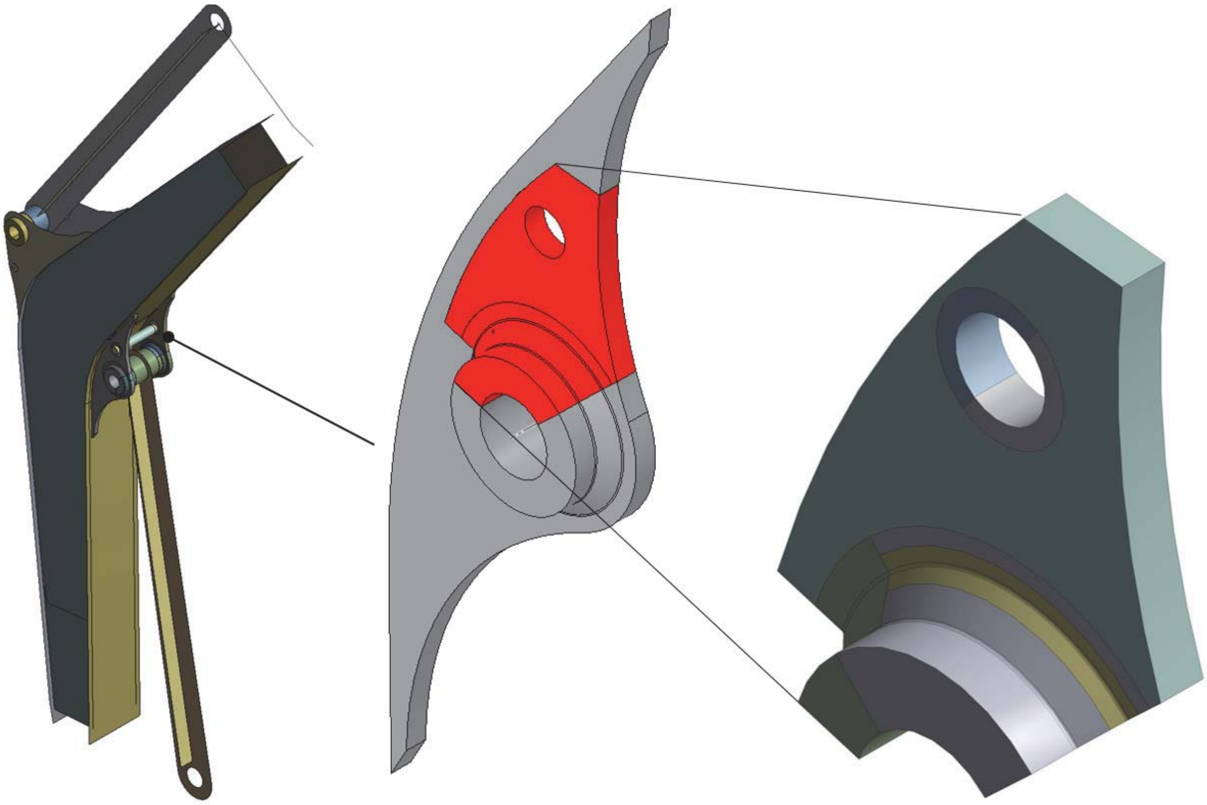

Figure 52: Geometry of the sub-model..

6.3 Results

6.3.1 Stress and deformation

When looking at the load sequence defined in Figure 42, four possible load cases occur. Figure 54 depicts lateral view of the boom global model deformation for three of

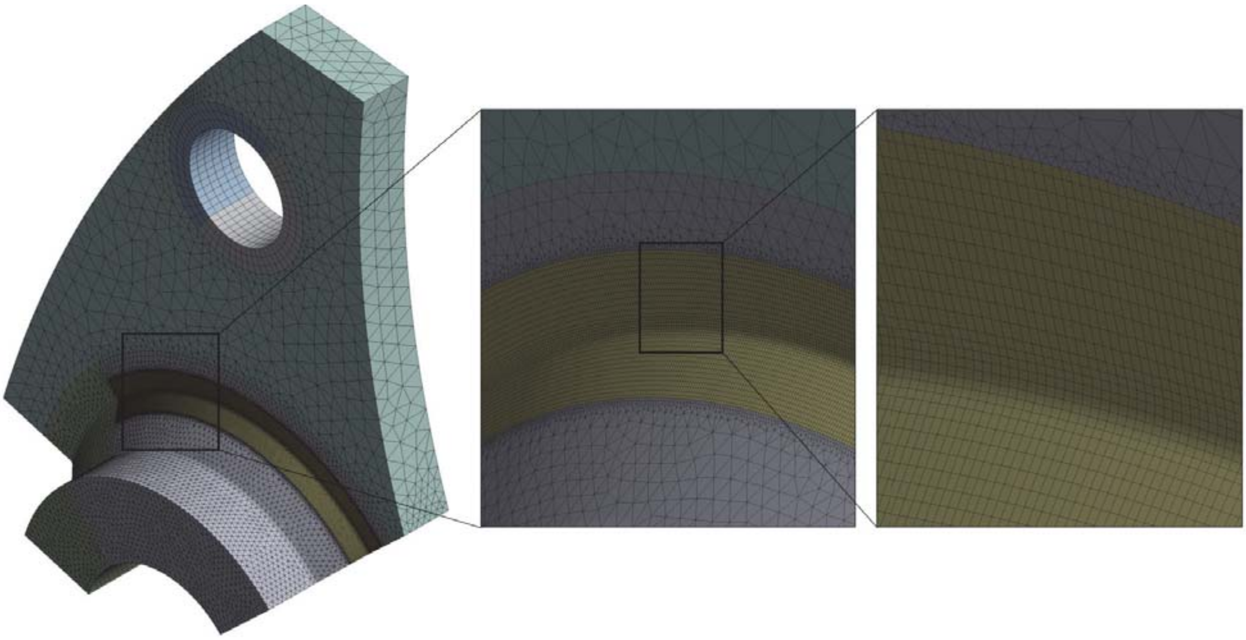

Figure 53: Sub model mesh of excavator boom lower aft looking forward left side plate.

the possible load combinations (fourth is non-loaded boom in sequence 02). This figure illustrates that side solid plates in the lower pinned joint are in turns loaded in tension and compression. Because fatigue relevant parameter is principal stress acting perpendicularly to the weld, in case of tension maximum principal stress is used, whereas in case of compression minimum principal stress is critical. Stress range directly influencing fatigue resistance is hence sum of maximum and minimum principal stresses taken from respective load cases.

Figure 55 depicts minimum principal stress for the first load step of sequence 01. In this load case side plate of the pinned joint is predominately loaded in compression with stress peak at the weld toe on the inner plate surface. Figure 56 depicts maximum principal stress for the second load step of sequence 01. Again stress peak exists in the same location as in load case 1, but in this case plate is predominantly subjected to tension. Figure 57 depicts minimum principal stress for the first load step of sequence 02.

To further illustrate deformational and stress behaviour of the plate, front view is presented for the above mentioned load cases (see Figure 58). The deformation is not in scale, nevertheless it is easily recognized how critical location is loaded.

Figure 59 shows sub-model results for the principal stresses of interest for all three possible load cases.

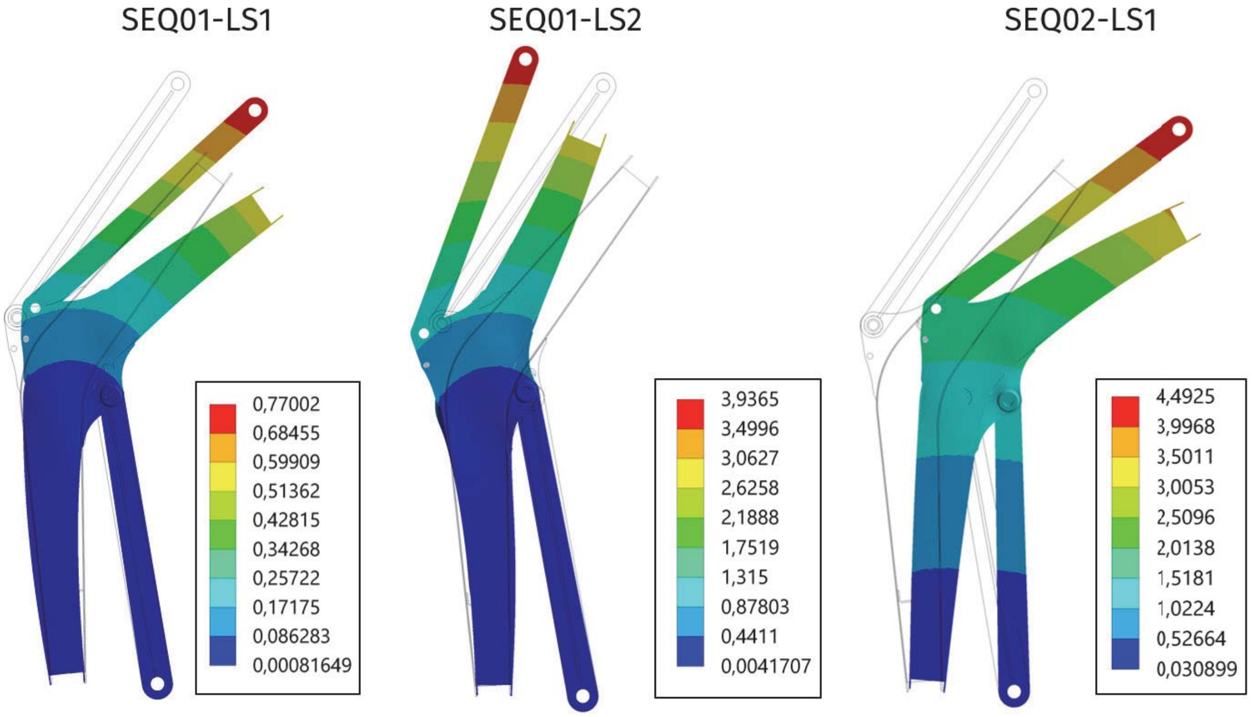
SEQ01-LS1
0,77002
0,68455
0,59909
0,51362
0,42815
0,34268
0,25722
0,17175
0,086283
0,00081649
SEQ01-LS2
3,9365
3,4996
3,0627
2,6258
2,1888
1,7519
1,315
0,87803
0,4411
0,0041707
SEQ02-LS1
4,4925
3,9968
3,5011
3,0053
2,5096
2,0138
1,5181
1,0224
0,52664
0,030899

Figure 54: Deformation of the global model of the boom for three different loads. **left)** Sequence 01 load step 1, **middle)** Sequence 01 load step 2, **right)** Sequence 02 load step 1. Deformation is displayed in substantially enlarged scale.

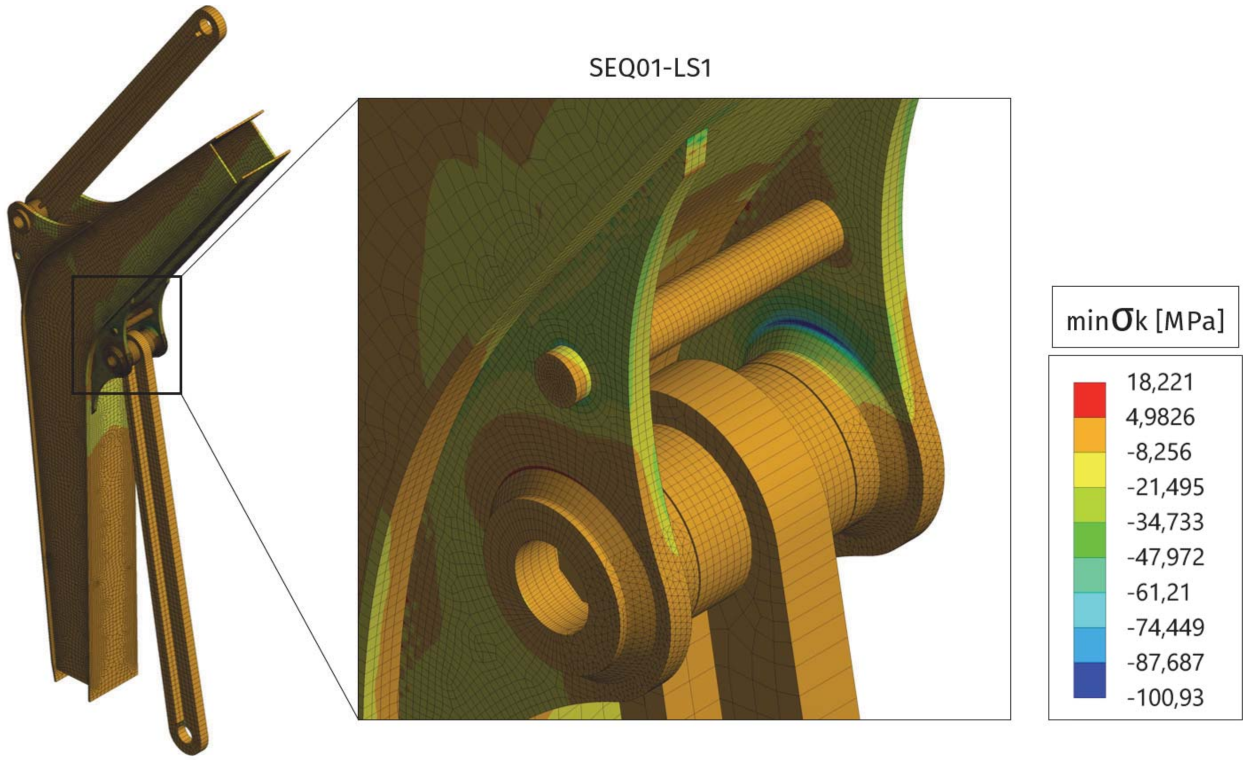
SEQ01-LS1
minσk [MPa]
18,221
4,9826
-8,256
-21,495
-34,733
-47,972
-61,21
-74,449
-87,687
-100,93

Figure 55: Minimum principal stress in the boom. Load sequence 01; load step 1.

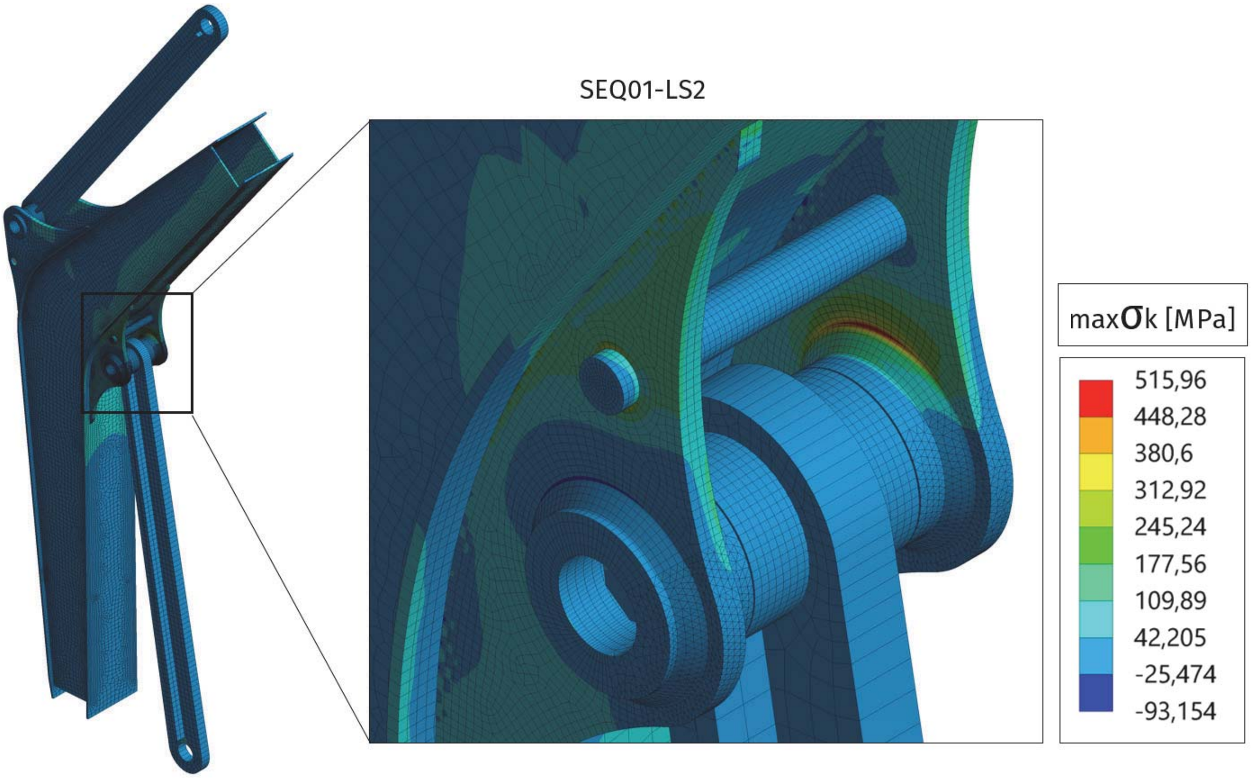
SEQ01-LS2
maxσk [MPa]
515,96
448,28
380,6
312,92
245,24
177,56
109,89
42,205
-25,474
-93,154

Figure 56: Maximum principal stress in the boom. Load sequence 01; load step 2.

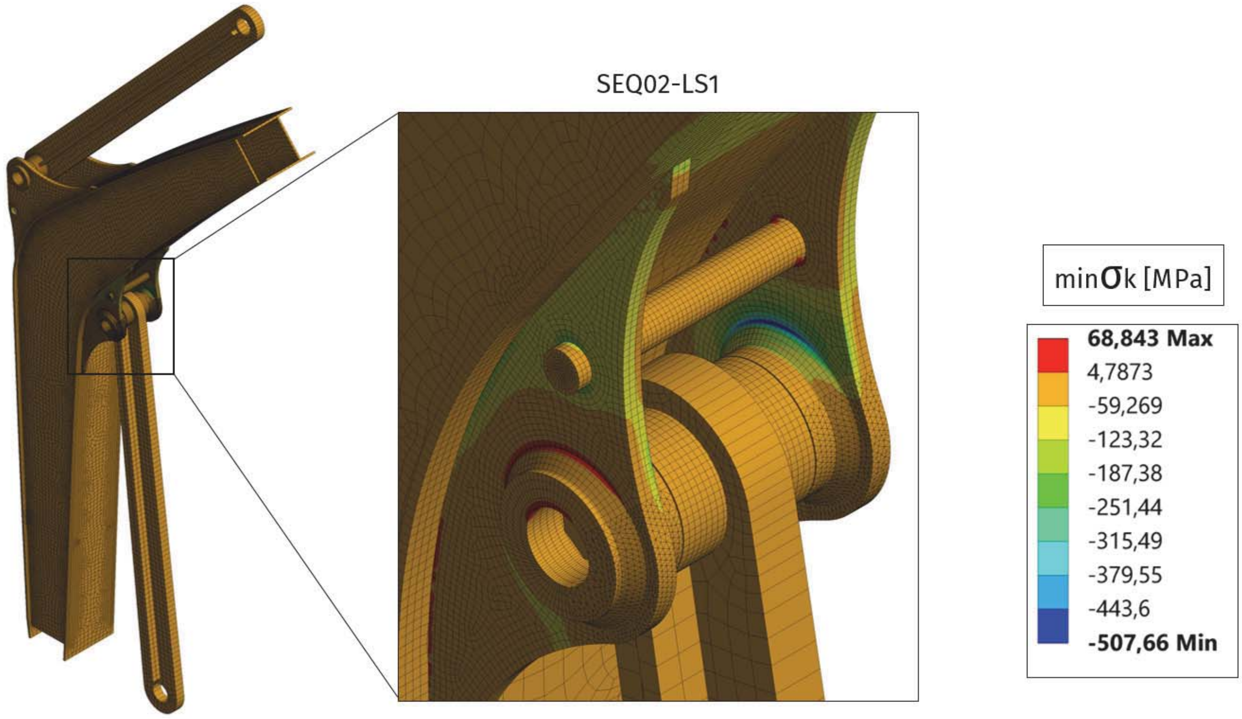
SEQ02-LS1
minσk [MPa]
68,843 Max
4,7873
-59,269
-123,32
-187,38
-251,44
-315,49
-379,55
-443,6
-507,66 Min

Figure 57: Minimum principal stress in the boom. Load sequence 02; load step 1.

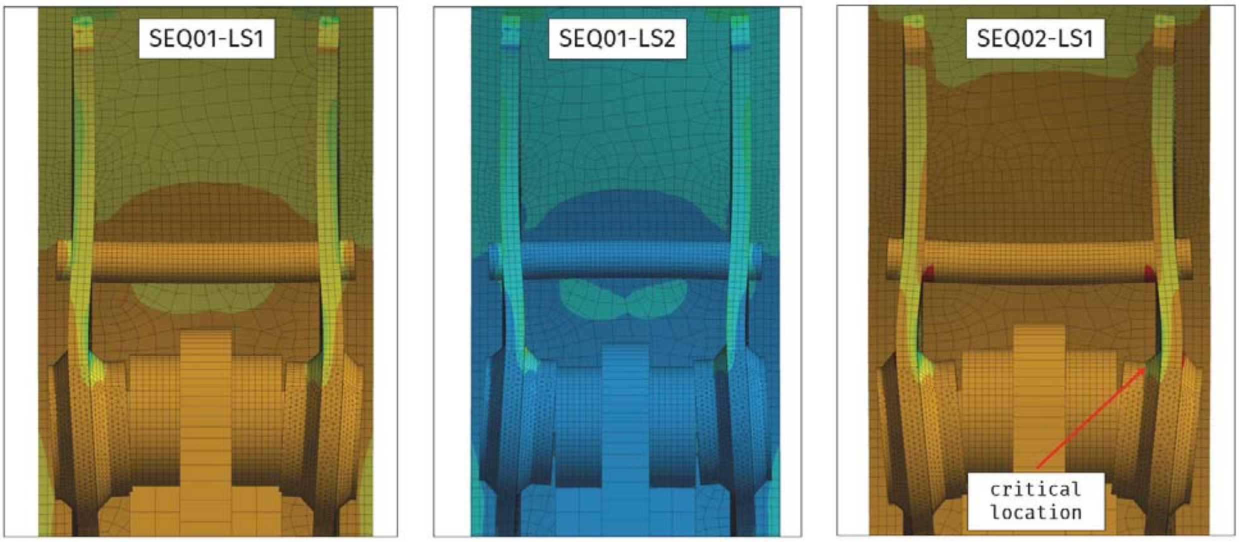
SEQ01-LS1
SEQ01-LS2
SEQ02-LS1
critical location

Figure 58: Deformation of the pinned joint. **left)** Sequence 01 load step 1 with minimum principal stress map, **middle)** Sequence 01 load step 2 with maximum principal stress map, **right)** Sequence 02 load step 1 with minimum principal stress map.

Finally, Figure 60 shows effective stress range in the toe region of the weld for the two considered load sequences. The exact stress range peak positions differ in each model, therefore the endurance needs to be calculated across the whole toes surface to get the

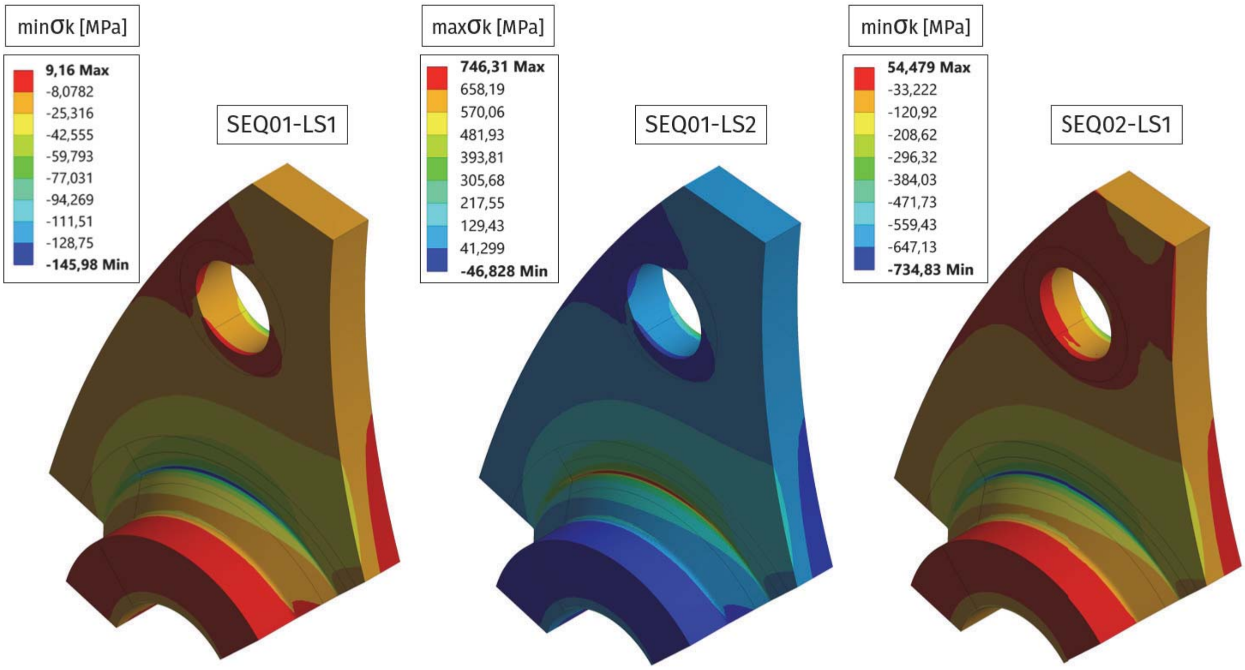
minσk [MPa]
9,16 Max
-8,0782
-25,316
-42,555
-59,793
-77,031
-94,269
-111,51
-128,75
-145,98 Min
SEQ01-LS1
maxσk [MPa]
746,31 Max
658,19
570,06
481,93
393,81
305,68
217,55
129,43
41,299
-46,828 Min
SEQ01-LS2
minσk [MPa]
54,479 Max
-33,222
-120,92
-208,62
-296,32
-384,03
-471,73
-559,43
-647,13
-734,83 Min
SEQ02-LS1

Figure 59: Sub-model principal stress results. **left)** Sequence 01 load step 1 with minimum principal stress map, **middle)** Sequence 01 load step 2 with maximum principal stress map, **right)** Sequence 02 load step 1 with minimum principal stress map.

worst possible nodal combination of the two loading sequences.

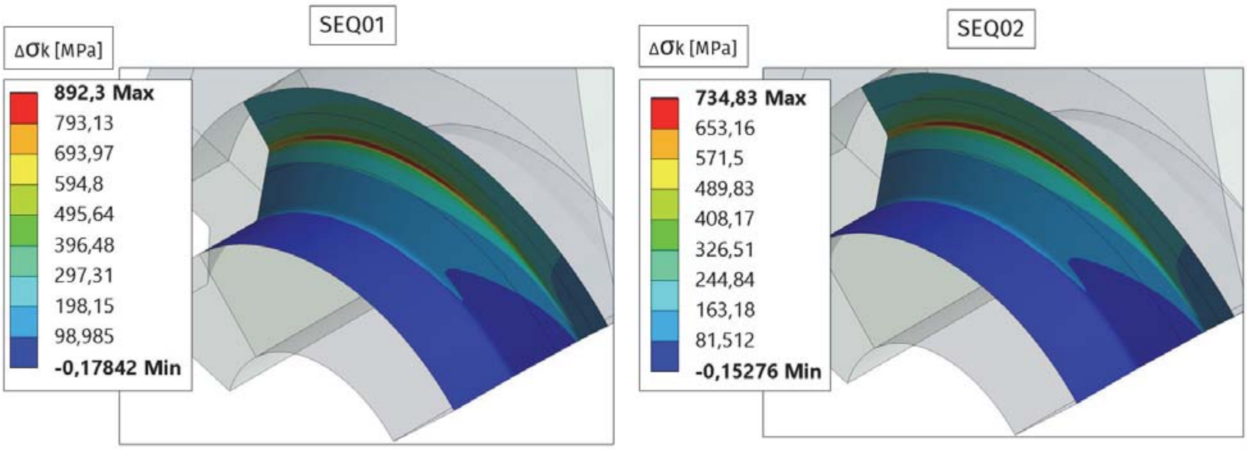
SEQ01
ΔσK [MPa]
892,3 Max
793,13
693,97
594,8
495,64
396,48
297,31
198,15
98,985
-0,17842 Min
SEQ02
ΔσK [MPa]
734,83 Max
653,16
571,5
489,83
408,17
326,51
244,84
163,18
81,512
-0,15276 Min

Figure 60: Effective stress range in the weld toe for the two considered load sequences.

6.3.2 Endurance

Endurance was determined on the basis of above mentioned stress range and S-N curve FAT225 representing 97.7% survival probability. For the damage accumulation the Palmgren-Miner rule was used (see equation 3). Under assumptions that one cycle is defined as one period of loading sequence (ie. +-+), that both of the loading sequences consist of 6 cycles and during loading the sequence 01 is repeated 9 times after which sequence 02 is repeated 11 times, the endurance can be calculated as:

$$N = D\left(\frac{n_{01}}{N_{01}} + \frac{n_{02}}{N_{02}}\right)^{-1} n_{cb} \tag{7}$$

, where D is fatigue damage ratio (implicitly $D = 1$), n_i is number of cycles in sequence i (for sequence 01 we consider $n_{01} = 6 \cdot 9 = 54$), N_i is endurance at effective stress range $\Delta\sigma_{k,i}$ and n_{cb} in number of cycles in the whole loading block. Once we substitute mathematical representation of S-N curve (equation 2) into the equation we get:

$$N = D\left(\frac{n_{01}}{\frac{C}{\Delta\sigma^m_{k,01}}} + \frac{n_{02}}{\frac{C}{\Delta\sigma^m_{k,02}}}\right)^{-1} n_{cb} \tag{8}$$

In case of FAT225 curve $C = 2.28e11$ and $m = 3.0$. Due to the fact that maximum of effective stress range differs for both sequences we cannot input them in the equation.

The endurance needs to be calculated for whole area of the weld toe from which location with worst combination of both sequences will be obtained. Just to illustrate the calculation we will assume that the effective stress range peaks occur in one location. At worst we obtain conservative envelope knowing that the actual endurance cannot be smaller than the result.

$$N = 1.0\left(\frac{54}{\frac{2.28e11}{892.3^3}} + \frac{66}{\frac{2.28e11}{734.83^3}}\right)^{-1} 120 = 1.0\left(\frac{54}{32\,066} + \frac{66}{57\,414}\right)^{-1} 120 = 1.0 \cdot 352.1 \cdot 120 = 42\,349.3 \tag{9}$$

The result indicates that were the effective stress range peaks locations same for both load sequences, the endurance would be $42\,349$ cycles (352 loading blocks). The above made calculation was made under assumption that effective stress range in critical location is in both sequences higher than constant amplitude fatigue limit (knee point in the S-N curve).

Endurance was calculated in Ansys for the whole weld toe region and results are displayed in Figure 61. We can see, that sequence effective stress peaks were quite close as endurance in critical location $N = 42\,420$ is very close to the conservative assumption made above.

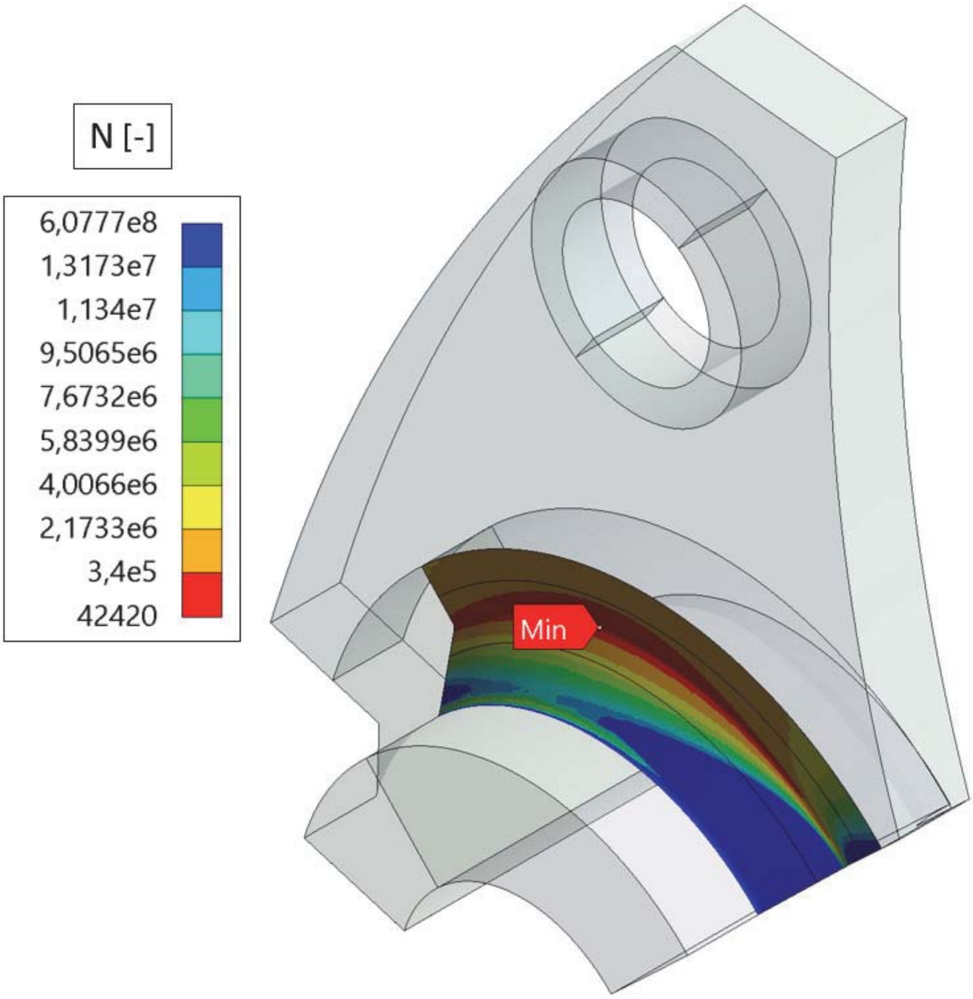
N [-]
6,0777e8
1,3173e7
1,134e7
9,5065e6
7,6732e6
5,8399e6
4,0066e6
2,1733e6
3,4e5
42420
Min

Figure 61: Endurance in the area of the weld toe notch. Isometric view of the submodel.

7 Conclusion

In this thesis, fatigue assessment by means of effective notch stress approach was researched. First, reader was presented with most common methods of fatigue assessment of structural details of welded joints in terms of: nominal stress approach, structural stress approach and effective notch stress approach. Each of the discussed methods has its clear advantages and disadvantages. Nominal stress approach is great for common details as very little effort for fatigue evaluation is needed. Structural stress approach is relatively forgiving in terms of mesh creation and is also very well linked to direct strain measurement and evaluation. Effective notch stress approach can be said to be most expensive with regard to computational effort that needs to be extorted to get meaningful results. Its greatest advantage nevertheless lies in its straightforward implementation by means of fictitious notch creation especially in cases where other methods struggle (non tabulated geometry, complex detail geometry).

After theory connected to the welded joints fatigue assessment was presented, small scale model was built and a sensitivity of modelling and meshing methods on fatigue resistance was tested. Greatest advantage was existence of fatigue tests of actual detail samples hence method precision could have been tested. It was mentioned that number of fatigue test samples was on the edge of statistical insignificance hence creation of general conclusions with respect to analysis results correctness is not advised. Based on the results, it can however be said, that in terms of elements type IIW recommendation, once discretization is close or better than recommended by IIW, all element types with quadratic displacement seem sufficient. Based on the comparison with the experimental results, it can be said that the effective notch stress approach based on FAT225 with 97.7% survival probability was for the given case rather conservative. Even after offsetting the S-N curve to 50% survival probability the results were still significantly lower than experiment average. This may have been caused by number of factors for example better level of welding technology or low number of experimental results.

In last part of this thesis, effective notch stress approach was applied to fatigue assessment of large-scale model of a boom from small-sized excavator. Critical location was easily determined based on the global model. Afterwards sub-model of critical location was created and results evaluated. Analysis itself was mostly presentation of effective notch stress approach utilization as actual fatigue testing results of the boom under given load sequence were unknown.

References

[1] Hobbacher A., *Recommendations for Fatigue Design of Welded Joints and Components*. International Institute of Welding, doc. XIII-2151r4-07/XV-1254r4-07, (Paris, France, October 2008)

[2] Niemi E., *Stress determination for Fatigue Analysis of Welded Components*. IIW doc. IIS/IIW-1221-93, The Iternational Institute of Welding, (1995)

[3] Fricke W., *Guideline for the fatigue assessment by notch stress analysis for welded structures* . Woodhead Publishing Limited, (England, Cambridge, 2008)

[4] Radaj D., Sonsino C.M., Fricke W., *Fatigue assessment of welded joints by local approaches*. Woodhead Publishing Limited, (England, Cambridge, 2006)

[5] Radaj D., Vormwald M., *Advanced Methods of Fatigue Assessment*. Springer-Verlag Berlin Heidelberg, (2013)

[6] Sosino C.M., Fricke W.,de Bruyne F., Hoppe A., Ahmadi A., Zhang G., *Notch stress concepts for the fatigue assesment of welded joints - Background and applications*. International Journal of Fatigue, 2012;34:2-16

[7] Aygul M., *Fatigue Analysis of Welded Structures Using the Finite Element*. Chalmers university of technology, (Sweden, Gothenburg, 2012)

[8] Růžička M., Hanke M., *Dynamická pevnost a životnost*. Nakladatelství ČVUT, (1992)

[9] `http://www.engineeringarchives.com/img/les_fatigue_meanstressequations_1.png` (access: 17.01.2016)

[10] `http://cdn-5.psndealer.com/e2/dealersite/images/newvehicles/2014/nv386604_1.jpg` (access: 31.7.2016)

[11] `http://assets.bobcat.com/images/excavators/e26/151128-t6k2002-11v1-fc_mg_full.jpg` (access: 31.7.2016)

A Analysis of geometry A

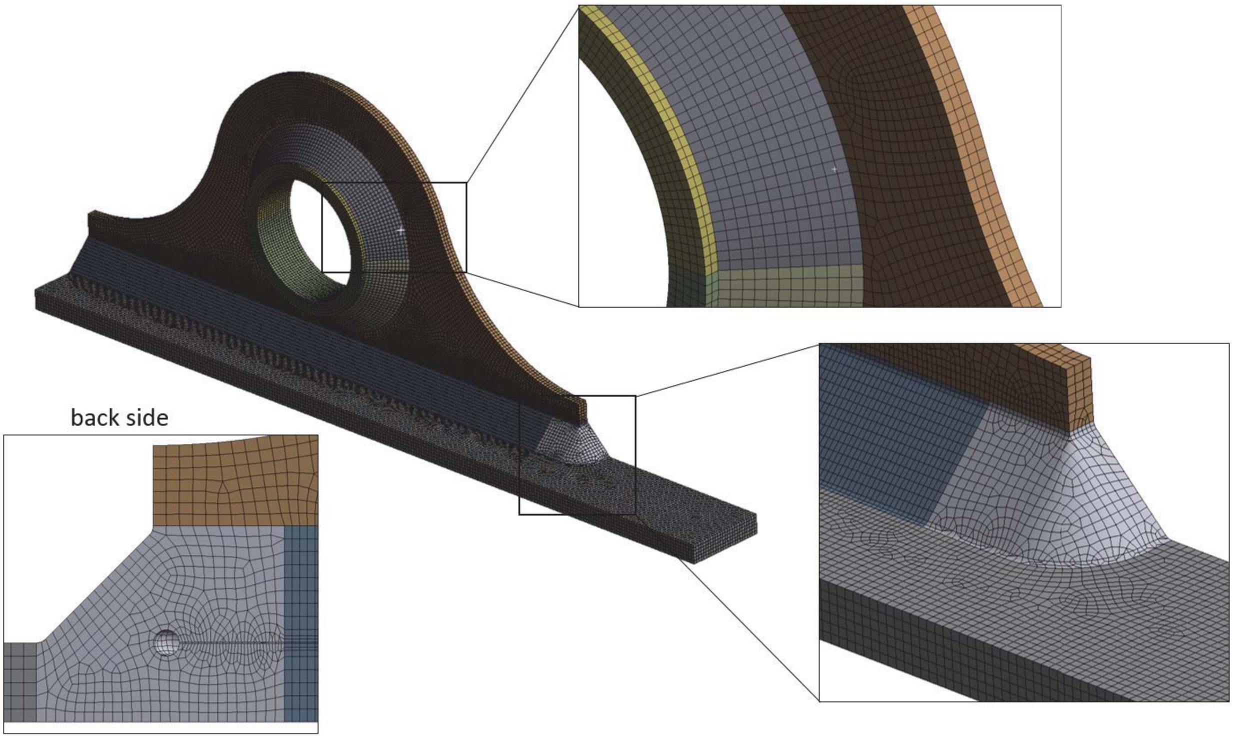

Figure 62: Global mesh for the weld edge geometry A.

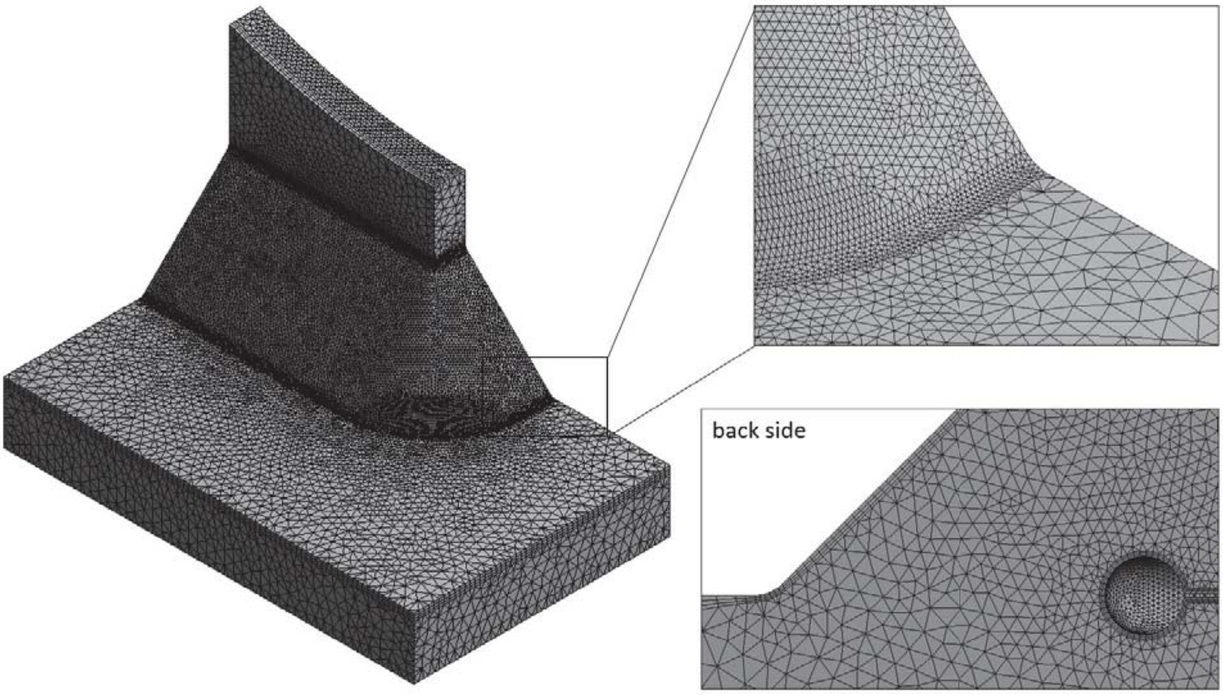

Figure 63: Sub-model for the weld edge geometry A, tetra meshing method.

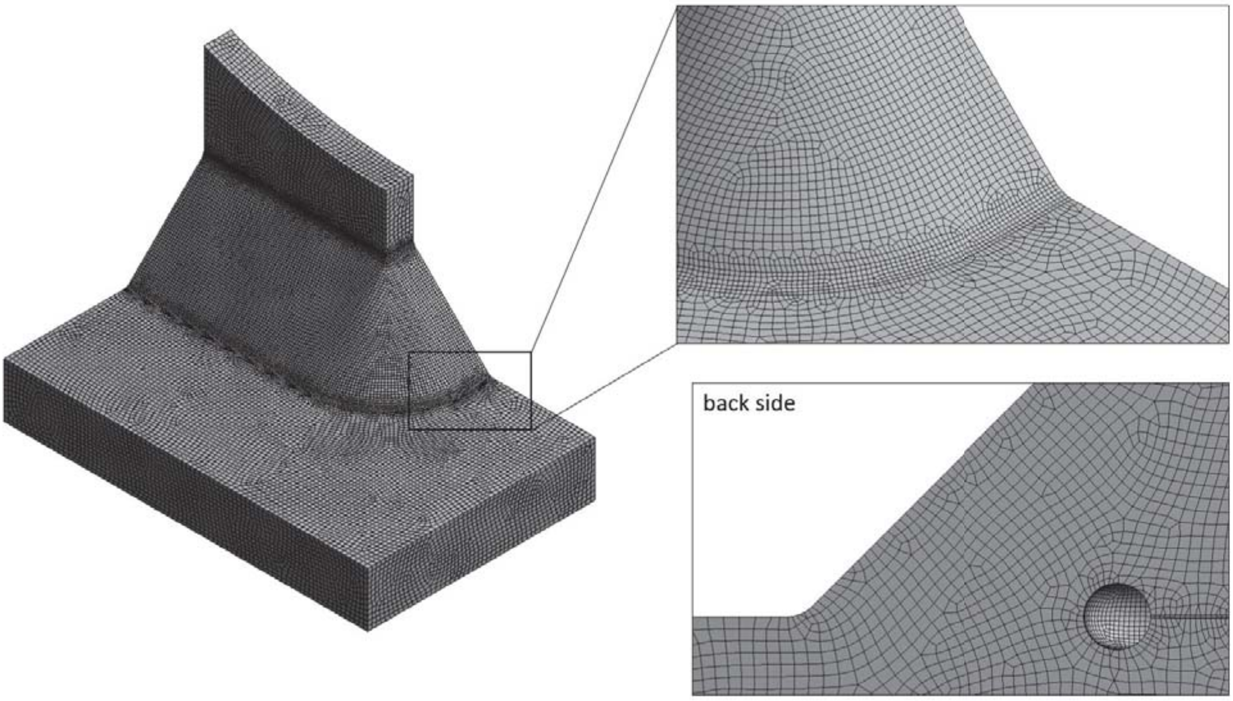

Figure 64: Sub-model for the weld edge geometry A, hex dominant meshing method.

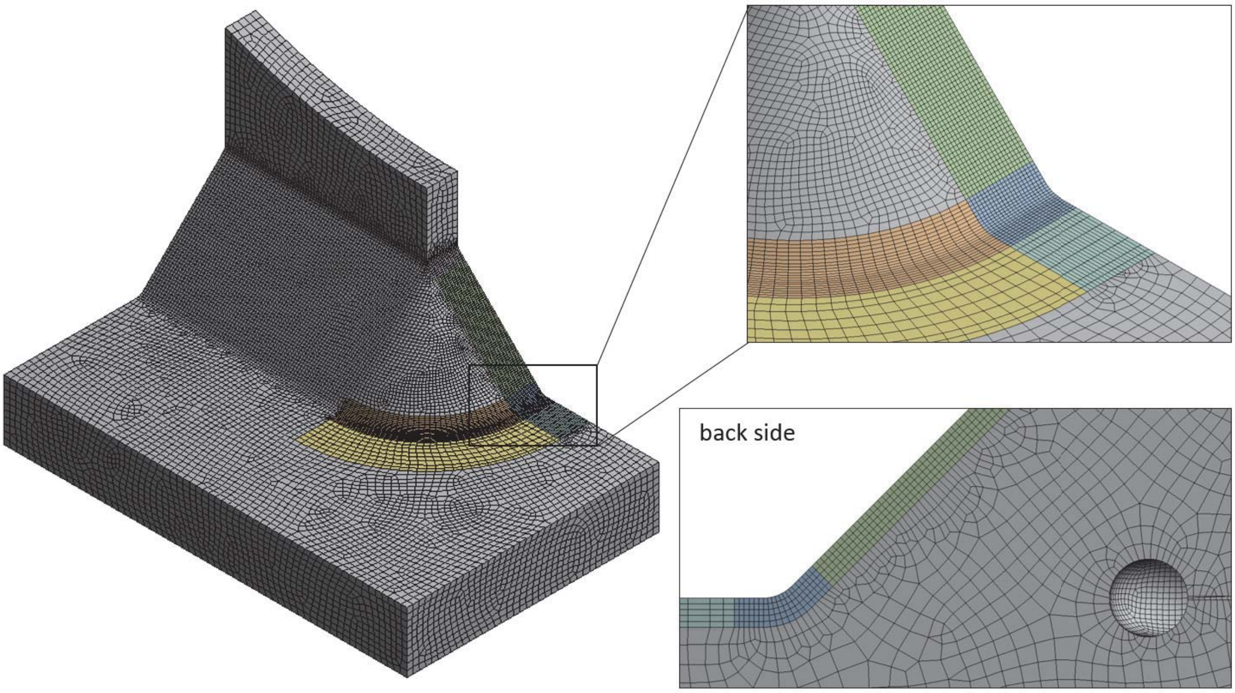

Figure 65: Sub-model for the weld edge geometry A, hexa meshing method.

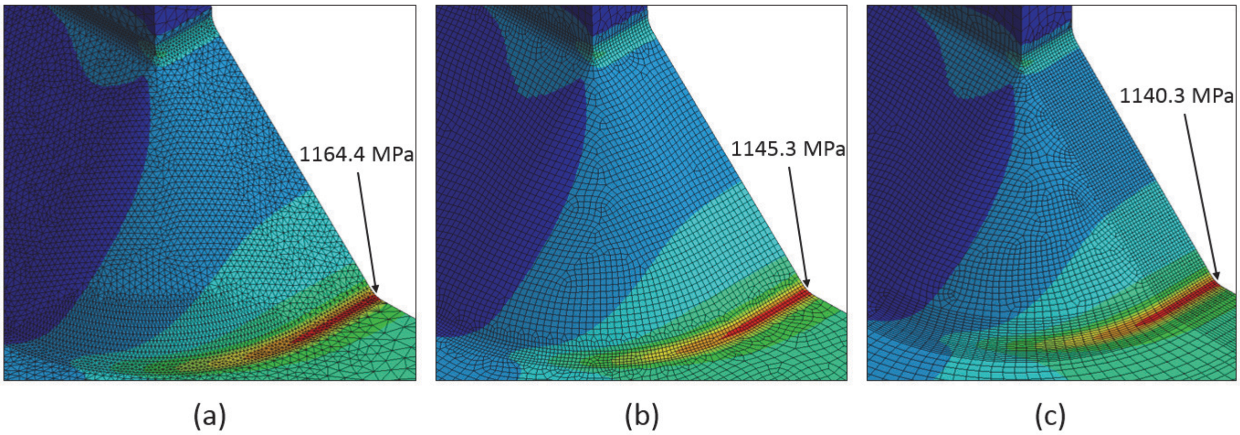
1164.4 MPa
1145.3 MPa
1140.3 MPa
(a)
(b)
(c)

Figure 66: Maximum principal stress in sub-model for the weld edge geometry A, $F = 2\,500N$. Meshing method **(a)** tetra, **(b)** hex dominant and **(c)** hexa.

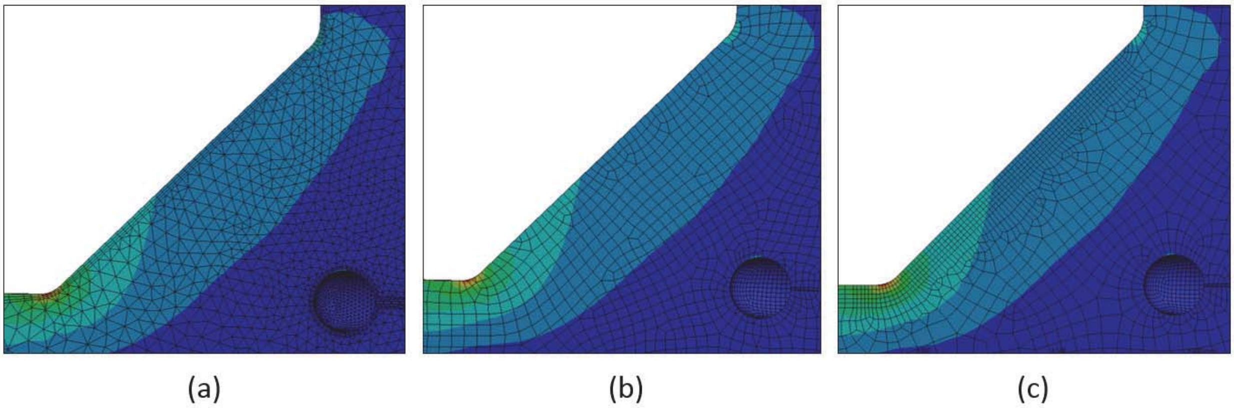

Figure 67: Depth-wise stress gradient in critical location of sub-model for the weld edge geometry A, $F = 2\,500N$. Meshing method **(a)** tetra, **(b)** hex dominant and **(c)** hexa.

B Analysis of geometry B

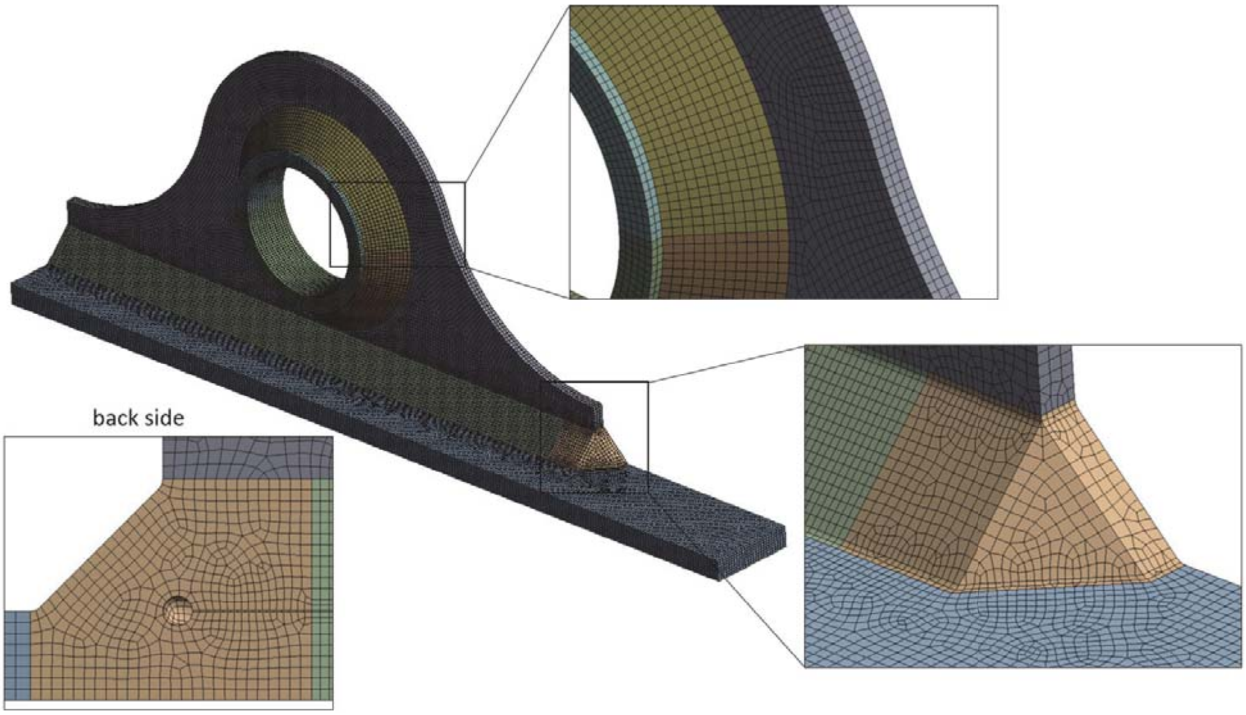

Figure 68: Global mesh for the weld edge geometry B.

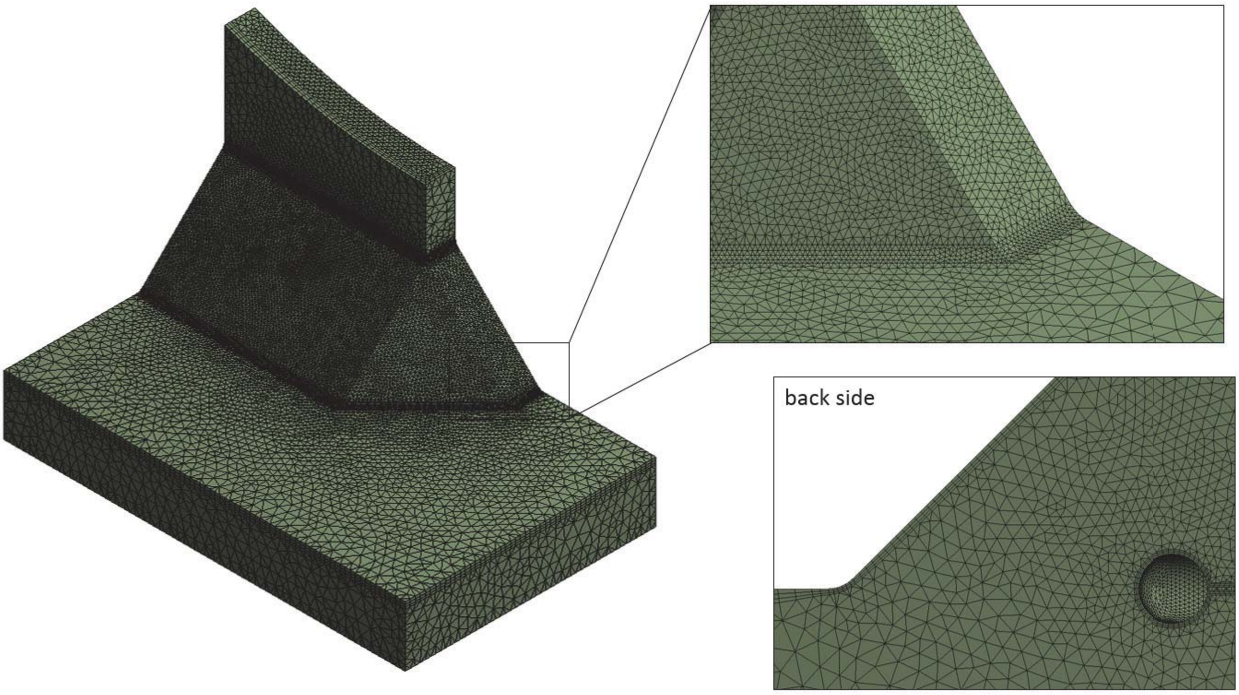

Figure 69: Sub-model for the weld edge geometry B, tetra meshing method.

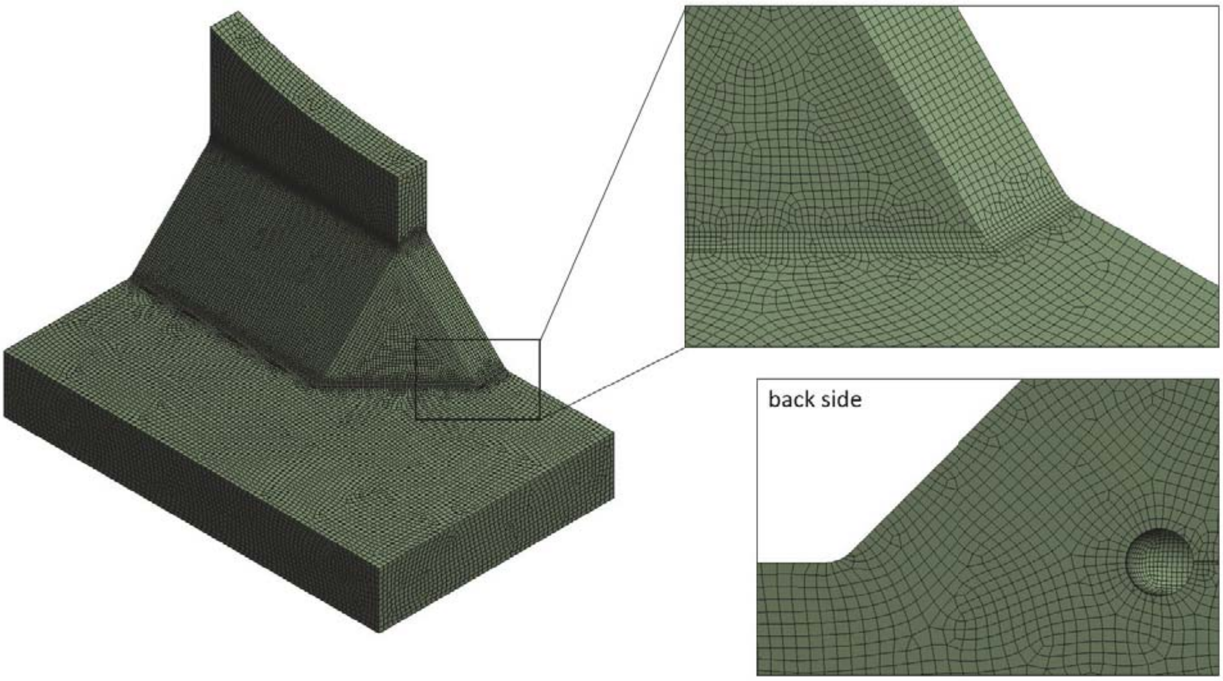

Figure 70: Sub-model for the weld edge geometry B, hex dominant meshing method.

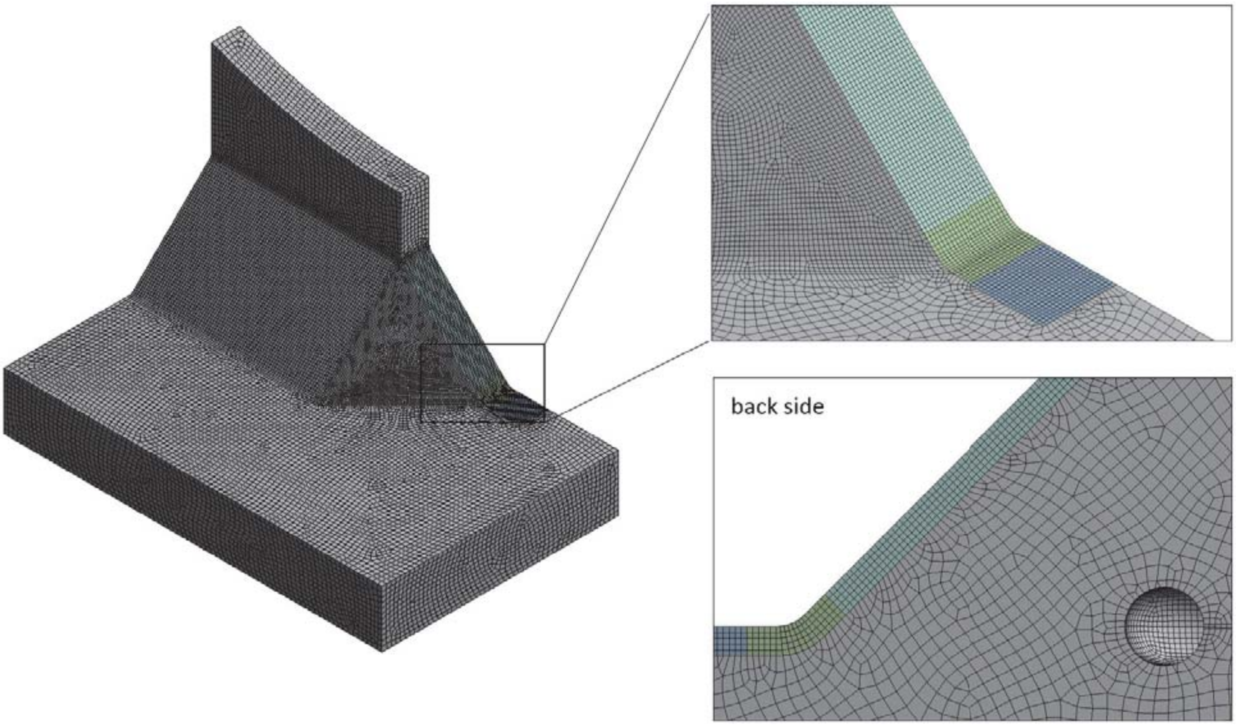

Figure 71: Sub-model for the weld edge geometry B, hexa meshing method.

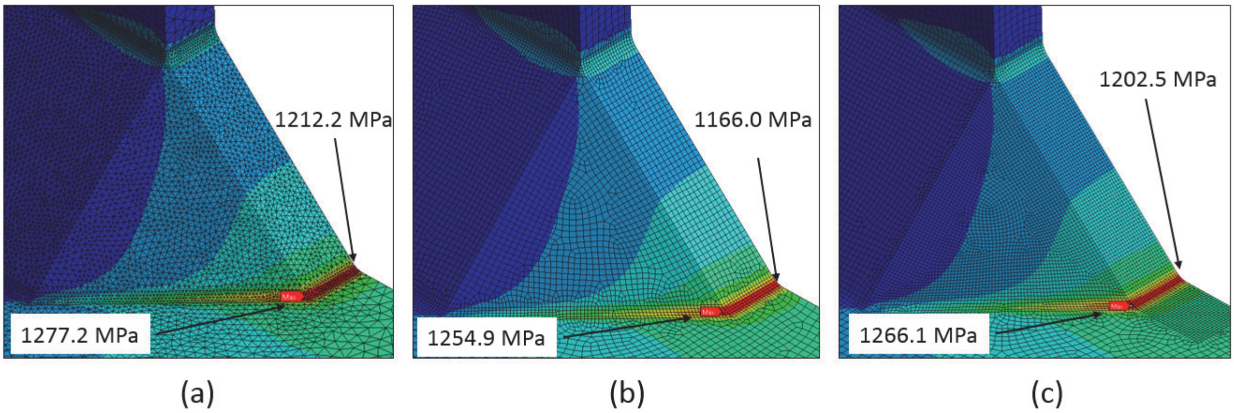
1212.2 MPa
1277.2 MPa
Max
1166.0 MPa
1254.9 MPa
Max
1202.5 MPa
1266.1 MPa
Max

(a) (b) (c)

Figure 72: Maximum principal stress in sub-model for the weld edge geometry B, $F = 2\,500N$. Meshing method **(a)** tetra, **(b)** hex dominant and **(c)** hexa.

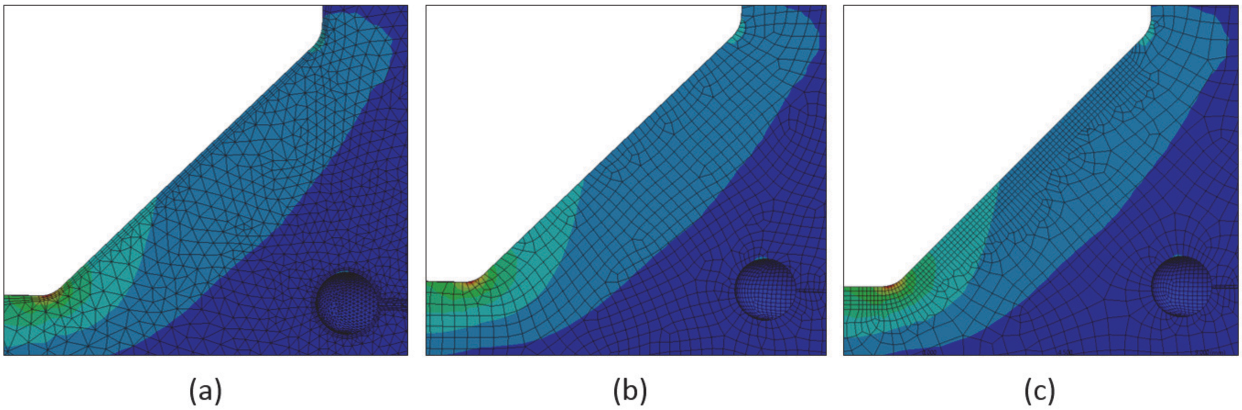

(a) (b) (c)

Figure 73: Depth-wise stress gradient in critical location of sub-model for the weld edge geometry B, $F = 2\,500N$. Meshing method **(a)** tetra, **(b)** hex dominant and **(c)** hexa.

C Analysis of geometry C

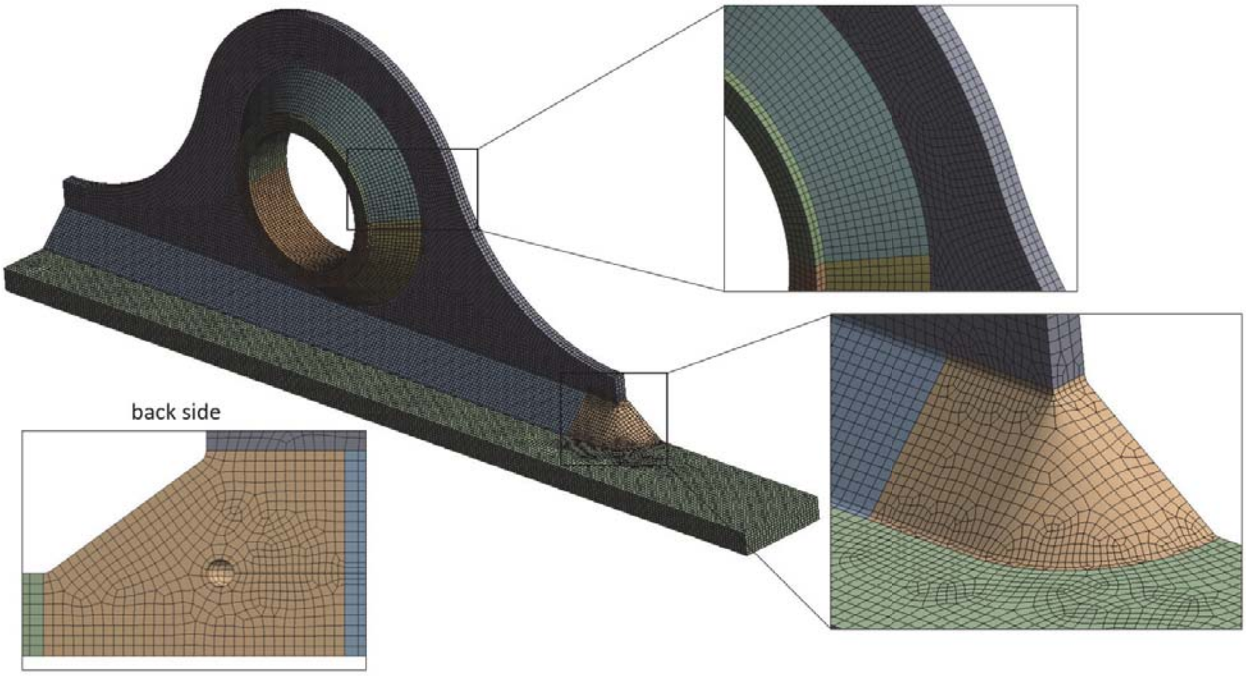

Figure 74: Global mesh for the weld edge geometry C.

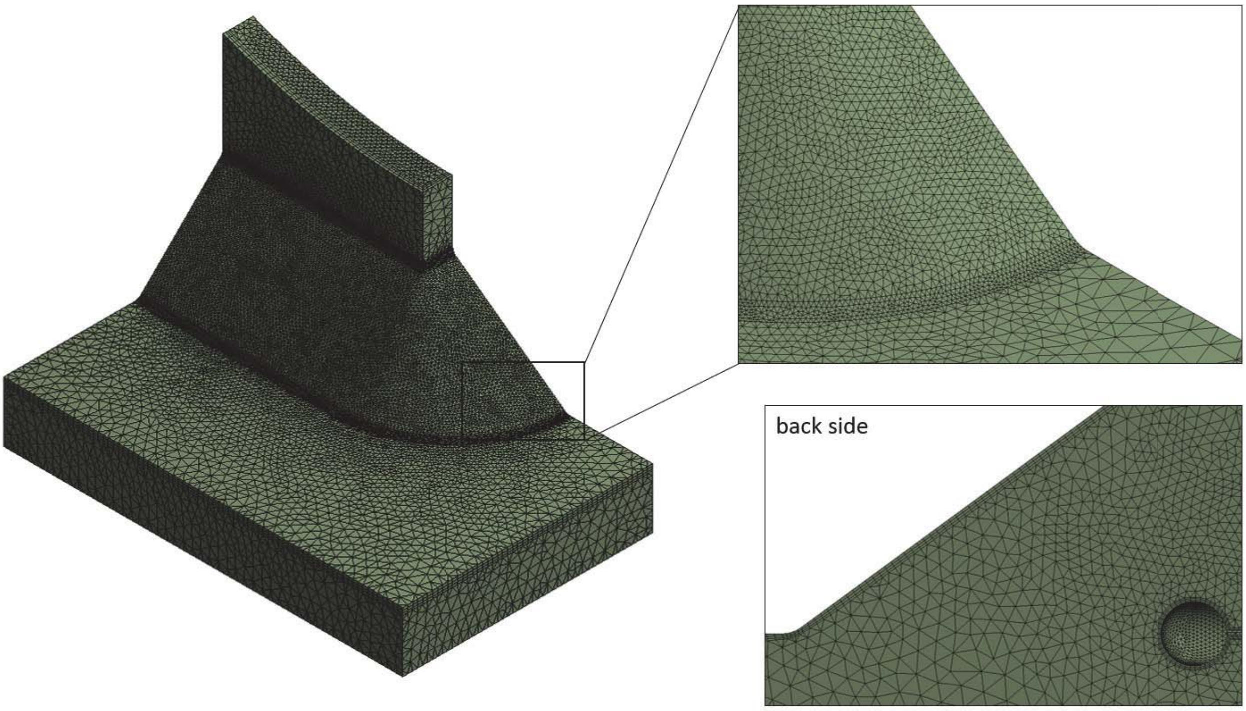

Figure 75: Sub-model for the weld edge geometry C, tetra meshing method.

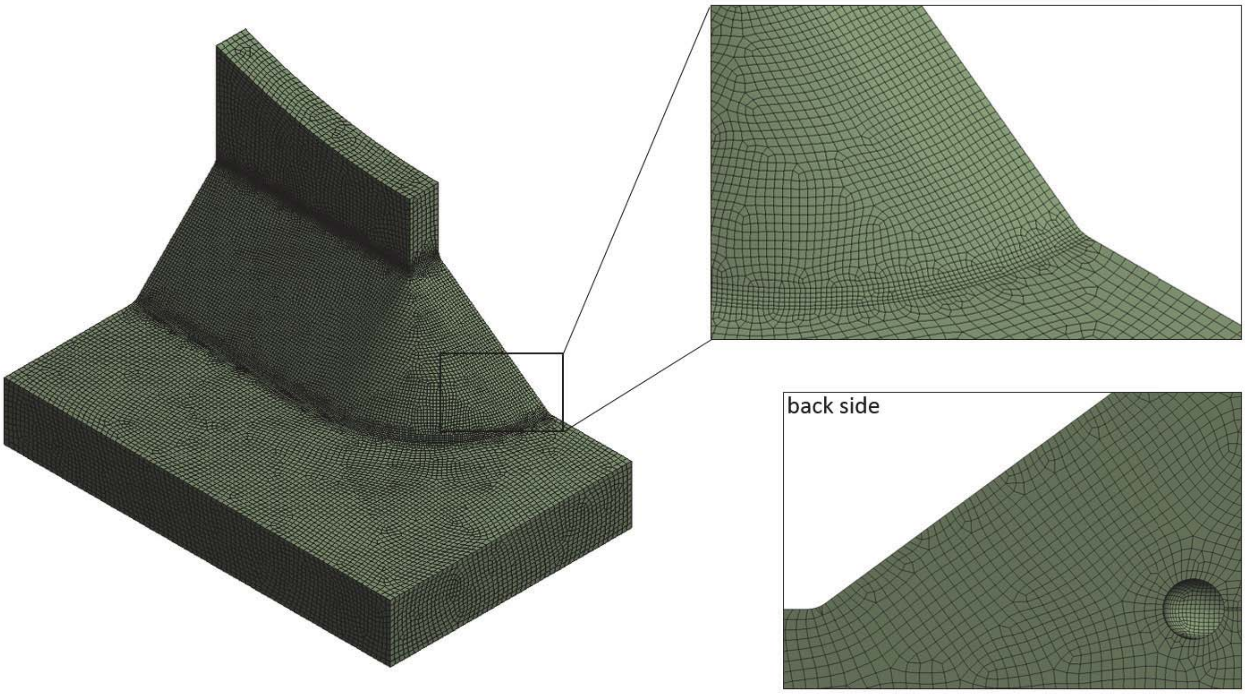

Figure 76: Sub-model for the weld edge geometry C, hex dominant meshing method.

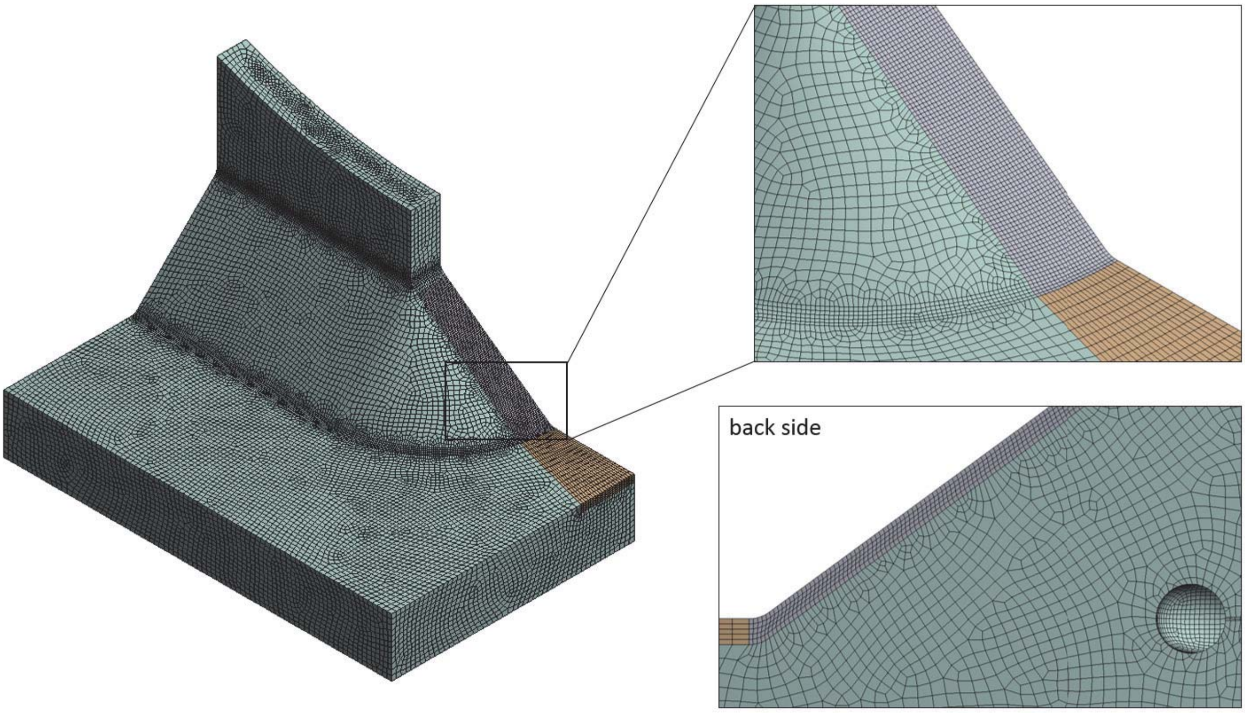

Figure 77: Sub-model for the weld edge geometry C, hexa meshing method.

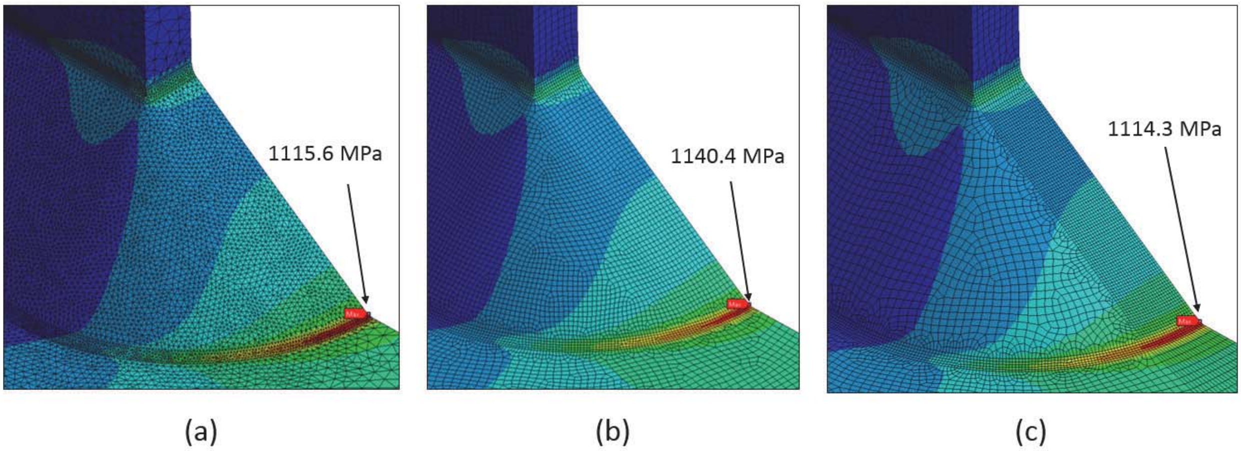
1115.6 MPa
1140.4 MPa
1114.3 MPa
Max
Max
Max

(a) (b) (c)

Figure 78: Maximum principal stress in sub-model for the weld edge geometry C, $F = 2\,500N$. Meshing method **(a)** tetra, **(b)** hex dominant and **(c)** hexa.

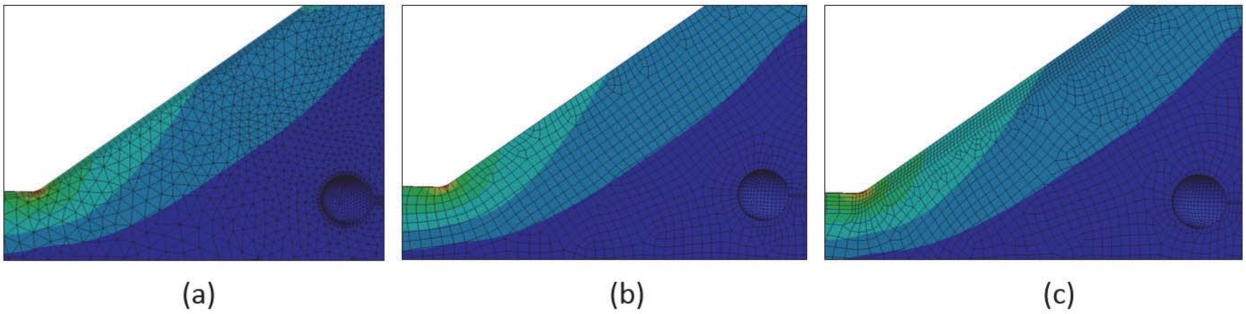

(a) (b) (c)

Figure 79: Depth-wise stress gradient in critical location of sub-model for the weld edge geometry C, $F = 2\,500N$. Meshing method **(a)** tetra, **(b)** hex dominant and **(c)** hexa.

D Nomenclature used in excavator description

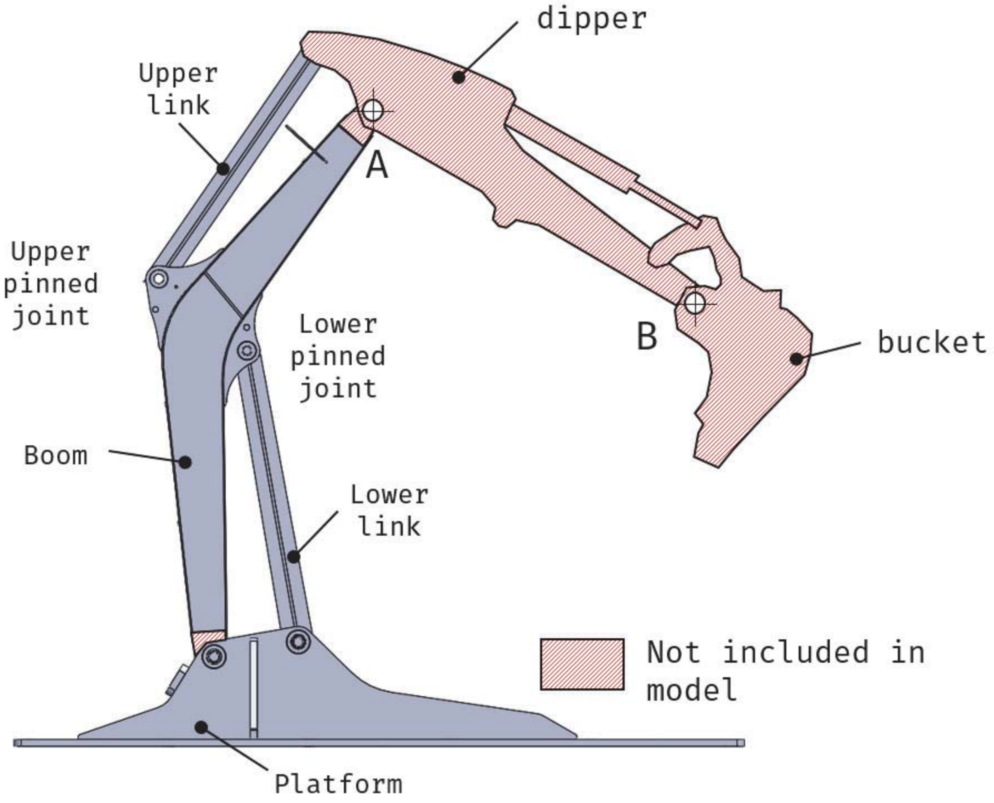
dipper
Upper link
A
Upper pinned joint
Lower pinned joint
B
bucket
Boom
Lower link
Not included in model
Platform

Figure 80: Nomenclature used in description of excavator model.